AN EXPERIMENTAL AND NUMERICAL INVESTIGATION OF THE STEADY STATE FORCES IN SINGLE POINT INCREMENTAL SHEET FORMING

A Thesis

by

MAHESH NAIR

Submitted to the Office of Graduate Studies of
Texas A&M University
in partial fulfillment of the requirements for the degree of

MASTER OF SCIENCE

August 2011

Major Subject: Mechanical Engineering

AN EXPERIMENTAL AND NUMERICAL INVESTIGATION OF THE STEADY STATE FORCES IN SINGLE POINT INCREMENTAL SHEET FORMING

A Thesis

by

MAHESH NAIR

Submitted to the Office of Graduate Studies of
Texas A&M University
in partial fulfillment of the requirements for the degree of

MASTER OF SCIENCE

Approved by:

Chair of Committee,	Jyhwen Wang
Committee Members,	Xin-Lin Gao
	Michael Johnson
Head of Department,	Dennis O'Neal

August 2011

Major Subject: Mechanical Engineering

ABSTRACT

An Experimental and Numerical Investigation of the Steady State Forces in Single Incremental Sheet Forming. (August 2011)

Mahesh Nair, B.En., Birla Institute of Technology and Science, Pilani

Chair of Advisory Committee: Dr. Jyhwen Wang

Incremental sheet forming process is a relatively new method of forming which is increasingly being used in the industry. Complex shapes can be manufactured using this method and the forming operation doesn't require any dies. High strains of over 300 % can also be achieved. Incremental sheet forming method is used to manufacture many different components presently. Prototype examples include car headlights, tubs, train body panels and medical products.

The work done in the thesis deals with the prediction of the steady state forces acting on the tool during forming. Prediction of forces generated would help to design the machine against excessive vibrations. It would help the user to protect the tool and the material blank from failure. An efficient design ensures that the tool would not get deflected out of its path while forming, improving the accuracy of the finished part.

To study the forces, experiments were conducted by forming pyramid and cone shapes. An experimental arrangement was set up and experimental data was collected using a data acquisition system. The effect that the various process parameters, like the

thickness of the sheet, wall angle of the part and tool diameter had on the steady state force were studied.

A three dimensional model was developed using commercial finite element software ABAQUS using a new modeling technique to simulate the deformation of the sheet metal blank during incremental sheet forming. The steady state forces generated for any shape, with any set of parameters used, could be predicted using the numerical model. The advantage of having a numerical model is that the forces can be predicted without doing experiments.

The model was used to predict the steady state forces developed during forming of pyramid and cone shapes. The results were compared and were seen to be reasonably close to the experimental results. Later, the numerical model was validated by forming arbitrary shapes and comparing the value obtained from simulations to the value of the measured steady state forces. The results obtained from the numerical model were seen to match very well with the experimental forces for the new shapes. The numerical model developed using the new technique was seen to predict forces to a reasonable extent with less computational time as compared to the models currently available.

DEDICATION

This thesis is dedicated to the two most important women in my life, my mother and my girlfriend.

There are no words to describe the support that a mother offers her son. Your love has helped me a lot mother.

My girlfriend has loved, encouraged and supported me every day, for the past two years. I am fortunate to have you in my life.

ACKNOWLEDGEMENTS

Two frogs jumped into a large vessel of milk and couldn't get out. The frogs kept swimming around trying to find a way out. But try as they might, they were unsuccessful to get out. The first frog realizing the fruitlessness of his attempts gave up and sank to the bottom. The second frog refused to accept defeat and swam on and on. Came morning and he found that he had churned the milk to butter. With one final push, he jumped out of the bowl to safety.

I would like to thank Dr. Jyhwen Wang for his invaluable guidance at every step in this project. He has truly been a mentor to me in every sense of the word and I would forever be grateful to him for advising me, not just about tackling the thesis problem but also about life in general. His words have helped me push myself on, with the belief that the solution would present itself if I kept on trying.

I express my gratefulness to Dr. Alex Fang for lending the dynamometer. I am also deeply indebted to Bright for helping me in the initial phase of the thesis. I haven't ever met anyone with so much energy as him. Cheng-Kang Yang was always available to help me when I encountered problems in ABAQUS. My sincere gratitude to Adam for helping me machine the fixture and teaching me to operate various machines.

I am thankful to my friends and family who helped me see through many rough days, I would also like to express my gratitude to the supercomputer facility and to the MMET and Mechanical Department for providing me with excellent facilities.

Thank you for making me the second frog.

TABLE OF CONTENTS

Page

Page

LIST OF FIGURES

FIGURE Page

FIGURE Page

FIGURE Page

FIGURE Page

LIST OF TABLES

1. INTRODUCTION: STEADY STATE FORCES IN INCREMENTAL SHEET FORMING

Incremental sheet forming (ISF) is a metal forming process which rose to prominence at the beginning of the 1990s. ISF is a highly localized deformation process in which a tool, whose path is programmed to follow a particular trajectory, moves over a sheet metal and forms the desired shape. Three dimensional models of the part are designed using commercially available CAD/CAM software FeatureCAM and CNC codes are generated by the same software. The codes are then fed into the CNC machine. Figure 1 shows the components necessary to perform single point incremental forming.

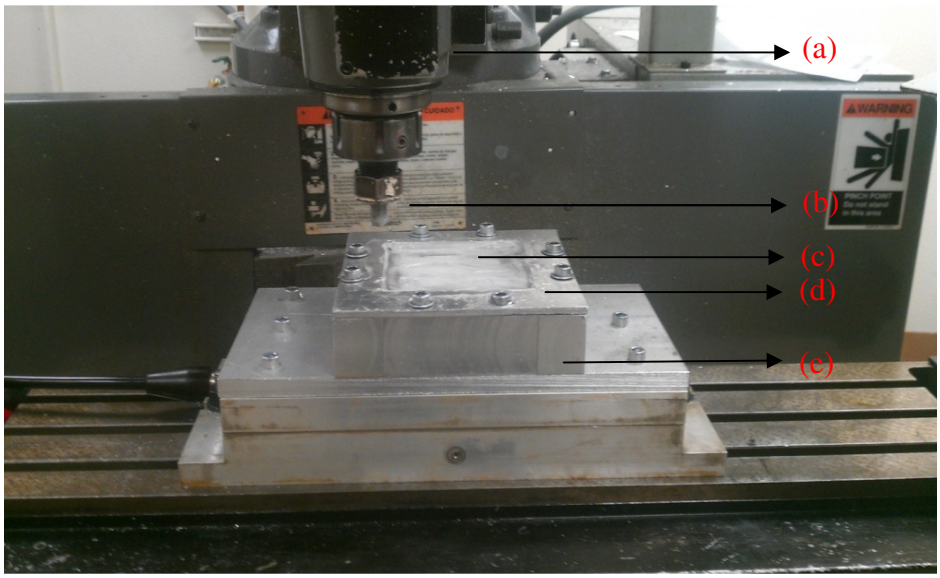

Fig. 1. Components necessary for incremental sheet forming.

This thesis follows the style of Journal of Materials Processing Technology.

With reference to Figure 1, the basic components needed to perform incremental forming include a Computer numerically controlled (CNC) machine (a), forming tool which deforms the sheet metal to form the desired shape (b), sheet metal work piece (c), a fixture which clamps the metal blank securely (d) and (e).

The path followed by the forming tool to form a cone shape is shown in Figure 2. The distance between each increments of the tool, referred to as the step size, is marked by the symbol υ. The symbol α represents the wall angle of the shape. The arrows depict the motion of the tool.

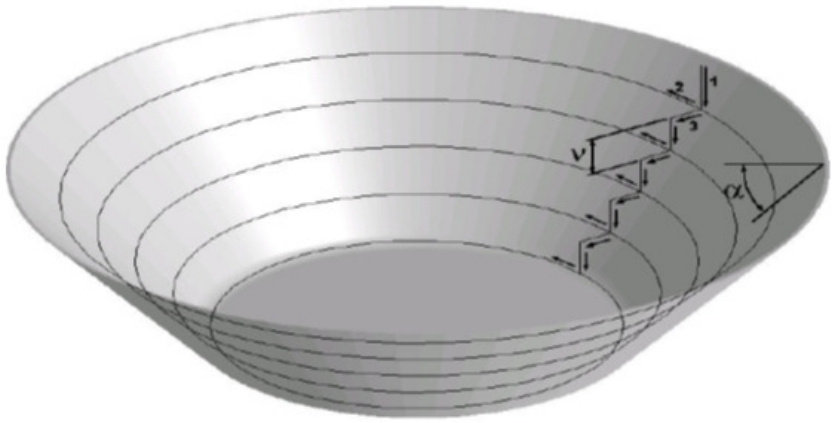

Fig. 2. Contour tool path used for incremental forming of a cone, Duflou et al. (2005).

ISF method has many advantages. Firstly, the forming operation does not require any dies to create the shape; this is why it is generally referred to as “die less forming”. The lack of requirement of expensive dies makes ISF a perfect manufacturing process

when rapid prototypes of shapes have to be made. The second major advantage of this process is that high strains of over 300 % can be achieved by ISF.

The primary focus areas of research in ISF include the study of formability and factors affecting it, the prediction of the springback of the sheet and the prediction of the forces generated during forming. Prediction of forces generated would help the user to protect the tooling and the material blank from failure. It would also help to design the machine against excessive vibrations and also to ensure that the tool will not get deflected from its path while forming. This would ensure higher dimensional control of the parts formed.

The forces acting on the tool while forming a pyramid having an angle of 45 degrees, with a step size of 1.27 mm, using a tool having a radius of 6.35 mm on a sheet having thickness of 0.8 mm are shown in Figure 3. Initially, when the tool pushes down on the metal, the response of the sheet metal is more of elastic deflection than plastic deformation. This phenomenon explains the low force acting on the tool at the start of the forming operation. However with several passes of the tool, the sheet metal gets plastically deformed and the elastic deflection reduces, thus increasing the force on the tool. After several passes of the tool over the sheet metal, the stiffness of the sheet does not increase much. At this stage, it was noticed that the forces required by the tool to deform the sheet tend to remain the same with each pass. Figure 4 illustrates the physical location of the tool at the start of the forming.

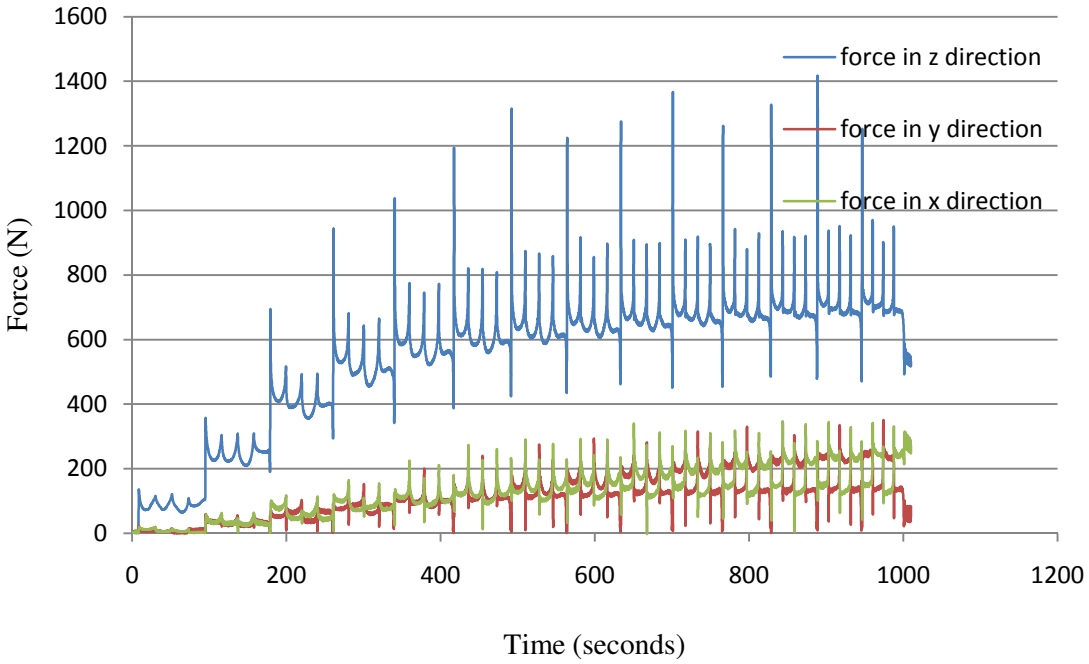

Fig. 3. Forces generated during incremental sheet forming.

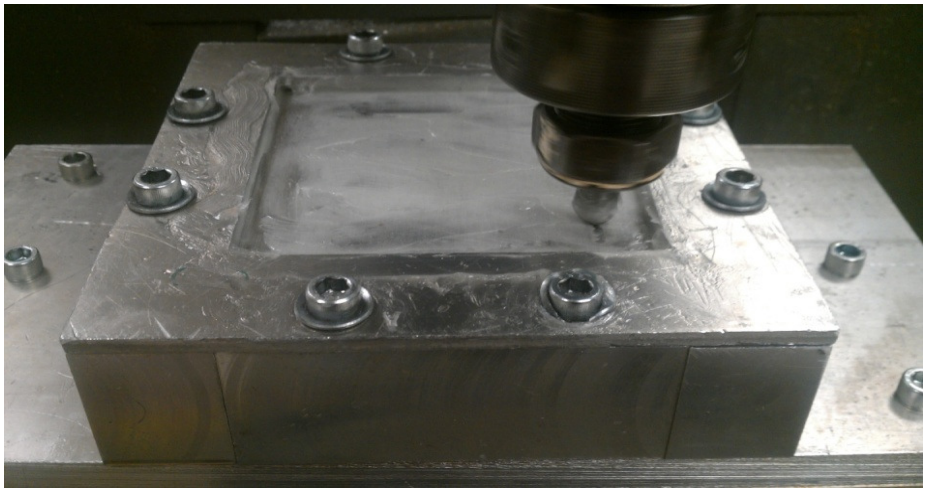

Fig. 4. Start of the first pass of the forming tool.

The forces acting on the tool once the sheet metal has been sufficiently stiffened are shown in Figure 5. It is noticed that the force values tend to follow a similar pattern over time. The peak (a) in Figure 5 represents the point when the tool reaches the corner of the pyramid and takes a step down. This point signifies the start of a new pass of the tool. Points (b), (c) and (d) represent the force acting on the tool when it reaches the other 3 corners of the pyramid. Point (e) signifies the force acting on the tool when it is just about to finish the pass. The constant force which lies between the peak values (a), (b), (c) and (d) represent the force acting on the tool when it is at a location between any two corners of the pyramid.

The condition where the amount of force required for deforming the sheet metal is approximately the same after each pass, can be called as the steady state condition. The forces generated during each pass of the tool, after the steady state conditions have been reached, are defined as the steady state forces. Figure 6 shows the physical region where the steady state conditions prevail.

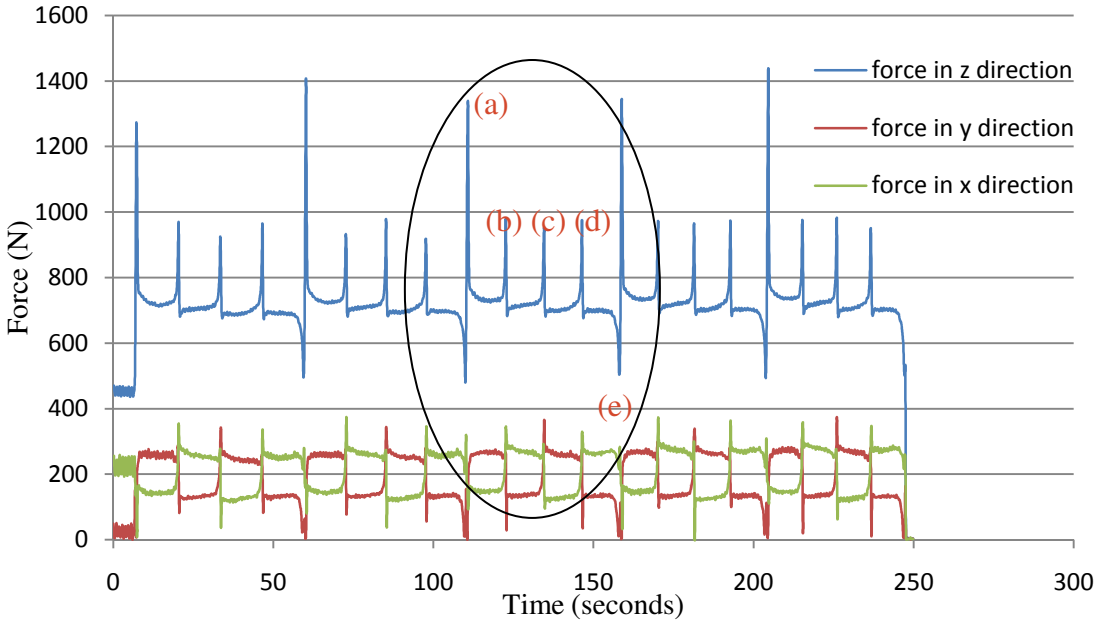

Fig. 5. Steady state forces.

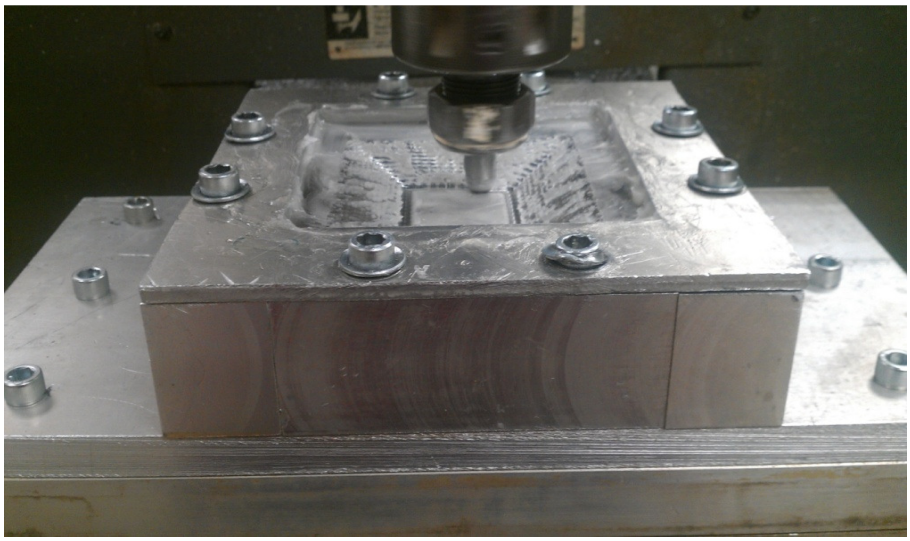

Fig. 6. Steady state condition.

The thesis deals with the prediction of the steady state forces generated during incremental sheet forming. A numerical technique which takes lesser computational time than the models currently available is developed to predict the forces generated. To investigate the steady state forces, it was necessary to perform experiments. Experiments were conducted to measure the forces generated while forming pyramid and cone shaped parts.

The first phase involved the design of the fixture which could be used for running the experiments. Once the design of the fixture was completed using SolidWorks, the next step was to manufacture it. The manufacturing of the fixture completed the first stage of the thesis. To measure the forces, it was also necessary to make the forming tool and have a data acquisition system which could measure the forces acting on the tool during forming. The data acquisitioning system included a table mount dynamometer which was connected to an amplifier. The output of the amplifier was connected to the input terminals of an analog to digital converter which would convert the analog signals to a digital format. Further details about the manufacturing of the fixture and the setting up of the hardware necessary for conducting experiments can be found in the third section.

Once the fixture was made, several experiments were performed to calculate the forming forces generated when sheets having thickness of 0.8 and 1.27 mm were used. Aluminum alloy 5052 sheets were selected to be the blank material. Pyramid and cone shapes having outer dimensions of 101.6 mm and a depth of 25 mm were decided to be used. Tools having radii of 6.35 mm and 9.525 mm were manufactured. Shapes having

wall angles of 30 and 45 degrees were formed. The main motivation for conducting the experiments was to study the effect of the input parameters on the forming force. The forces generated during forming of pyramid and cone shapes would be measured and the vector sum of the steady state forces would be compared. Results of the experiments conducted are presented in Section 4 of the thesis.

The next task was to develop a numerical model which could effectively model the steady state forces using finite element code ABAQUS. Standard three dimensional analysis was done and the results were compared with the experiments. The model developed attempted to simulate only the peak forces and the force developed when the tool was in between the corners. The tool path simulation started from a point which was sufficiently deep, thus assuming that the sheet metal was fully stiffened at that depth. Therefore it was logical to expect that the force experienced by the tool to further deform the sheet metal would be the steady state force. The depth was decided based on experience obtained after performing lot of experiments. This is a method which has hitherto been untried and it can save a lot of computational time. The numerical model developed is mentioned in detail in the fifth section.

The results obtained from the numerical model thus developed are compared with the measured steady state force values. Finally, arbitrary shapes were created and the force values obtained for the new shapes were compared with the predicted values. This was done to validate the numerical model developed.

2. BACKGROUND

Previous work related to the formability and force prediction in single point incremental forming is discussed in this section. Few analytical and numerical models which have been developed are also explained.

Incremental sheet forming (ISF) is a metal forming process which rose to prominence at the beginning of the 1990s. Hagan and Jeswiet (2003) have explained about the different types of sheet forming methods like the stretch expanding, two path method, incremental backward bulge forming and others including CNC incremental sheet forming. Jeswiet et al. (2005b) have given a brief description about some of the different variations of the incremental sheet forming process. Figure 7 shows some of these variants.

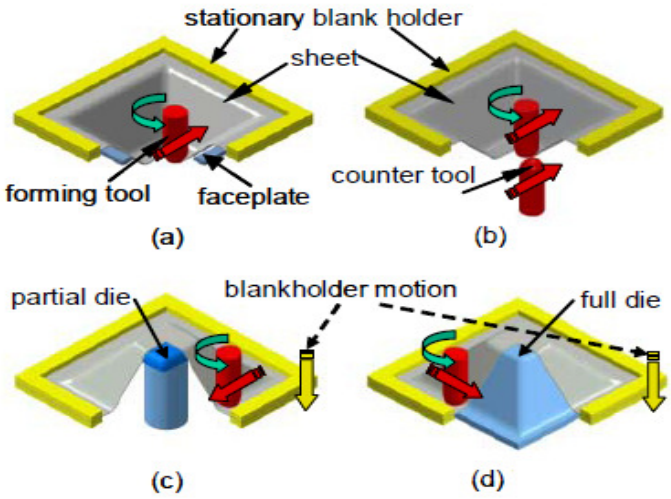

Fig. 7. Variations of the incremental sheet forming process : (a) single point incremental forming , (b) incremental forming using a counter tool , two point incremental forming using (c) partial die and (d) full die, Jeswiet et al. (2005c).

2.1. Applications of incremental sheet forming

Incremental sheet forming is a great production method for batch production runs and many prototypes have been made for common products. Jeswiet et al. (2005a) manufactured a solar cooker cavity and also fabricated a prototype of a headlight for a car company Jeswiet and Hagan (2001), as shown in Figure 8. Several other asymmetric shapes including tubs, noise shields for automotives, motorcycle gas tanks and also ankle supports which are used in medicine have also been made Jeswiet (2005), Jeswiet and Hagan (2003). Amino et al. (2002) manufactured fenders and hoods for a Honda automobile using incremental sheet forming methods. Several new methods of incremental sheet forming are coming up which includes the use of laser to perform

incremental sheet forming Duflou et al. (2007a) and incremental sheet forming of sandwich panels Jackson et al. (2008).

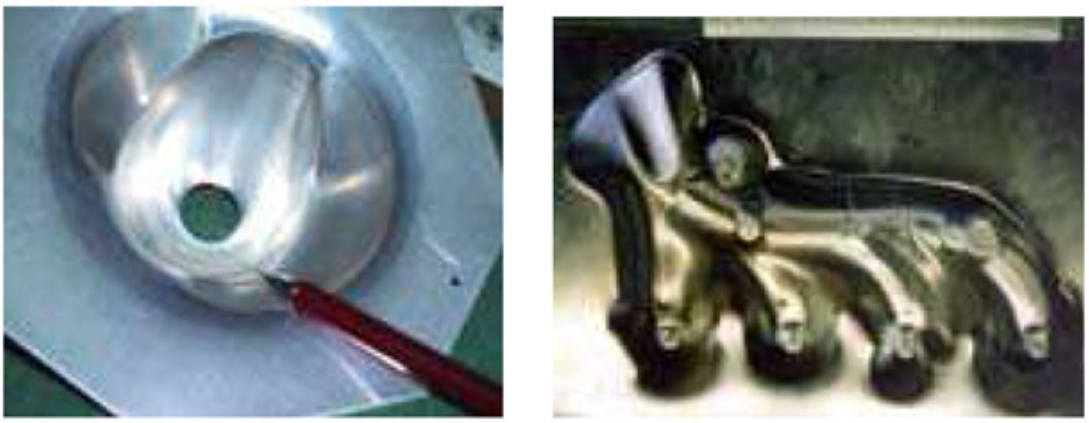

(a) (b)

Fig. 8. Rapid prototype products made using incremental sheet forming: (a) headlight Jeswiet and Hagan (2001), (b) automobile noise shield, Jeswiet et al. (2005c).

A thorough review of the history and development of the process of incremental sheet forming have been given by Hagan and Jeswiet (2003), Ham and Jeswiet (2008). These papers discuss the research currently being undertaken in the field of ISF. Some of the research topics include the study of formability and strains achieved during forming, factors affecting dimensional accuracy of the final parts and methods to improve it and forces generated during ISF. Jeswiet and Ali (2000) have given a thorough description of the entire ISF process. They have mentioned about the experimental set up required to perform ISF, about how to design parts and generate CNC codes using commercially

available softwares. They made several complex shapes and showed that “incremental micro-plastic forming” was a feasible process.

2.2. Formability

Ham and Jeswiet (2008), Ham and Jeswiet (2006) highlight the various parameters which influence formability during incremental forming. The effect of step size, wall angle, the feed rate and the spindle rotation speed on formability were analyzed. The material formability was found to increase when smaller step sizes, lower wall angles and thicker sheet were used. Formability also increased when higher spindle rotation speed and smaller tool were used. A smaller tool increases formability as the friction at the tool tip increases due to the larger concentration of forces. The increase in the thickness of the metal blank improves formability due to the fact that there would more material to deform in a thicker material and higher depths could be reached without the material thinning enough to cause fracture. The various parameters that affect the formability of the material during forming are shown in Figure 9.

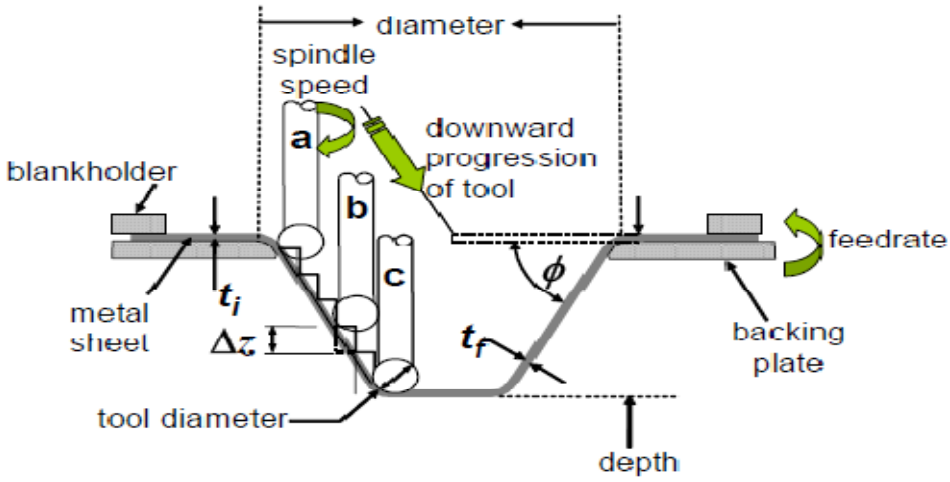

Fig. 9. Parameters which influence formability, Ham and Jeswiet (2006).

Filice et al. (2002) researched on the forming limit diagram for the incremental sheet forming process. They performed experiments for three different straining conditions which were pure uni-axial stretching condition, bi-axial stretching and a new testing condition which was in between the uni-axial and bi-axial stretching condition. They measured the major and minor strains using circular grids which were imprinted on the sheets before forming. The forming limit diagram for the incremental sheet forming was found to be a straight line with a negative slope which differed from the traditional forming limit diagram. They reasoned that the difference in the forming limit diagram was due to the ISF process following a heavily localized deformation mechanism with straining conditions ranging between uni-axial and bi-axial stretching.

In a later paper Jeswiet and Young (2005) made five different shapes from 1.21 mm thick Al 3003-0 sheets using a contour tool path and constructed a forming limit

diagram for the incremental sheet forming process. It was seen that strains of over 300% could be achieved for all 5 different shapes. The general trend of the forming limit curve was similar to the results obtained by Filice et al. (2002). It was concluded that high strains could be obtained in incremental sheet forming compared to the conventional forming method. Figure 10 shows the difference in the forming limit curve between the incremental and conventional forming processes.

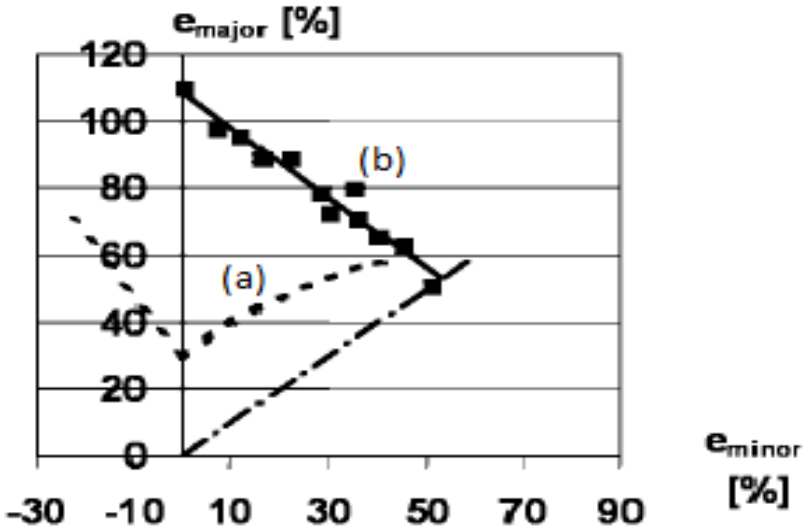

Fig.10. Forming limit curve, (a) conventional forming and (b) incremental sheet forming, Filice et al. (2002).

Jeswiet et al. (2002) tested the forming parameters which affect incremental sheet forming using a conical and a pyramid shape. A 3 axis CNC milling machine was used with a high carbon steel tool having a diameter of 12.7 mm diameter. 1.3 mm thick Aluminum 3003-0 sheets were used and all the parts had a constant increment size of

0.254 mm. They observed that the maximum forming angle increased as the thickness of the sheet increased. Jeswiet et al. (2005b) have mentioned the influence of material process parameters on the overall formability of the forming process by highlighting the influence of step size, spindle rotation, tool radius and directionality of travel. The authors reported that the formability decreased on increasing the step size because of the sheet metal blank undergoing more severe deformation conditions when higher step size were used. Formability was seen to increase when higher spindle rotation speeds were used due to the increase in the local heating and reduction of friction at the interface between the tool and the sheet.

Kim and Park (2002) investigated the effect that process parameters like contact friction between the tool and the sheet and anisotropy of the sheet have on the formability of the sheet. The authors highlighted that a certain amount of friction was necessary for better formability as the presence of friction was seen to increase the pressure of the tool acting on the sheet thus improving the formability. However using a higher friction value than the nominal one would cause the sheet to crack. Anisotropy of the sheet was also seen to have an influence in the formability of the sheet with the formability increasing when a smaller tool was used along the transverse direction and larger diameter tool along the rolling direction.

The various factors and their effect on formability that are mentioned in Reddy and Cao (2010) are summarized. Formability was seen to have an inverse relation to step down distance and the tool diameter. Since the sheet is anisotropic, formability increases in the transverse direction. Spiral tool path increases the formability as compared to the

contoured tool path. A higher tool speed and thicker material were seen to produce higher formability. It was also seen that a low friction value between the tool and the sheet metal blank helped to increase the formability although a high friction value damaged the tool and reduced the surface quality of the part produced. Lubrication dint seem to have any effect on the material formability, however the presence of lubricants is quite necessary to ensure high surface finish is obtained.

2.3. Mechanisms

Although extensive research has been done on the formability and the various factors which affect it during incremental sheet forming, the mechanism behind the forming process is still not fully understood. Understanding the mechanism of incremental sheet forming would help to predict forces generated during forming. Jeswiet and Ali (2000) conducted various experiments to study the effect of thickness on the formability. Conical and pyramid shapes having different wall angles were manufactured and it was seen that the wall thickness value agreed well with the value predicted by the spinning model developed by Sortais et al. (1963).

Shim and Park (2001) performed straight groove test to assess the formability of aluminum sheet and noticed that the strain was highest at the corners and low at the sides. A state of biaxial stretching at the corners and plane strain stretching at the sides were reported by them. During a closed-loop test of the tool path, it was noticed that for the same amount of tool depth, more deformation occurred at the corners than along a

straight edge and this was the reason cracks occurred mostly at the corners during forming.

Park and Kim (2003) manufactured a triangular cone using the contour step process to study the deformation mechanisms and the authors observed that as the curvature of the tool radius increased, the deformation went from plane-strain stretching to biaxial stretching. Cracks were explained to occur at the corners more frequently during incremental forming because of the dominating presence of bi-axial stretching in the corners. Kim and Park (2002) studied the deformation of the sheet during incremental sheet forming. In the straight line test, a state of biaxial stretching was noticed at the starting and end points while between these points, the mechanism was plane-strain stretching. The authors noted that the formability was greatest when the minor strain was zero, or during the plane-strain stretching phase. Jackson and Allwood (2009) mentioned that predominantly stretching and shear occurred in the plane perpendicular to the tool and shear in the plane parallel to the tool in incremental forming. The shear in the direction of the tool is thought to be as a result of friction and is the most significant strain component.

Emmens and Van den Boogaard (2009) have recapitulated the stabilizing deformation mechanisms which are found in incremental sheet forming. They mentioned that incremental sheet forming is a highly localized process and also mentioned about six different mechanisms which could explain the stabilization due to localization. The six mechanisms mentioned were “contact stress, bending under tension, shear, cyclic straining, geometric inability to grow and hydrostatic stress”. Out of the six mechanisms,

it is widely thought that bending under tension is the primary deformation mechanism in incremental sheet forming as is also thought by Marciniak et al. (2002). Silva et al. (2008) developed a model based on membrane analysis with frictional force acting in the plane of the tool. They took a local shell element and performed a force balance on the shell in the circumferential, thickness and meridional directions. They identified that the flat surface and the rotation symmetric surfaces were under plane strain conditions while the corners were biaxially stretched which led to their thinning and cracking while forming.

2.4. Force measurement

Prediction of forces acting on the tool during forming is a major research area in the field of incremental sheet forming. Jeswiet and Szekeres (2005) discussed about forces developed during incremental forming of pyramid and cone shape. 1.21 mm thick 3003-0 Aluminum alloy sheets were used. For measuring forces, a cantilever type of sensor was mounted to the spindle of the forming tool. It was seen that the axial force was larger than the combined rotational forces, which meant that the major energy went into pushing the tool down into the sheet metal surface. Another interesting observation was that at some points, the rotational force would be negative; this was reasoned to be due to the springback of the sheet which pushed the tool back and exerted a force in the opposite direction resulting in the negative values of the force. It was noted that the draw angle was an important factor in incremental sheet forming to determine if the part could be made in a single pass or required multiple passes. Many cones were made having

different wall angles and it was observed that the forming force generated increased with the wall angle.

Duflou et al. (2005) used a Kistler 9265B six component table mount dynamometer to measure forces generated during forming. Experiments were done to learn the effect of three different process parameters which are the vertical step size, the tool diameter and the wall angle on the forming force. 1.2 mm thick aluminum 3003-0 sheets were used to form cone having a maximum diameter of 180 mm. The cone had a wall angle of 50 degrees. The tool used had a diameter of 10 mm and a step size of 0.5 mm. The parameters were changed one at a time and the forces were obtained in the three principal directions and were studied to learn the effect of each parameter on the force.

The first observation noted was that the force values started from zero and increased uniformly at the starting. Later when a fair amount of depth was reached, the force values were seen to be fairly constant. This was explained to be due to the fact that the tool takes a certain number of contours before fully being in contact with the sheet and also certain number of passes are required before the end effects which maybe induced due to starting too near the backing plate can be neglected. He divided the forces obtained into two broad regions. One was the peak forming force which was defined to be the highest force generated. The second region, which had a fairly constant value and fell after the maximum peak region, was called the settled force. It was seen that the peak force and the settled force increased as the tool diameter increased. Specimens with wall angles which varied between 20 to 60 degrees were made and it

was seen again that increasing the wall angle increased the force. Increase in the wall angle also resulted in increased straining of the sheet metal blank after every pass, which led to higher forces. It was also concluded that out of the three parameters, the vertical step size had the least significant impact on the forming force.

Duflou and Tunckol (2006) conducted experiments to study the effect that the boundary and part geometry exert on the forming force. Experiments were also performed with a spiral tool path to check if there were any differences in the forming forces generated as compared to the step wise contour followed by the tool. To study the effect of the end boundary conditions, cones having diameters of 90 mm to 60 mm were formed in an orifice of 91 mm. The cone had a wall angle of 70 degrees. It was seen that the peak axial force was 580 N on the part with zero proximity to the boundary and 460 N for the part with 30 mm proximity thus proving that boundary conditions did play a part initially in the forces generated during forming. It was seen that after the nominal angle was reached and a sufficient depth was traversed, the steady state forces were the same for both parts. This was reasoned out to be due to the fact that the tool contact evolved only after a certain number of contours and also it was thought that the effects of boundary conditions reduce considerably after a certain number of passes. It was also seen that the spiral tool path gave the same steady state forces as compared to the contour tool path.

To investigate the influence of the part geometry, two pyramids were formed. One had an initial wall angle of 30 degrees followed by a wall angle of 60 degrees and the other had a wall angle of 60 degrees. The other dimensions were kept the same, it

was seen that the settled force was similar in both the cases and thus the steady state forces were seen to be same irrespective of the part geometry. However no comparisons were made between cone and pyramid shapes.

Ambrogio et al. (2007) contributed to the force prediction problem by studying the influence of the tool diameter, tool pitch, the thickness of the sheet metal used and the wall angle on the tangential force component. The tangential force component was defined to be the product of the force in the vertical direction and the sine of the wall angle of the part. It was shown in a paper by Filice et al. (2006) that the tangential component was the main criterion for failure of the sheet metal blank. They further concluded that the most important factor which controls the forming force is the wall angle of the part. It was seen that a monotonic decrease in the value of the force after the peak force had reached, indicated impending failure of the material. An increase in the tool diameter was found to delay the steady state conditions being reached during forming. This was reasoned out to be due to the longer bending phase which is imposed on the sheet metal when a larger tool is used.

Petek et al. (2009) performed experiments to obtain the effect of the wall angle, tool rotation, vertical step size, tool diameter and lubrication between the tool and the sheet on the force generated. Cone specimens were made from DC05 draw steel having a thickness of 1mm. The base parameters were a wall angle of 65 degrees, forming depth of 60 mm, tool rotation of 40 rpm, tool diameter of 10 mm and a vertical step size of 0.5 mm. The lubricant used was SYLAC 80-05. It was noted that the force increased as the wall angle, vertical step and the tool diameter increased. The force magnitude increased

almost linearly with the increase in the step size. To study the effect of lubrication, experiments were done with and without the use of lubrication at a rotational speed of 40 rpm. It was seen that when lubricant was not used, the material developed cracks and this was due to the large value of friction between the tool and the specimen which increased the temperature due to the heating effect and also led to the kneading of the sheet material. However the force values were the same and it was concluded that the presence of lubrication leads to a better quality surface but it doesn't influence the magnitude of the forces.

Durante et al. (2009) conducted a study on the influence of tool rotation on the forming forces and it was noticed that the rotation didn't affect the vertical force quite a lot but it reduced the value of the in-plane forces.

Filice et al. (2006) did a wide variety of experiments and they noticed the force patterns do not depend on the history of forming. If for instance the wall angle was increased during forming, then instantaneously the force would increase, but after a few passes, the force would get back to the original value.

Several interesting trends in the forming force were observed which were categorized as three main types of curves. Firstly after the peak force is formed, the force value remains constant and this was explained by them to be due to the compensation between the effects of strain hardening, which increases the force required to deform a material and sheet thinning which reduces the force. The end effect of these effects is a steady value of the force. This trend was observed for low wall angles.

The next type of trend was a polynomial force trend which is observed for high but not severe wall angles, wherein the curve showed a low negative gradient after the peak and this was due to the thinning which takes place during stretching which reduces the force required to form the material. In the third case when high wall angle were used, the force decreased monotonically and this indicated onset of failure. In this trend known as the monotonically decreasing force trend, the sheet thinning dominates over the strain hardening and thus the force continually decreases.

Ambrogio et al. (2006) devised a method for detecting failure in the sheet during incremental forming based on studying the trends of the force generated. It was reasoned that till the force reached a peak value, bending was the most dominant mechanism after which stretching mechanism began and the forces trend then obtained were a factor of sheet thinning and work hardening effects. Figure 11 shows the three force trends.

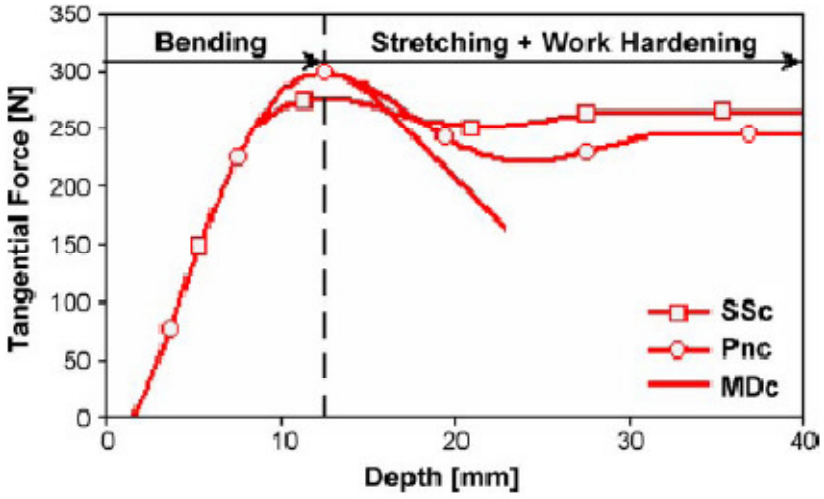

Fig. 11. Force trends showing the governing mechanisms, Ambrogio et al. (2006).

2.5. Analytical and numerical models for force prediction

Once the parameters which affected the force and their influence were found, the next attempt was to model the deformation process. The advantage of developing an analytical or numerical model which could effectively model the steady state forces is that it could be a very powerful tool to predict the steady state forces generated for any shape and any process parameter used.

Duflou et al. (2007b) developed a model to predict the force required to form parts having complex shapes with varying wall angles. The prediction would be based on the forces measured while forming parts with uniform wall angles. The research involved forming cones having an initial diameter of 128 mm and a depth of 30 mm. Annealed Al 3003-0 and Al 3103-0 alloys were used as the sheet metal blank. The input parameters that were included in the analysis were the vertical step size, the tool diameter, the wall angle and the thickness of the blank. Several experiments were conducted by changing one or more parameters at a time. Using a commercially available statistical data analysis package, the results obtained from the 27 different conditions were combined and formed into three multi-linear regression equations. Their experimental studies were based on experiments which were designed according to the "face centered- central composite design" The in-plane forces had been combined into one equation, while the other two equations were for the maximum peak vertical force and the settled vertical force. The three equations had the process parameters and their interaction terms as the variables and were second degree in nature.

A hyperbolic part and hemispherical part were chosen as the complex shapes whose force values would be predicted as these both geometries had continuously changing wall angles. The hyperbola started with a wall angle of 5 degrees and then constantly increased till it reached an angle of 72 degrees. The force prediction was not applied till the wall angle reached a value of 40 degrees, this is because firstly the tool wouldn't have made enough passes to reach a nominal contact area value and also the slope angle was not long enough for the force to have a nominal steady value. There was a maximum error of 9.6 % for the vertical force and 13.8 % for the in-plane force for the hyperbolic part.

The hemisphere has an initial wall angle of 72 degrees which decreases uniformly. It was seen that the steady state force value decreased due to localized necking and thinning. Due to this there was a large error of 23.9 % between the predicted and measured value of the in-plane forces. The conclusion of the regression model was that the predicted values had a lot of deviation when the results were extrapolated outside the nominal wall angle range of 40-60 degrees.

Aerens et al. (2010) presented a new approach for the forces which are formed in incremental forming based on results derived from experiments and also from analysis done using finite element simulations. The aim was to establish equations which could be used to calculate forces for different materials. Firstly truncated cones were formed and the forces were measured. Five different materials having different tensile strength and different thickness were used to perform the experiments. The post processing of the results and the development of the equations were done partly by using regression

techniques and partly by using the results obtained from finite element simulations and also the physics of the process. The work done to model the plastic deformation zone is documented in the following paper by the authors Eyckens et al. (2008).

Small scale models were made to learn the contact properties between the tool and sheet interface and the results were used to model forming forces. Three regression equations were developed for each material. Finite element simulations were done for the case of a tool forming a cone. The contact zone between the tool and the sheet metal blank were studied. From the results, the contact area was approximated to be a ribbon having constant width and from geometry, relations were developed between the radial and the axial force. Combining the relations obtained from the numerical simulation and the regression equations, a new set of equations were developed. These equations were dependent on the process parameters and the tensile strength of the material. The formulae developed were compared to the experimental value and the error was seen to vary from 1.1 % to 26.8 % as the process parameters were changed. The formulation also included the tensile strength as a material input parameter.

Bouffioux et al. (2008) performed line tests to verify the accuracy of tool force prediction using finite elements. Brick elements which had three layers along the thickness and shell elements were used. The coefficient of friction used was 0.05. It was seen that shell elements predicted the same force when a coarse and fine mesh was used. Also shell elements were seen to take much less computational time than brick elements.

He et al. (2005b) performed simulation of a cone with wall angle of 50 degrees using two different finite element codes, Lagamine and Abaqus. They compared the

force results obtained and it was seen that the force values predicted by the Lagamine model was over 30 % more than the values predicted by Abaqus. They also performed the same simulation using the Implicit and Explicit approach and they found that the latter approach reduced the computation time by a factor of four. However using the explicit approach could reduce the accuracy of the prediction.

Henrard et al. (2005) modeled a cone with a wall angle of 50 degrees with 8 node brick elements using finite element code, Lagamine. Three layers of brick elements were used along the thickness. Hill and Lankford coefficients were used to characterize the material. The cone had a final depth of 40 mm and maximum diameter of 180 mm. The forming tool had a radius of 6.35 mm and the step size was 0.5 mm. The simulation was done for only one-quarter of the cone and it was noticed that simulation of each pass took around 15 to 20 hours using a 8 CPU machine "(MIPS R12000 at 400 MHz)" with the Lagamine code. Force required to deform the material was obtained, however it was not compared to any experiments values. It was mentioned that a very fine mesh and a complete model of the cone was necessary to get accurate force results. However the authors suggested that this was not a feasible option due to the long computational time involved. Simulations were done to study the effect of friction on the total forming force and it was seen that there was a 4 % increase in the force when the friction coefficient was increased from 0.05 to 0.15. By performing a strain analysis using the model, they established that influence of the tool was "well-localized" and that the area which is beyond one-tool diameter is not deformed.

He et al. (2005a) simulated the forming process of a 40 degree pie of a cone. Brick elements having 6 and 8 nodes were used. Three layers were used along the thickness and each layer had about 2640 elements. The isotropic Von Mises yield criterion was adopted. The cone had similar dimensions to the cone described in Henrard et al. (2005). The forces got from numerical method were compared to the measured force and it was seen that the calculated force overestimated the experimental force by about 30%. The large error in the predicted values were thought out to be due to the isotropic Von Mises yield criterion being used in the analysis where in reality the material exhibits anisotropy. Another reason for the inconsistency between the results was the inaccuracy in describing the friction between the tool and the sheet metal. Figure 12 presents the results obtained by He et al. (2005a).

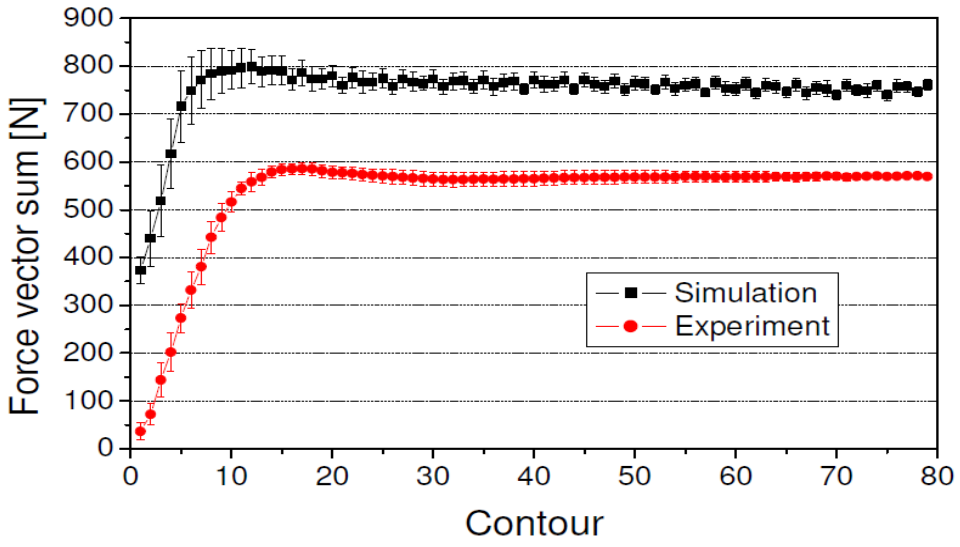

Fig.12. Comparison between the measured values and numerical value, He et al. (2005a).

The numerical model was further developed by Flores et al. (2007) by incorporating a kinematic hardening law instead of isotropic hardening law. The previous Von Mises and Swift model was changed to a Von Mises, Swift and Ziegler model. It was seen that the results obtained from kinematic hardening were closer to the experimental values when compared to the isotropic hardening model.

Analytical models were developed to calculate forces. Iseki (2001) developed a force model which could predict the radial and axial forces. He used a simplified plane strain membrane model using the assumption that the sheet metal which was in contact with the tool stretched uniformly. Finite element analysis was done in ABAQUS where the deformation was modeled for a quadrangular pyramid shell which was made from annealed aluminum. The plane strain model did not include the effect of friction or anisotropy. The model was not used to predict any forces obtained from experiments.

Pohlak et al. (2007) refined the model developed by Iseki by including the effects of plastic anisotropy into the model. The model was described better by using Hill's second and higher order yield criteria. However no experimental force prediction was done using the model. The authors developed a numerical model using LS-DYNA where forming of a pyramid was simulated the. Lankford stress coefficients and the yield stresses were other parameters used apart from the data obtained from the stress strain curve. The numerical model was compared with experimental data collected during forming of a pyramid and the model prediction showed good results when compared to the experimental data. The model couldn't however predict the peaks near the corner which was observed in the results got from the experiments. For both the models

developed by Iseki (2001) and Pohlak et al. (2007), it is necessary to approximate the width of the elongated strip after deformation to calculate the forces.

Marciniak et al. (2002) developed an elementary analytical model to predict the force generated during forming operation based on the principle of Bending-Under-Tension. However no comparisons were made to any experimental or numerical work.

2.6. Research objectives

Although Incremental Sheet Forming could theoretically be used to produce a wide variety of products, it has still not received much attention in the industry. Based on the review done, the main disadvantages of the ISF process are mentioned below:

1) The machining time taken is very large compared to the standard processes like stamping and deep drawing.
2) The large geometric error of the final product as compared to the target product. The reason for the dimensional inaccuracy is that sheet thinning takes place during forming which increases the difference between the desired and the obtained dimensions in a part.
3) Large setting up time and cost of the machine which performs Incremental Sheet Forming.
4) The deformation mechanism is still not well understood although several theories have been put forward to explain ISF.
5) There is a need for an effective analytical or numerical model which could predict the forces arising during ISF effectively.

The present work done in the thesis develops an effective numerical model to predict the forces. Prediction of forces is quite necessary to design the machine from failure. Knowledge of the forces beforehand could also help to reduce excessive vibrations and ensure that the tool wouldn't get deflected out of its path while forming thus increasing the dimensional control of the process.

Although experiments could be performed to get the forces generated, manufacturing the fixture and setting up of the whole data acquisition system would take a lot of time and money. Thus it is of the utmost importance to develop a numerical or analytical model which could predict forces without the need to do experiments. The nature of forces generated during incremental sheet forming and the effect of parameters on the forces generated during forming are studied by conducting experiments.

The disadvantage of the numerical models currently available is the large computational time needed to get the force results. To overcome this problem, it is necessary to develop a numerical model which would not only be able to predict forces accurately but also obtain the results with much less computational time. Developing such a numerical model is the endeavor of the present research.

3. MANUFACTURE OF FIXTURE AND EXPERIMENTAL SET-UP

This section describes the basic components required to perform experiments in incremental sheet forming and to measure the force data during forming. Information regarding the manufacture of the fixture is also discussed briefly.

3.1. Introduction

The objective of building the experimental set up was to perform experiments and measure the forces generated during forming. Several components are required to effectively collect the data. A table mount dynamometer was used to measure the forces developed in the x, y and z directions. The dynamometer gives a voltage output which is commensurate with the magnitude of the forces generated. An amplifier was connected on the output side of the dynamometer to amplify the weak signals received from the dynamometer. The amplified signals which are in an analog format are converted into digital signals using an analog to digital converter. A data acquisition software which was installed in the computer would capture the forces generated during the experiments. The voltage values that are measured by the data acquisition software were exported to Microsoft Excel. The final magnitude of the forces is obtained by multiplying the voltages by the appropriate scaling factor.

A fixture which would hold the sheet blank during the forming operation was designed and manufactured. A metal frame was also manufactured to firmly clamp the sheet metal. The fixture was mounted on top of the dynamometer. Another component

necessary for performing incremental sheet forming is the forming tool. Forming tools were made using the manual lathe and then polished to obtain a high surface finish.

A commercially available software FeatureCAM was used for modeling the 3 dimensional models of the parts to be created. CNC codes of the part can be generated by the same software. These CNC codes are then fed into the CNC machine to do incremental forming.

3.2. Design and manufacture of the fixture

The main function of the fixture was to hold the work piece securely during forming. Since forming produces a large amount of localized stress, clamping the sheet metal firmly so as to prevent any sideways motion is of the utmost importance. A metal frame was also manufactured to be used as a clamp to prevent movement of the sheet metal blank. The sheet metal was placed in between the base of the fixture and the clamping plate. The arrangement was held firmly in place by using steel bolts.

The fixture was designed considering the dimensions of the dynamometer on which it was to be mounted. It was decided to build the fixture using five components. The first component was the base which was to be bolted onto the dynamometer. Since the base has to endure a lot of vibrations and forces, it was decided to make it 15.875 mm thick. The other four components are rectangular bars 50 mm thick which rise up vertically from the base plate. These four components provide a framework for holding the work piece on. The four components are bolted to each other using 9.525 mm diameter bolts. For designing and making 3D models of the components, commercial

software Solidworks 2009 x64 Edition SP4.1 was used. Figure 13 present the final design of the fixture.

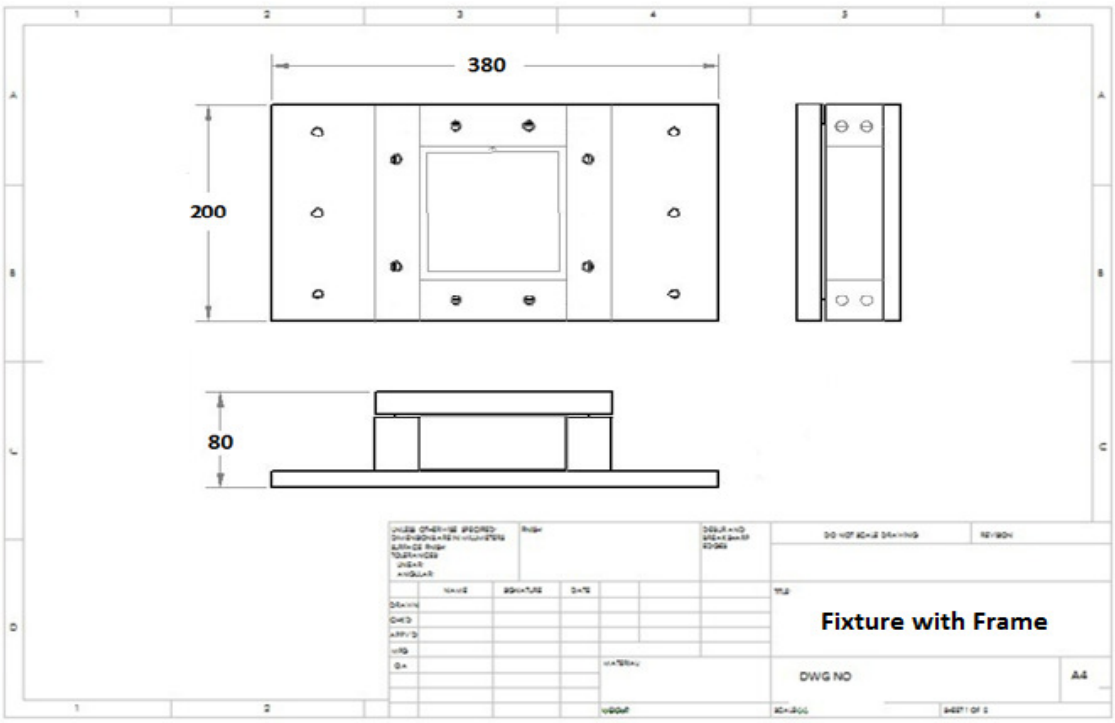

Fig. 13. Final fixture design.

3.2.1. Bolt design

Proper design of the bolts is of the utmost importance to ensure that the fixture does not fail. Also the forces generated during forming are transmitted from the sheet metal work piece to the dynamometer through the bolts, thus it is very important to ensure that the bolts don't fail by shear or by tension. To design the bolts, previous

experimental data was analyzed to get a fair idea about the magnitude of the forces which would be acting on the sheet metal. The maximum force was found to be of the order of 3000 N in the vertical direction and about 1700 N in the horizontal plane. It was noticed that the bolts which were used to join one bar with another were the most likely to fail by shear. Thus designing of the bolt against shear failure was considered to be the main criterion for failure. A steel socket scrap screw which was fully threaded and had a minimum tensile strength of 1241 MPa was selected. The Rockwell hardness value was C39 which ensured that the bolts would not fail for a maximum vertical load of 3000 N.

3.3. Manufacture of the components

The components were manufactured using aluminum alloy 6061-T651. The alloy was chosen due to its combination of high strength to withstand forces, its excellent machinability and its good resistance to corrosion. The sequences of operations done for machining the block from the stock size to the final dimensions are mentioned below:

1) Aluminum bar of length 90 mm and a width and height of 5 mm was ordered. The bar stock was cut into smaller bars keeping a tolerance of about 25 mm from the final required dimension by using a radial band saw.
2) The bar was machined down to the required dimension by face milling operation using the manual milling machine.
3) After the length and width was machined within a tolerance range of .0127 mm, holes having a diameter of 9.525 mm were drilled. Bridgeport CNC machine was used for drilling. The machine has accuracy within 0.00254 mm.

4) After the holes were drilled, chamfering tool was used to chamfer the edges of the part so that any burrs that could hinder the movement of the screw through the holes could be removed. Chamfering also improves the surface finish of the hole.
5) After chamfering, tapping operation was done to cut the threads inside the holes.
6) After the internal threads were created, the holes were cleaned to remove any debris. The rectangular bars were later assembled and mounted on the base piece which was in turn fixed to the dynamometer.

3.4. Design and manufacture of the tool

The main purpose of the forming tool was to produce a region of highly localized stresses on the sheet metal and thus produce the formed shapes by localized plastic deformation. The tool was mounted to the spindle of the CNC machine by using collets. It was decided to use a tool having circular cross-section and a hemispherical tip for the project. To study the effect of the tool diameter on the forming force, tools having radii of 6.35 mm and 9.525 mm were manufactured. The tools had a length of 50.8 mm and were made from 41L40 easy to machine high strength low alloy steel. The tools were manufactured using a manual lathe and later machining was done by CNC machine. To smoothen the surface to get a good surface finish, the tool tip was polished in stages by first using grit 320 paper and then moving onto grit 240 sand paper. After that the tool was further polished by using 0.05 micron size alumina powder, keeping the tool on the spindle of the CNC machine and rotating it at a low speed of 60 rpm. The final polishing

was done till the eccentricity of the tool was limited to just 1 in thousands per 25 mm. The tools used are shown in Figures 14 and 15.

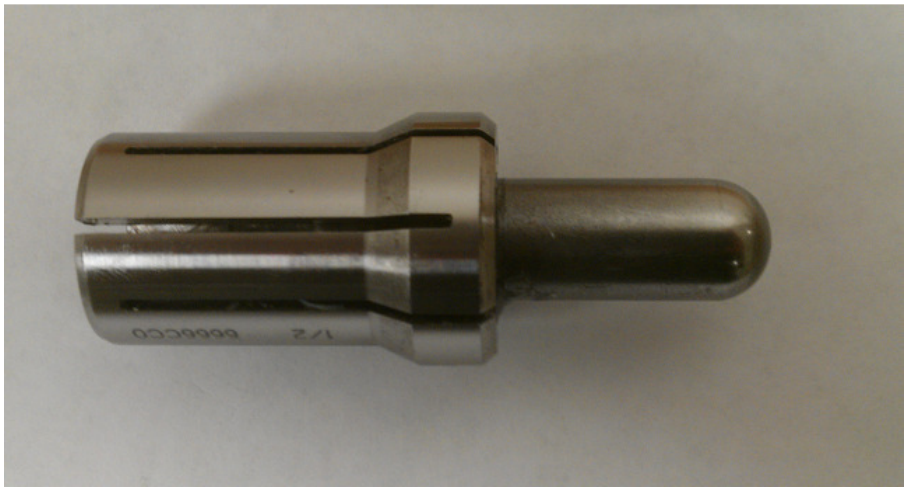

Fig. 14. Tool having radius of 6.35 mm.

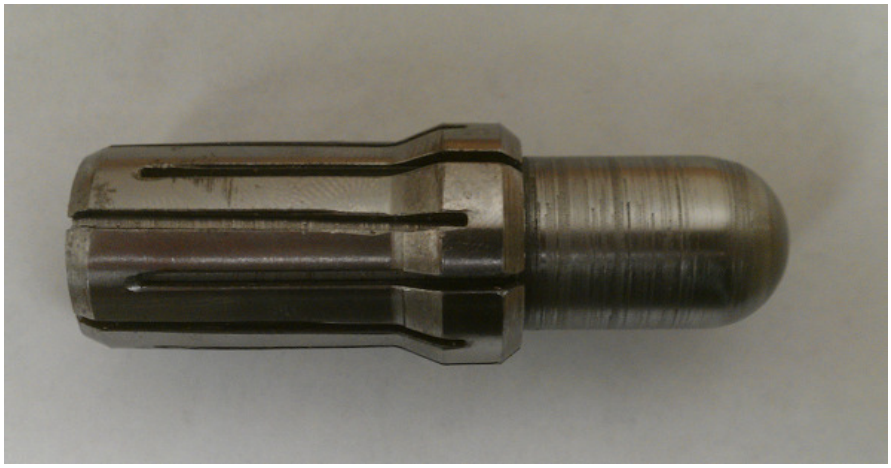

Fig. 15. Tool having radius of 9.525 mm.

3.5. Components of the data acquisition system.

The dynamometer is a device which measures force in the three principal directions. The dynamometer was installed on the table of the CNC machine. The fixture which holds the sheet metal is fitted on top of the table mounted dynamometer. Thick wire cables transfer electric signals from the dynamometer to the amplifier. The values of these signals are directly proportional to the force acting on the tool during the forming operation. The dynamometer was connected to a complimentary amplifier which magnifies the voltage values it receives from the dynamometer. The amplified signals were then fed into an analog to digital converter. The digital signals which come from the output side of the converter were then captured by the LabVIEW data acquisition software which is installed in the computer. A brief description of each of the components is mentioned below.

3.5.1. Dynamometer

The force measurement begins with the dynamometer. From literature, it was learnt that a table mount dynamometer was more reliable to measure forming forces than a force measuring system installed near the tool. The dynamometer used in the experiment was a MC 818 series dynamometer, manufactured by Advanced Mechanical Technology Inc (AMTI). It has four channels to measure the forces in the x, y and z directions and also the moment along the x axis. The dynamometer produces analog signals whose magnitude is directly proportional to the force produced. The force measurements are done using strain gages present inside the dynamometer.

After amplification, the analog signals were inputted to an analog to digital converter NI USB 6009. The manufacturer of the analog to digital converter is National Instruments. The analog to digital converter primarily converts the analog signals from the amplifier to digital signals and feeds it to the data acquisition software NIDAQ895-1 provided with the converter. The output readings from the data acquisition software were captured in an Excel spreadsheet.

3.5.2. Amplifier

The amplifier was used to amplify the weak signals which are fed as input from the dynamometer. The dynamometer sensitivities are in the order of microvolts/volt-unit-load. Thus, amplification is necessary to provide high level output signals.

The Missile command amplifiers (MCA) were developed to be used with AMTI's dynamometer. The gain of the amplifier could be adjusted using switches provided on the panel. The voltage gain used for the experiments was 4000. The maximum output of the amplifier is +/- 10 volts. The amplifier requires a 115 Volts AC, 50-60 Hz power supply as input power.

The amplifier had 9 different wires coming out from it. Four wires were for the three mutually orthogonal force direction and for the moment along the x axis while the other five are connected to the ground. Before making the connections, to ensure the safety of the equipment and the user, it was necessary to connect one of the ground wires to the body of the amplifier.

To minimize error in the voltage output, it was essential to balance the amplifier channels before starting the experiments. Each amplifier channel had a pair of LED

lights. When the LED's are lit, it indicates that the output reading would have a positive or negative error of more than 0.05 volts depending on which light is lit. To ensure that the initial output was zero, the potentiometer next to the lights had to be balanced till both lights go out. Balancing was performed after allowing for a 30 minute warm up time after switching on the amplifier.

3.5.3. Analog to digital converter

The analog to digital converter was used to convert the analog signals coming from the amplifier into digital signals which were captured by the data acquisition software. The converter used for the experiments was made by National Instruments and the model used is USB-6009. The maximum operating voltage range was +/- 10 volts.

A differential method of connection was employed to make the connection between the wires coming from the output side of the amplifier to the analog side of the analog to digital converter. In this type of connection, the value that enters into the converter is the value of the difference between the positive and negative terminals into which the wires coming from the amplifier are fed. The wire which measured force in the x direction was plugged into the port numbered 2 in the analog end of the converter. This was the positive terminal of the differential type of connection. A ground wire was then connected to the port numbered 3 which was the negative terminal, to complete the connection. In the similar way, the wires which measure force in the y direction and z directions were connected to ports 5 and 8 respectively while the corresponding ground wires were connected to adjacent ports 6 and 9 respectively.

Figure 16 illustrates the amplifier and analog to digital converter used for measuring the forces. The magnified signals which come from the amplifier are inputted into the analog to digital converter. From the converter, the output USB wire was connected to the Data Acquisition Software.

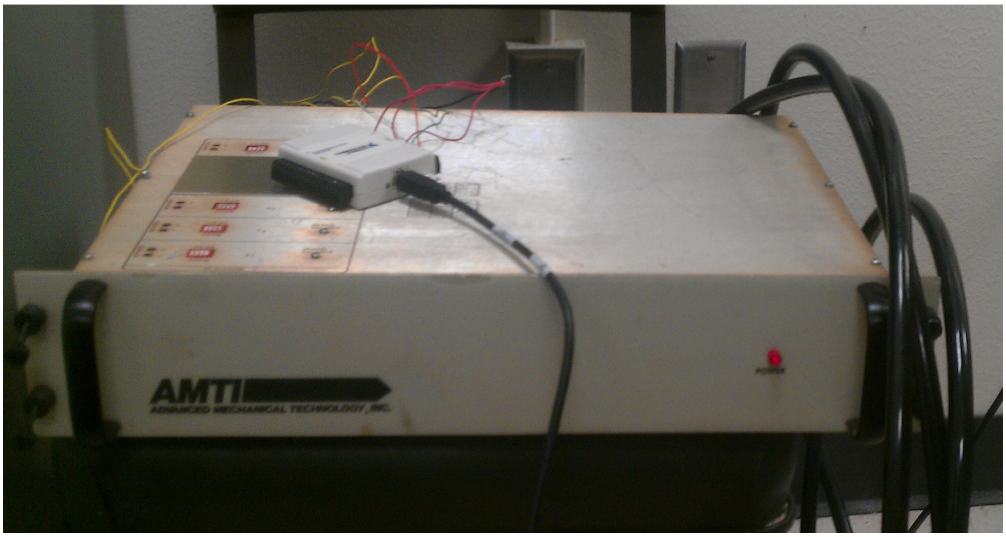

Fig. 16. Amplifier and analog to digital converter.

3.5.4. Data acquisition software

The data acquisition software used was LabVIEW Signal Express LE. The sampling rate used for the experiments was 5 Hz which meant that 300 data points were collected every minute. Digital signals measured by the software are exported directly to an Excel spreadsheet. The signals were multiplied by the appropriate scaling factor to obtain the forces.

4. INCREMENTAL SHEET FORMING EXPERIMENTS

The results of all the experiments conducted are presented in this section along with the input parameters that were used during forming of the parts.

4.1. Introduction

Experiments were conducted to measure the forces generated during forming. The effect of the input parameters on the forming force was studied. The forming forces were measured using the LabVIEW data acquisition software. A continuous sampling mode was selected for the data acquisition and the samples were collected at a rate of 5 Hz. The rate was chosen to limit the number of data points obtained to a range of 8000 to 12,000 points.

The total space available for manufacture was 125 x 125 mm square and it was decided to design the pyramid and cone to have a maximum initial length of 101.6 mm. The dimensions were chosen to ensure that the forming would take place at a fair distance from the boundary. The pyramid and cone shapes were to have a maximum depth of 25 mm. This was to ensure that the tool made several passes to fully stiffen the sheet. Once the sheet was fully stiff, the forces obtained would be the steady state forces. In all the experiments, separate force measurements were taken after the tool reached a depth of 19 mm. This depth was chosen from experience of the knowledge of steady state forces. Finally before running the experiments, an even coating of Vaseline was applied onto the surface of the sheet metal. This was to ensure that the surface remained

smooth so that wear damage to the tool due to the contact friction could be minimized. Lubrication also improves the surface finish of the finished part.

4.2. Test for repeatability

Three force measurements were performed with the same forming conditions to check the repeatability of the results. A pyramid having a wall angle of 30 degrees was chosen as the base model. The sheet used had a thickness of 0.8 mm and the forming tool had a radius of 6.35 mm. The step size used in the experiments was 1.27 mm. The results presented in Figures 17, 18 and 19 were the forces obtained in x, y and z directions respectively.

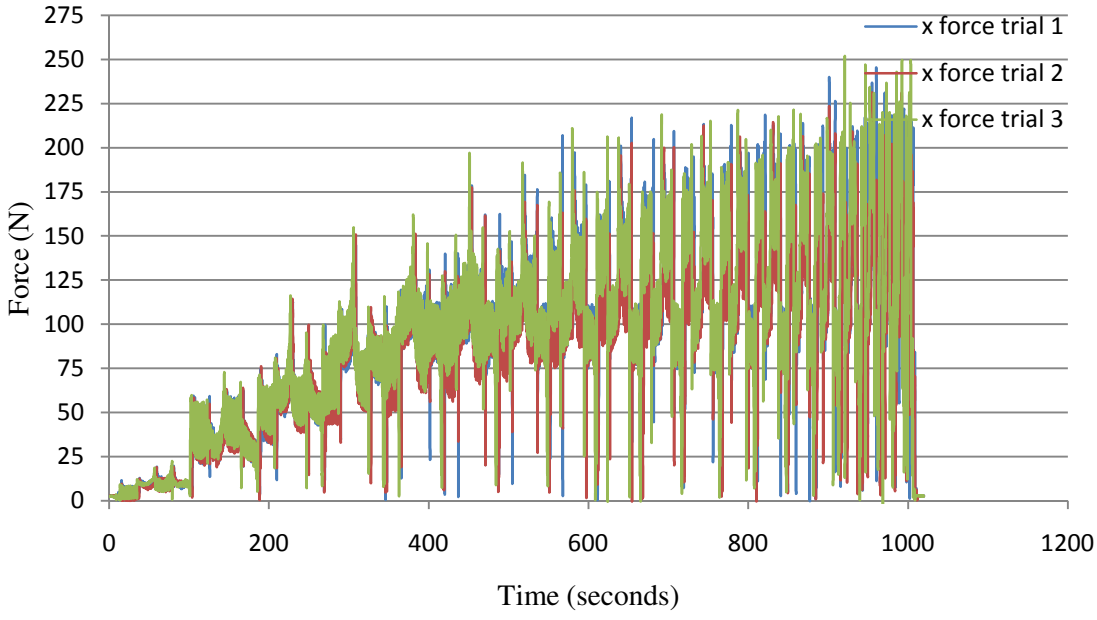

Fig. 17. Repeatability test - force in x direction.

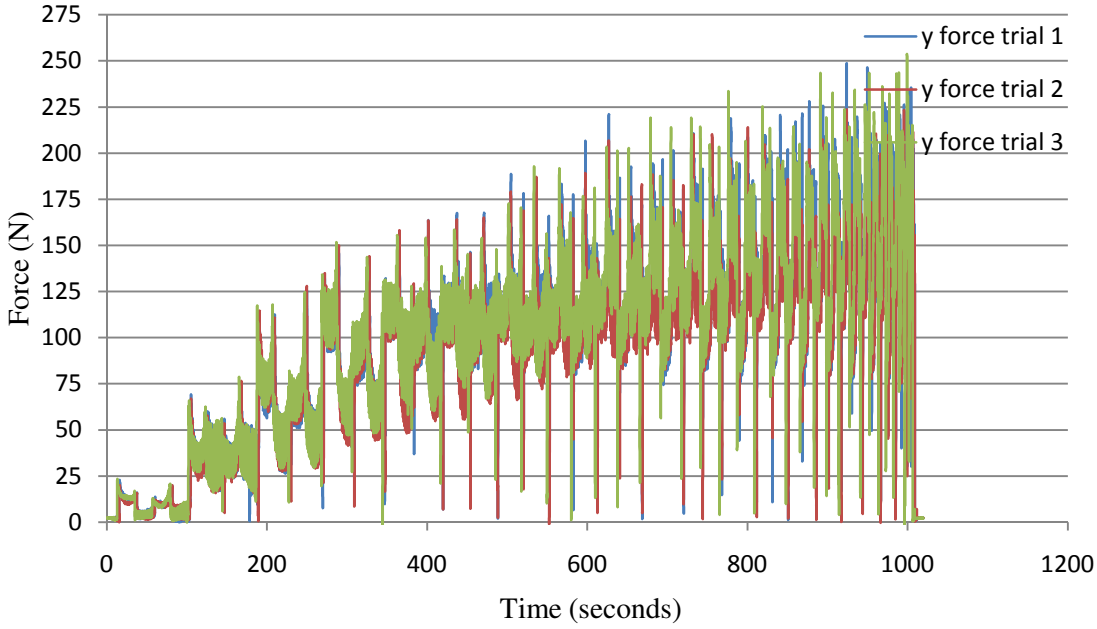

Fig. 18. Repeatability test - force in y direction.

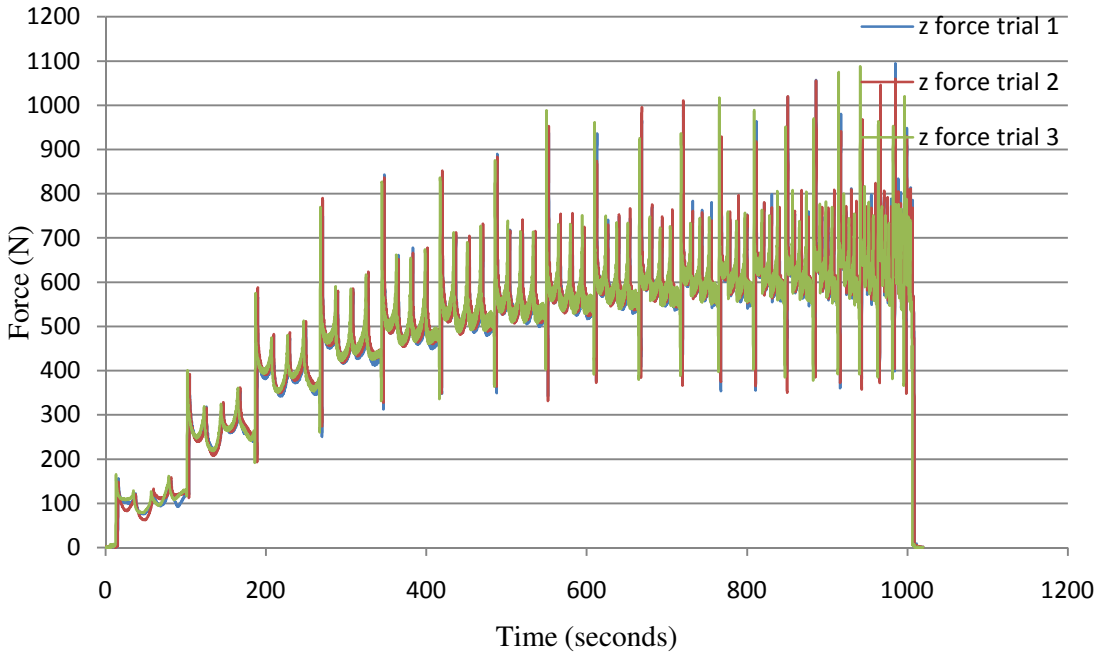

Fig. 19. Repeatability test - force in z direction.

The above figures showed that the results that were obtained from the data acquisition software were repeatable. The next section presents the results of the experiments performed.

4.3. Force measurements for pyramid shape

Two complete cycles of steady state forces developed during the forming of a pyramid having a wall angle of 45 degrees are shown in Figure 20. The tool used had a radius of 6.35 mm and a depth of 0.635 mm was given for each pass. The sheet had a thickness of 0.8 mm.

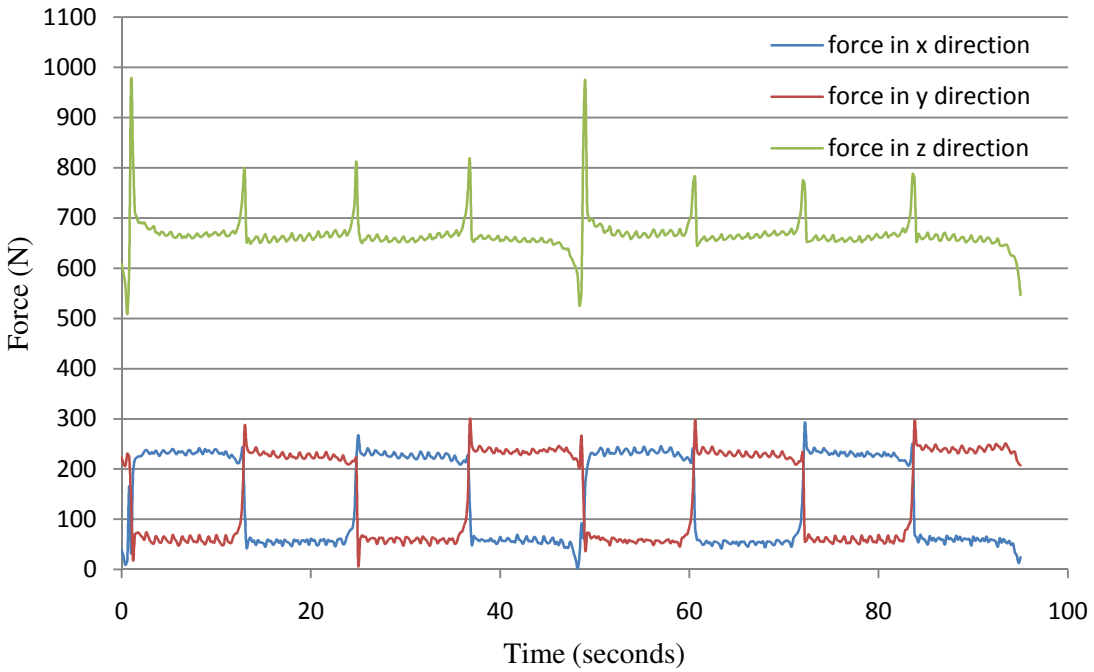

Fig. 20. Two cycles of the steady state force.

It was clear that the forces are fairly constant with every pass. It is worth noting a few observations with reference to Figure 20. Firstly it was seen that the x value of the force increased and reached a maximum value while the y force remained constant. After that, the x value reduced to reach a constant value while the y force increased to reach a maximum value during this time. This trend was seen to be repeated. The reason for this behavior of the graph was due to the motion of the tool in the respective direction. Initially while the x force was increasing, the tool was making a pass in the x direction along the walls of the pyramid while in the next phase, the tool changed direction by 90 degrees and started moving along the y direction thus increasing the y component of the force. The maxima of the forces were observed at the corners just after the tool had made a 90 degree bend and started to move in the new direction. This showed that the forces generated depend on the direction of motion of the tool.

It was seen that the value of the force between the peak forces, i.e. when the tool was moving along the side of the pyramid, are fairly constant and this was due to the nearly constant contact area between the tool and the sheet metal. It was inferred from the steady state force in the z direction that the vertical force did not depend on the direction in which the tool was moving. A sudden decrease was noticed in the forming force just before the pass was completed. This decrease was due to the fact that at that point, the sheet was already deformed and the force acting on the tool was solely due to the springback of the material. The vector sum of the forces for the above pyramid is shown in Figure 21.

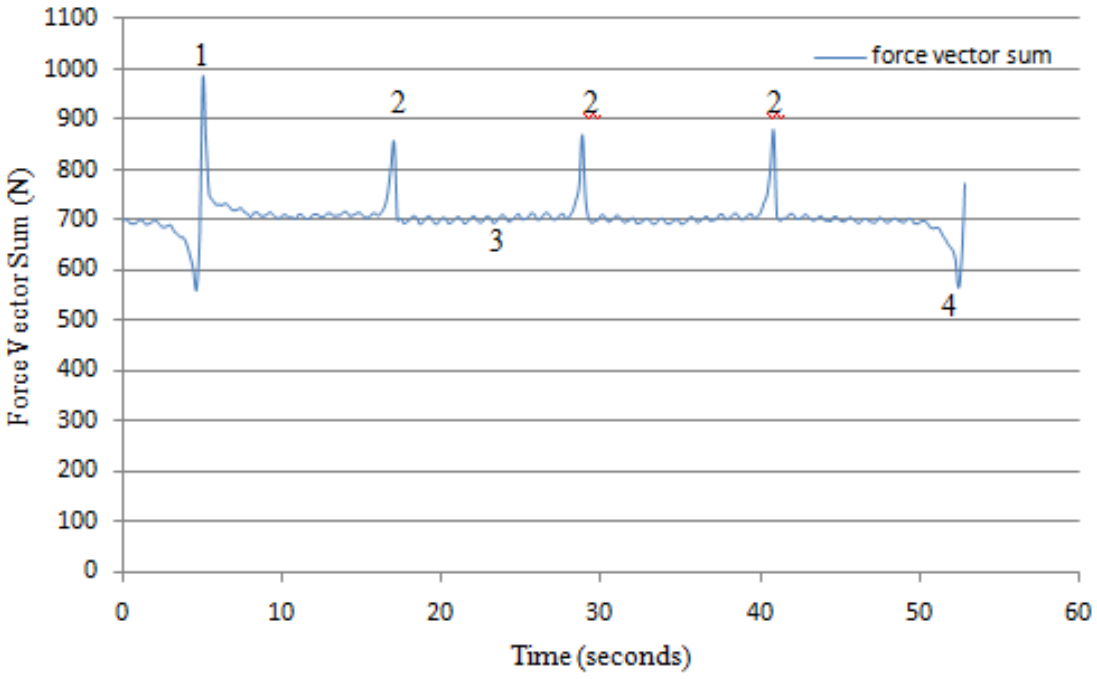

Fig. 21. Types of forces observed for the pyramid.

The force numbered 1 is the force acting on the tool when it reached a corner and made a step down. This signified the start of a new pass. The forces labeled as 2 were the forces measured when the tool was at the other three corners of the pyramid. This force was lesser than force 1 due to the fact that there was no step down at these points. The forces were higher than force 3 due to the increase in contact area between the tool and the sheet metal at these corners. Force 3 was the force acting on the tool when it was deforming the portion of the sheet metal blank between the corners. It can also be called as the deformation force. This force was constant due to the fact that the area between the tool and the sheet metal was a constant at these points. The last force under

consideration is the force value registered just before the end of a pass. This force was expected to be small because the metal was already deformed by the tool at the start of the pass and this force was the force acting on the tool due to the springback of the sheet.

4.4. Force measurements for cone shape

The forces developed in the three orthogonal directions during the forming of a cone having a wall angle of 45 degrees are shown in Figures 22 and 23. The tool having a radius of 6.35 mm was used and a depth of 1.27 mm was used for each pass. The sheet had a thickness of 0.8 mm.

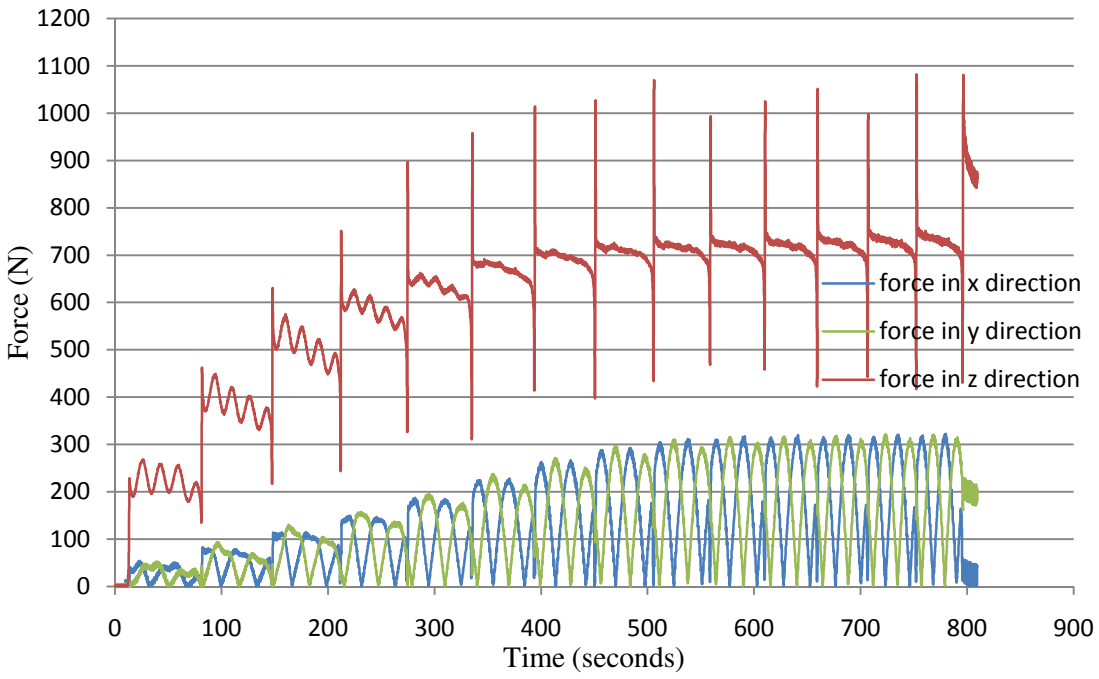

Fig. 22. Force profile obtained for a cone before the steady state has been achieved.

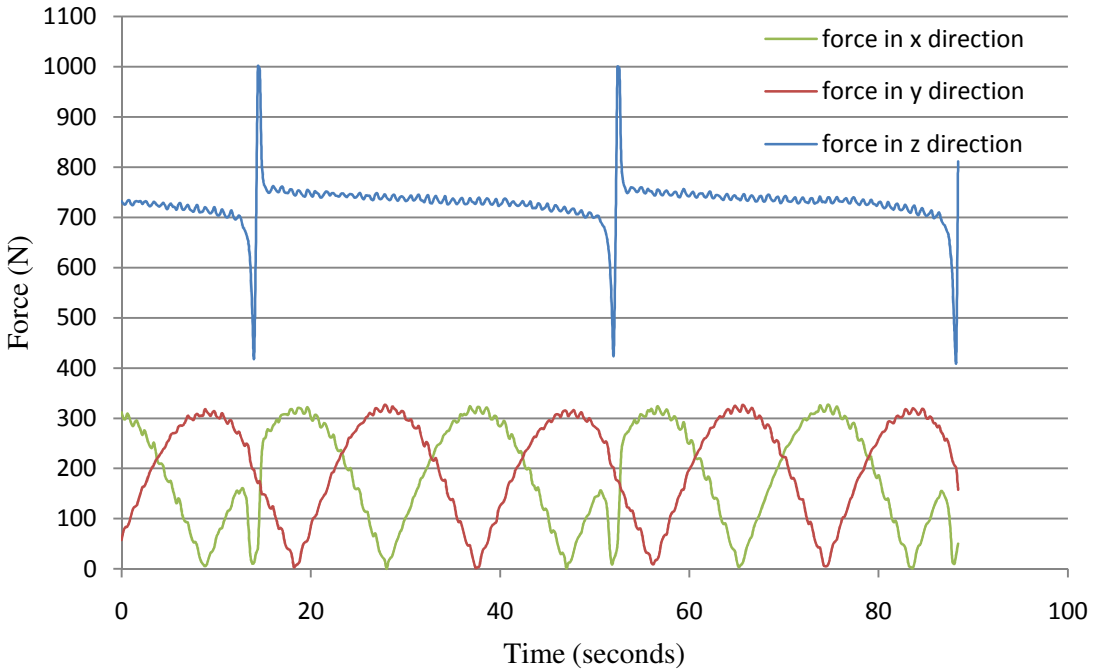

Fig. 23. Steady state force profile obtained for cone.

From the forces shown in Figure 23 it was seen that the x and y forces had a symmetrical arrangement. The z force had only one peak compared to four in the case of a pyramid, this peak arises when the tool made a vertical step downwards. The other smaller peaks were absent due to the fact that there were not any corners present in a cone and so there will be steady deformation force throughout till the tool took a step downwards increasing the force instantaneously.

The steady state vector sum of the forces obtained in a cone is shown in Figure 24. The figure shows the plot of the force vector sum against time obtained during forming of a cone having wall angle of 45 degrees. Radius of the tool was 6.35 mm and the step size was 1.27 mm. The sheet thickness was 0.8 mm.

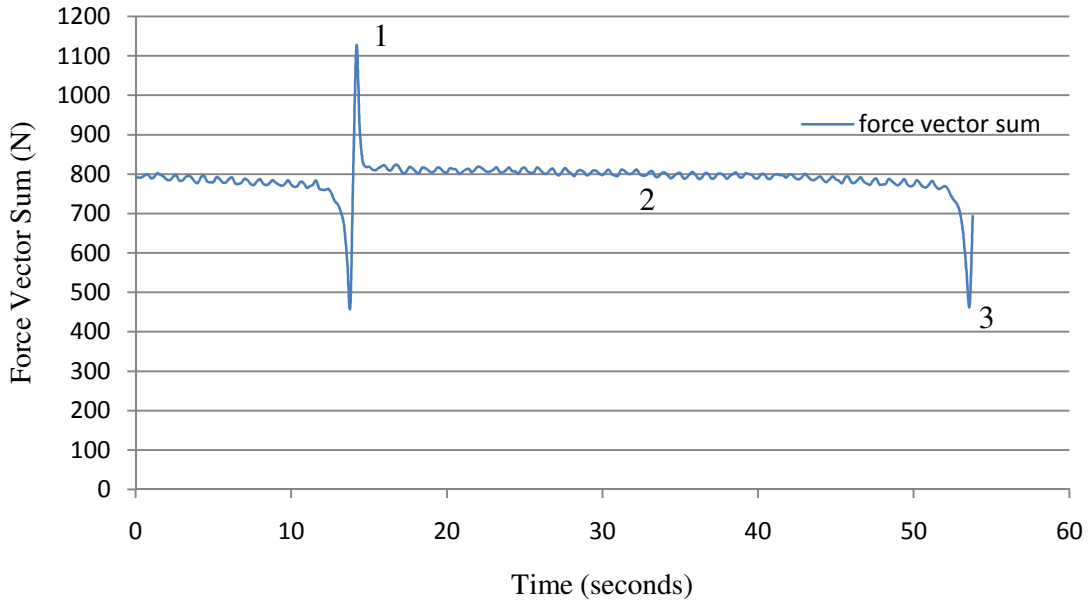

Fig. 24. Types of forces observed for the cone.

The force numbered 1 was the force on the tool when it made a step down. This signified the start of a new pass. The force labeled as 2 was the force measured when the tool was deforming the sheet metal at any other point after the step down. Since the cone had no corners, there were no secondary peaks observed. Force 3 was the force measured just before the end of a pass. This was the force acting on the tool due to the springback of the sheet.

4.5. Parametric study

Once the experiments were conducted, the next aim was to find out the effect that the parameters had on the forming forces generated during ISF. The data obtained

experimentally would be analyzed to find out the influence of each of the parameters individually. The parametric study is presented below. For the sake of clarity, only the steady state force obtained during two passes of the tool are shown in all the figures presented in this section.

4.5.1. Effect of sheet thickness

To determine the effect that the thickness of the sheet had on the forces, sheets having thickness of 0.8 mm and 1.27 mm were used. A pyramid having a wall angle of 30 degrees was used and the tool used had a radius of 6.35 mm and the step size was 0.635 mm.

Figures 25, 26 and 27 present the experimental data obtained in the x, y and z directions respectively.

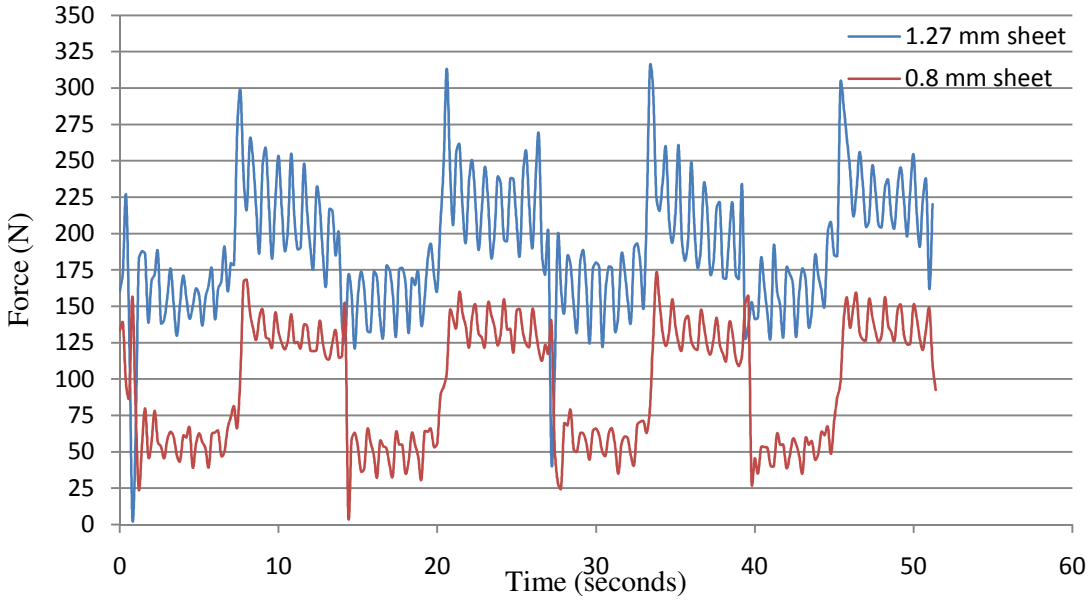

Fig. 25. Comparison of steady state force measured in x direction for 1.27 mm and 0.8 mm sheet.

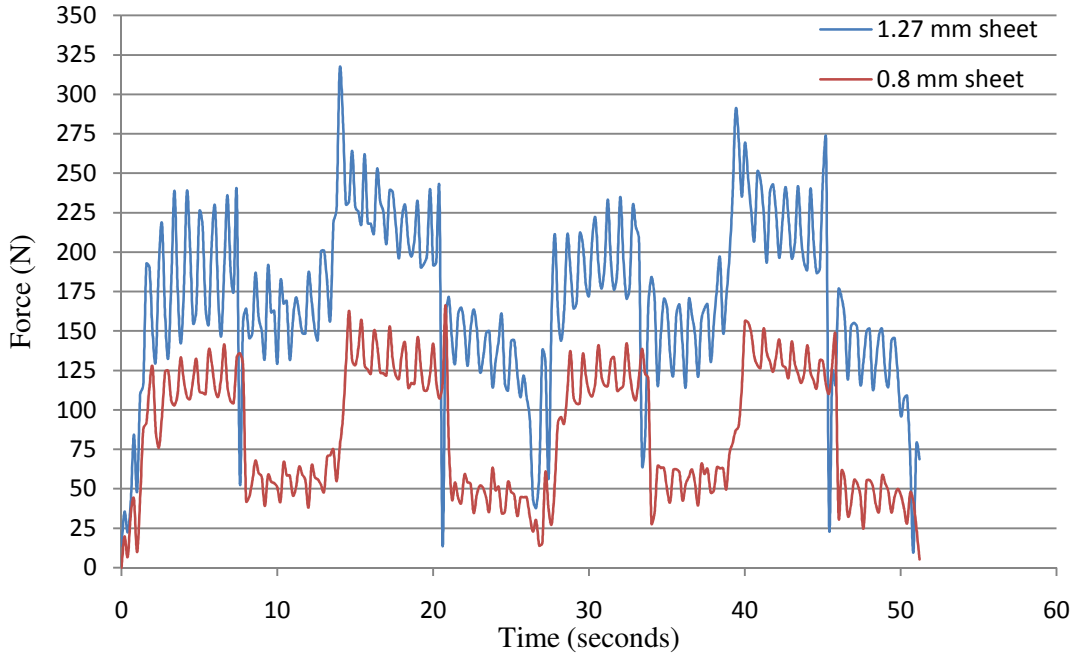

Fig. 26. Comparison of steady state force measured in y direction for 1.27 mm and 0.8 mm sheet

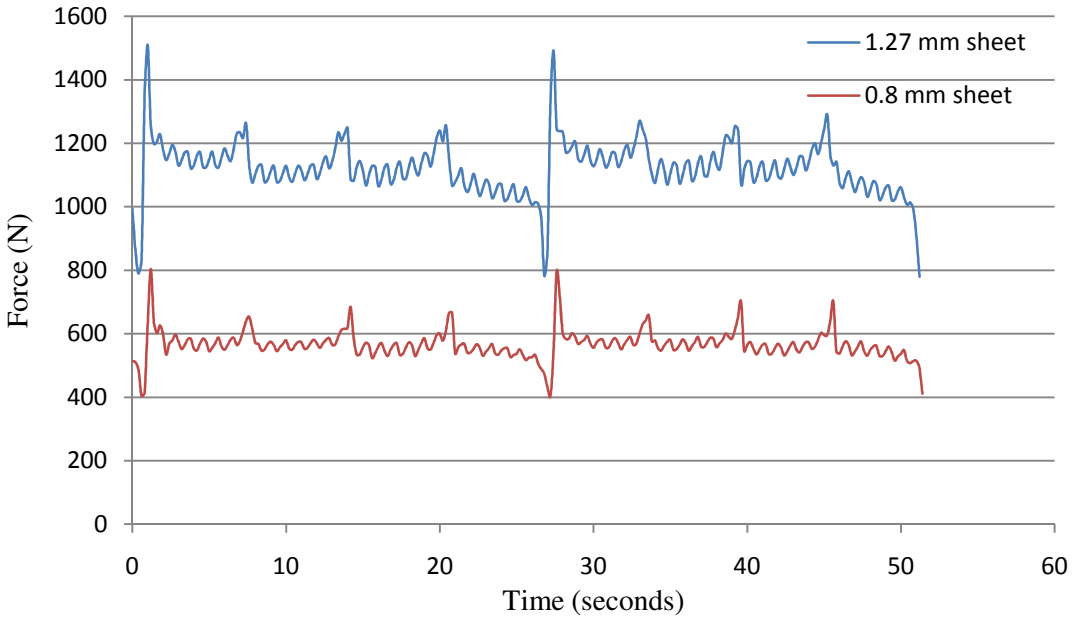

Fig. 27. Comparison of steady state force measured in z direction for 1.27 mm and 0.8 mm sheet.

It was observed that the forces required for forming were significantly more in the case of the sheet having thickness of 1.27 mm compared to the thinner sheet. This was because of the larger amount of material that the tool had to deform thus leading to an increase in the forming force.

The difference in the initial peak force, (numbered 1) was seen to be about 600 N in the z direction while it was around 100 N in the x and y directions. The same amount of difference was noticed for the secondary force peaks and the force when the tool was between the corners of the pyramid. The difference in the force due to the springback, (numbered 4) was seen to be about 400 N in the z direction while it was around 50 N in the x and y directions. Thus it could be seen that the forces numbered 1, 2 and 3 had the same difference in force values when sheet with different thickness were used. The force labeled as 4 had a different relation compared to the other three forces, this could be due to the fact that the amount of springback that the sheets had do not follow the same relationship that the other three forces had with respect to thickness of the sheet.

Although a thinner sheet takes less force to deform, the material would crack easier than a thick sheet due to thinning during forming. Thus the formability of a thin sheet is quite low and a certain amount of thickness is desired for successful forming.

4.5.2. Effect of step size

The magnitude of the step down that the tool made after each pass is an important parameter which had an effect on the measured forces. To study the effect of the step size, a pyramid having a wall angle of 45 degrees was formed. The tool used had a radius of 6.35 mm and the sheet thickness was 0.8 mm. The step sizes that were used

in the experiment were 0.635 mm and 1.27 mm. The results presented in Figures 28, 29 and 30 are the forces obtained in x, y and z directions respectively.

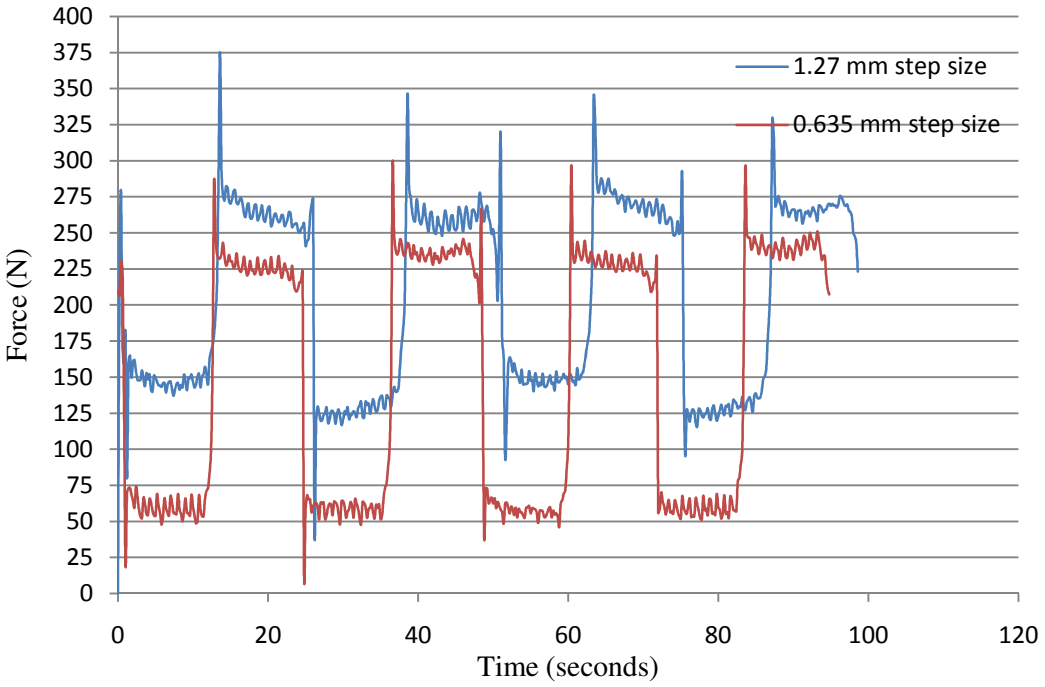

Fig. 28. Comparison of steady state force measured in x direction for 1.27 and 0.635 mm step size.

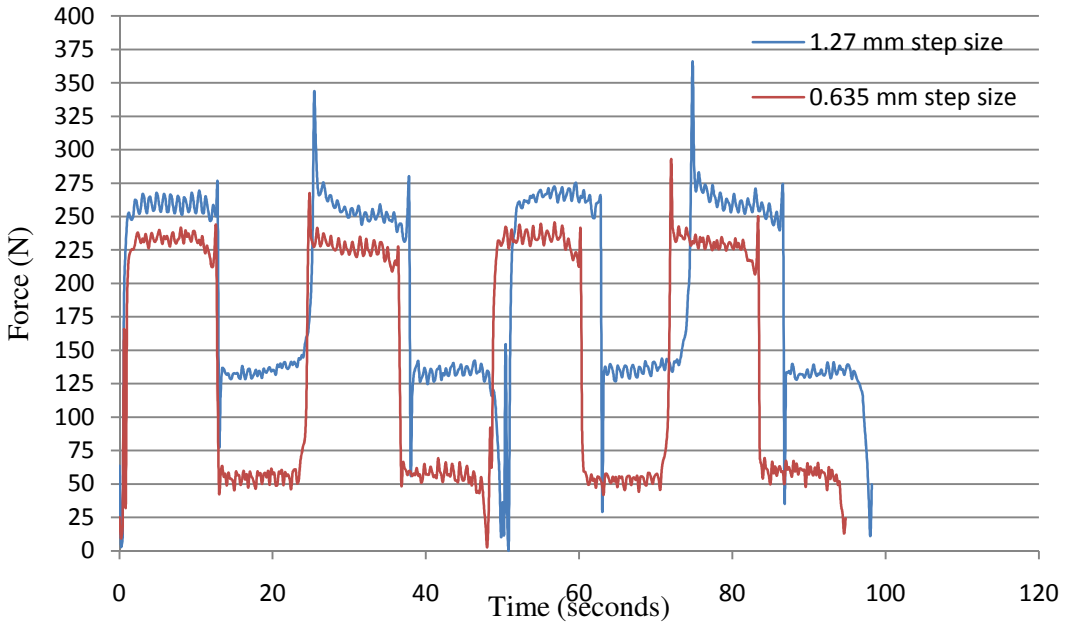

Fig. 29. Comparison of steady state force measured in y direction for 1.27 and 0.635 mm step size.

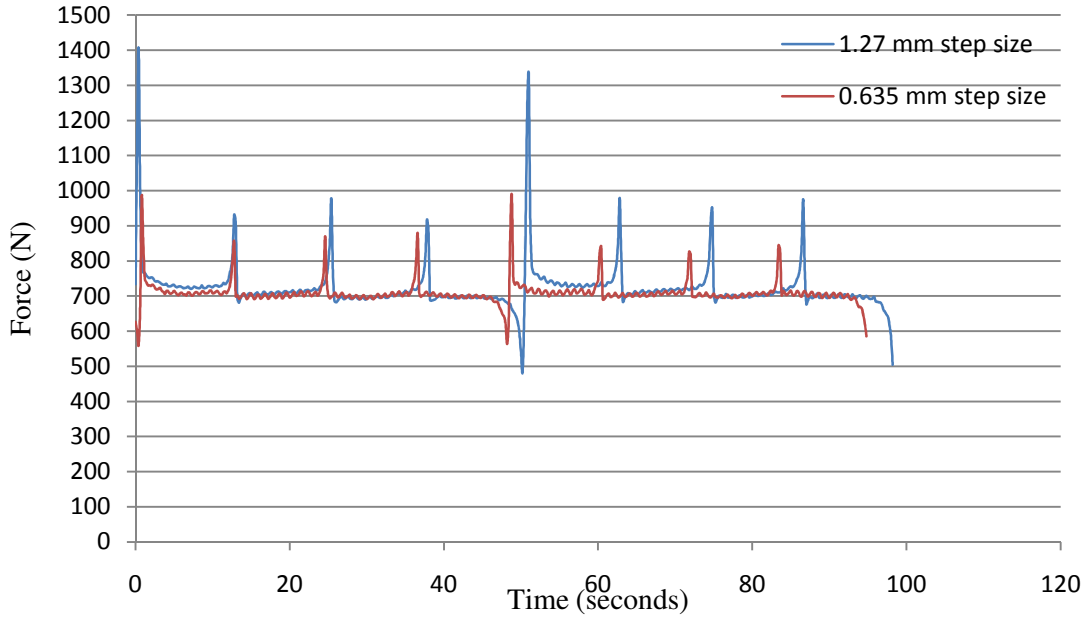

Fig. 30. Comparison of steady state force measured in z direction for 1.27 and 0.635 mm step size.

From the above figures, it was seen that the steady state force increased for the larger step size compared to the steady state observed for a step size of 0.635 mm.

From the graphs it was seen that the difference in the force 1 was about 400 N in the z direction and about 50 N in the x and y directions. The reason for the increase in the force was the increased stretching of the metal blank when a higher step size was used. Due to the increased stretching, the deformation conditions were more severe as explained by Jeswiet et al. (2005b) which lead to an increase in the overall force. It was seen that the force needed for deforming the sheet metal after the step down, numbered as 3, was almost the same in the x, y and z directions. The difference in the force just before the tool completed the pass was seen to be only around 100 N which is a minor increase.

On comparison with the force graphs obtained from the previous condition, it was noticed that the step size does not have a profound influence on the forces generated as sheet thickness does. The advantage of using larger step size to form the part was the reduction of time taken to form the part. However a larger step size was seen to leave impressions at the place where the tool made a step down which reduced the overall appearance of the final part. Hence smaller step sizes were generally preferred while creating shapes during incremental sheet forming due to the better appearance of the final part.

4.5.3. Effect of wall angle

Wall angle plays an important role in the generation of forming forces with a higher force being expected for a higher wall angle. The wall angle is the most important

criterion which determines formability of the material with the formability drastically reducing when the wall angles reaches high values. The wall angles chosen were of a medium range which was neither too small nor too large to cause failure.

For the experiments conducted to determine the effect of wall angle, pyramids having wall angle of 30 degrees and 45 degrees were used. The other parameters were kept the same, the tool used had a radius of 6.35 mm and a step size of 0.635 mm was used. The thickness of the sheet used in both cases was 0.8 mm. Figures 31, 32 and 33 present the forces obtained in x, y and z directions respectively.

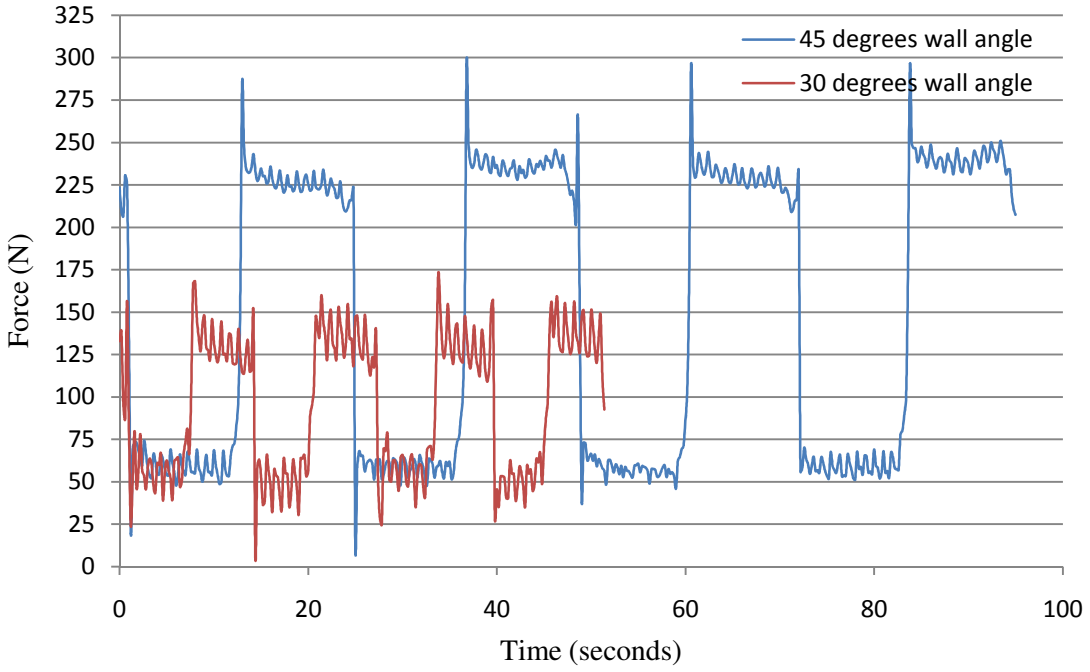

Fig. 31. Comparison of steady state force in x direction for 30 and 45 degrees wall angle

.

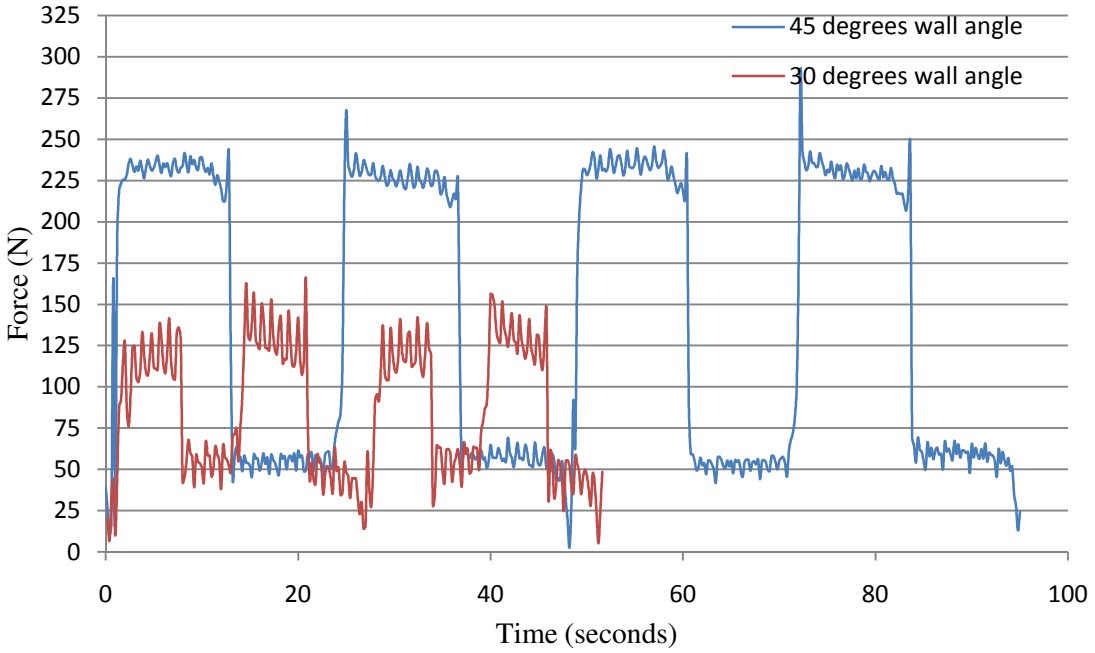

Fig. 32. Comparison of steady state force in y direction for 30 and 45 degrees wall angle.

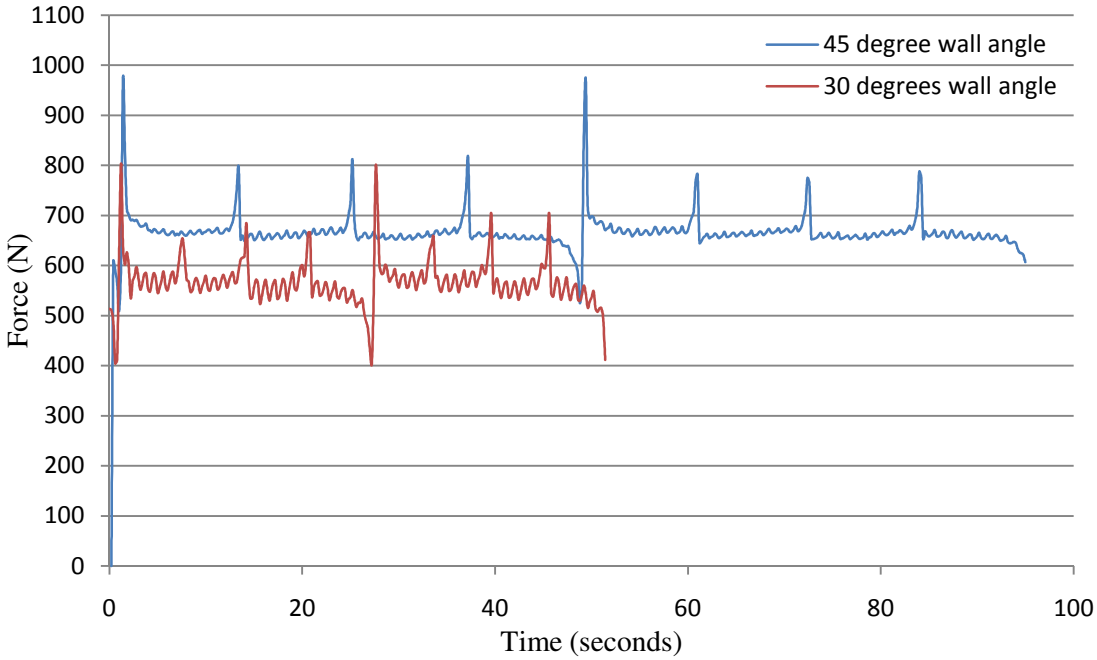

Fig. 33. Comparison of steady state force in z direction for 30 and 45 degrees wall angle.

From the above figures it was quite evident that an increase in the wall angle directly resulted in an increase in the force generated during forming. There is a moderate increase of about 100 N in the x, y and z directions for the deformation force. The difference between the initial peak values were seen to be around 200 N in the z direction.

The reason for the increase in the force was due to the fact that for higher wall angles, the material had a longer bending phase and thus it was stressed more with every pass as compared to the part with 30 degrees wall angle. The increase in the number of data points for the part with 45 degrees wall angle was due to the fact that the tool had more distance to traverse in the case of the part with the steeper wall angle.

The above results showed that the wall angle was a major parameter in the determination of forces. Filice et al. (2006) mentioned that the tangential component was the main criterion for sheet metal failure and that the wall angle was the single most important factor which controls forming force. It was also noticed that the wall angle had a lesser influence on the forming forces when compared to the effect that the blank thickness had on the forces.

4.5.4. Effect of tool diameter

The diameter of the tool was another major input parameter that determined the magnitude of the forming forces generated. To determine the effect that the tool diameter had on the forces, tools having radii 6.35 and 9.525 mm were used. A pyramid having a wall angle of 45 degrees was formed on a sheet having a thickness of 0.8 mm

with a step size of 1.27 mm. The force comparison results are presented below. Figures 34, 35 and 36 present the forces obtained in x, y and z directions respectively.

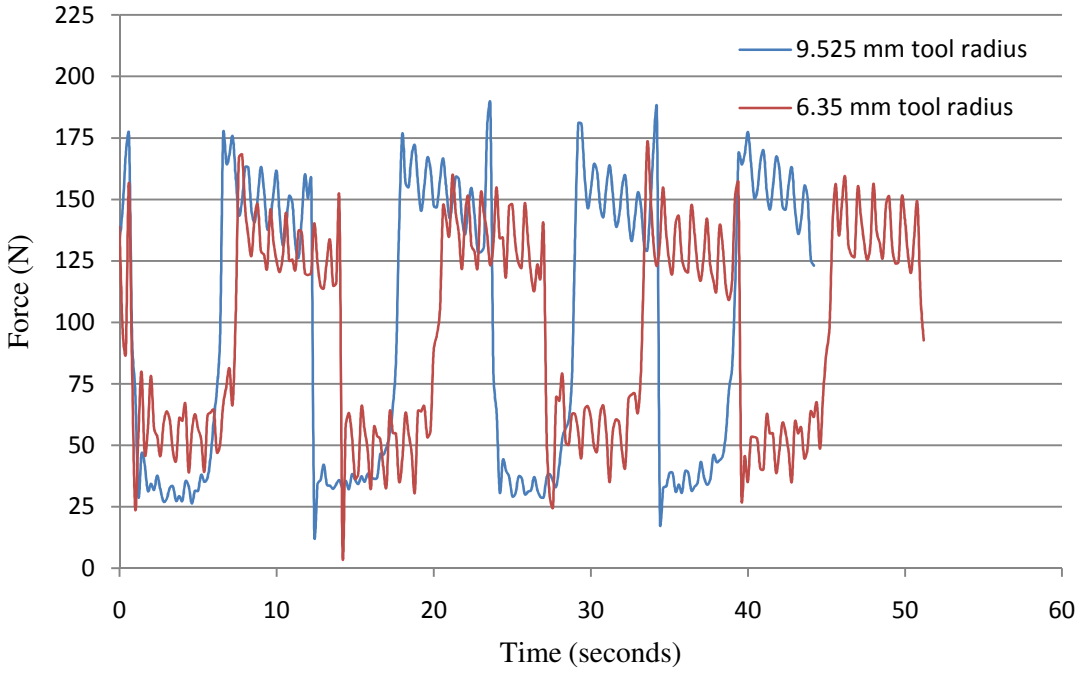

Fig. 34. Comparison of steady state force in x direction for 6.35 and 9.525 mm radii tools.

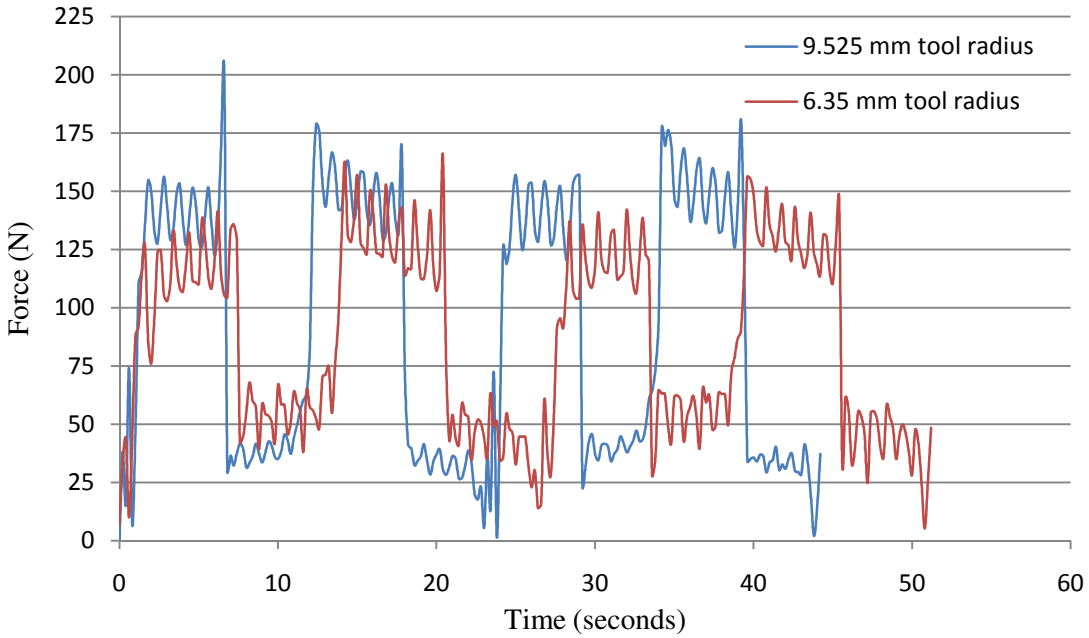

Fig. 35. Comparison of steady state force in y direction for 6.35 and 9.525 mm radii tools.

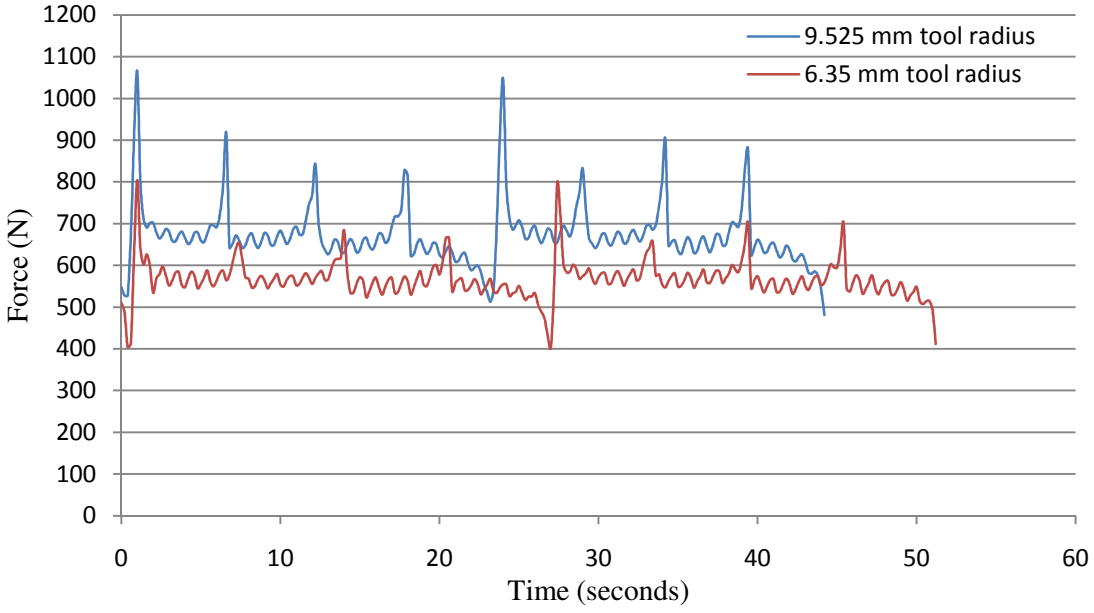

Fig. 36. Comparison of steady state force in z direction for 6.35 and 9.525 mm radii tools.

From the above figures it was seen that there was an increase in the steady state forces obtained when a tool having a larger diameter was used. The force difference obtained was found to be around 200 N for all the peak forces. This was due to the fact that the change in area was the same in both cases. The difference in force labeled 3 was approximately 100 N in the z direction and was almost the same in the x and y directions.

The reason for the increased force when a larger tool is used is due to the increase in deformation area between the tool surface and the sheet metal blank on each pass. A larger tool had a larger deformation area and thus it deformed more material with each pass which lead to a higher force as compared to a smaller tool.

It was also noticed that a larger tool gave a better surface finish to the parts as compared to the tool with 6.35 mm radius. Apart from the larger forces that arise when a larger tool was used, the maximum formability that the tool achieved was sufficiently lower than that achieved when a smaller tool was used. This was because a smaller tool concentrated the stresses effectively on a smaller area which increased the formability of the part, while in the case of the tool with a larger diameter, the contact pressure was spread across a large area which reduced the stress imparted to the metal.

4.5.5. Influence of the tool path on the forming force

Experiments were also conducted to check the influence of the tool path on the forming forces. For this extent, pyramid and cone shapes were designed and manufactured with the same set of input parameters. In the case of the pyramid, the tool followed a rectilinear path and the tool changed its direction to a mutually perpendicular

one when it reached the corners. The tool encountered four corners during forming of a pyramid which accounted for the small peaks that was visible in the force diagram, the higher spike was the effect of a step down when the tool was at a corner. In the case of the cone, the tool followed a circular profile and it did not encounter any edges. The only spike in the graph was when the tool made a vertical step downwards.

Figure 37 presents the steady state force data in the z direction obtained during forming of a cone and pyramid having wall angle of 45 degrees and a step size of 1.27 mm. The tool used had a radius of 6.35 mm and the thickness of the sheet was 0.8 mm. The pyramid and cone had similar outer dimensions of 101.6 mm and both were formed to a depth of 25 mm.

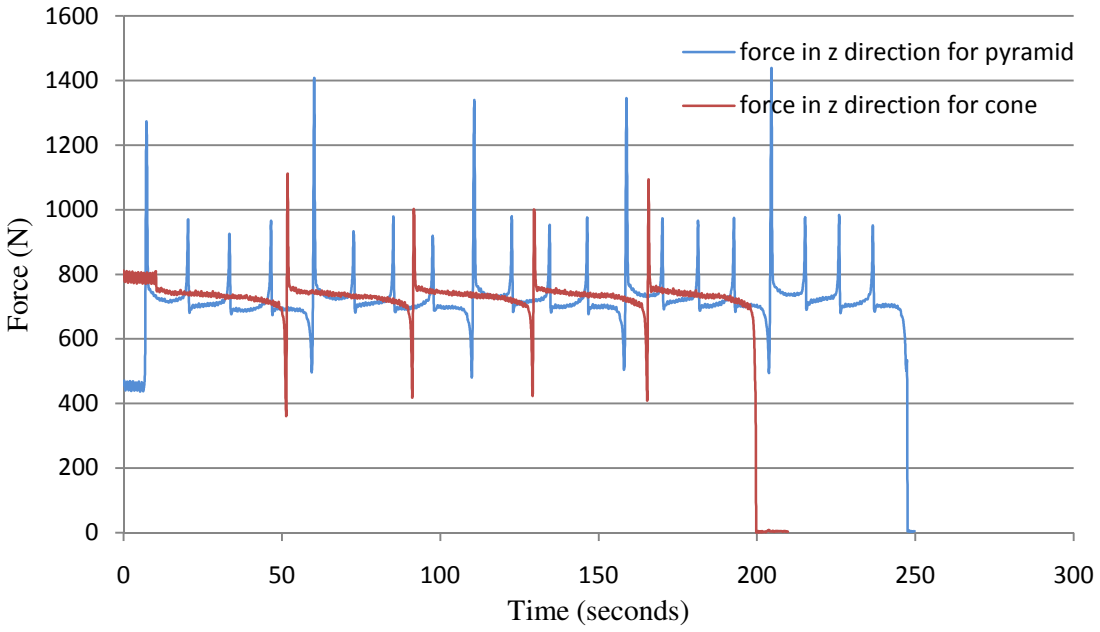

Fig. 37. Comparison of steady state force measured in z direction for pyramid and cone shapes.

It was seen from the figure that the deforming force was the same for both pyramid and cone. The force peak differed for the pyramid and the cone, this was due to the fact that the contact area changed when the tool reached the corner of the pyramid. The force peak was seen to be more for the pyramid due to the extra reinforcement the three edges provided.

The vector sum of the x and y forces were calculated and plotted in Figure 38. On comparing, it was seen that the magnitude of the flat portions was slightly higher for the case of the cone. This could be due to minor radial effects occurring in the case of the circular path taken by the tool during forming of the cone. However the difference was a small percentage of the total forming force.

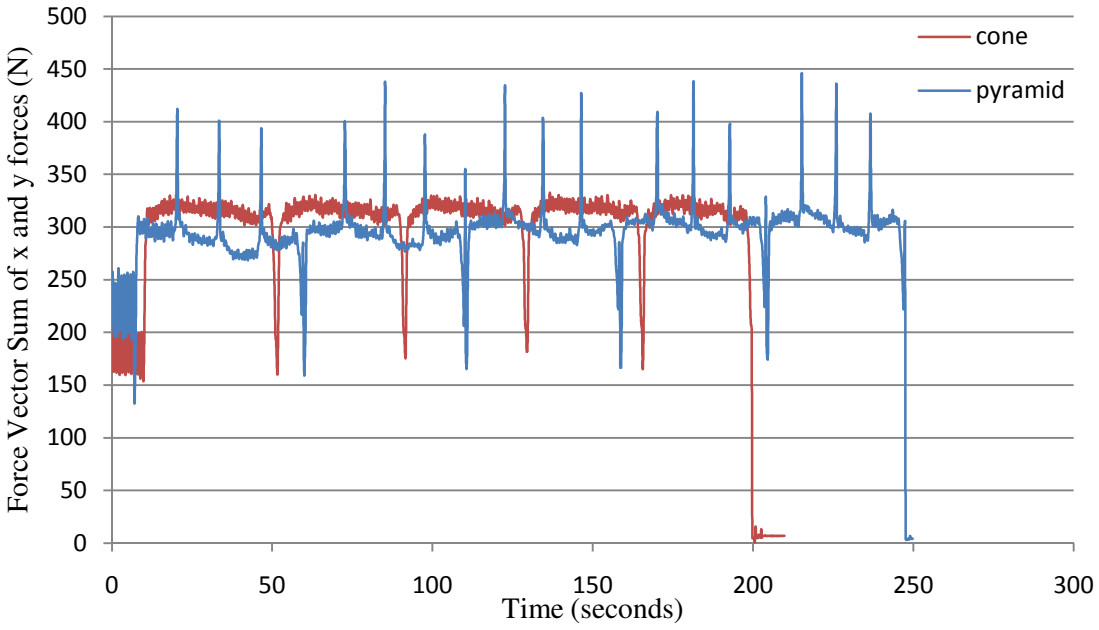

Fig. 38. Comparison of steady state force vector sum of the forces in x and y directions for pyramid and cone shapes.

The total force required to form the pyramid and cone shapes were obtained by vector addition of the forces in the three perpendicular directions. Figures 39, 40 and 41 present the forming force graphs for pyramid and cone shapes obtained from experiments.

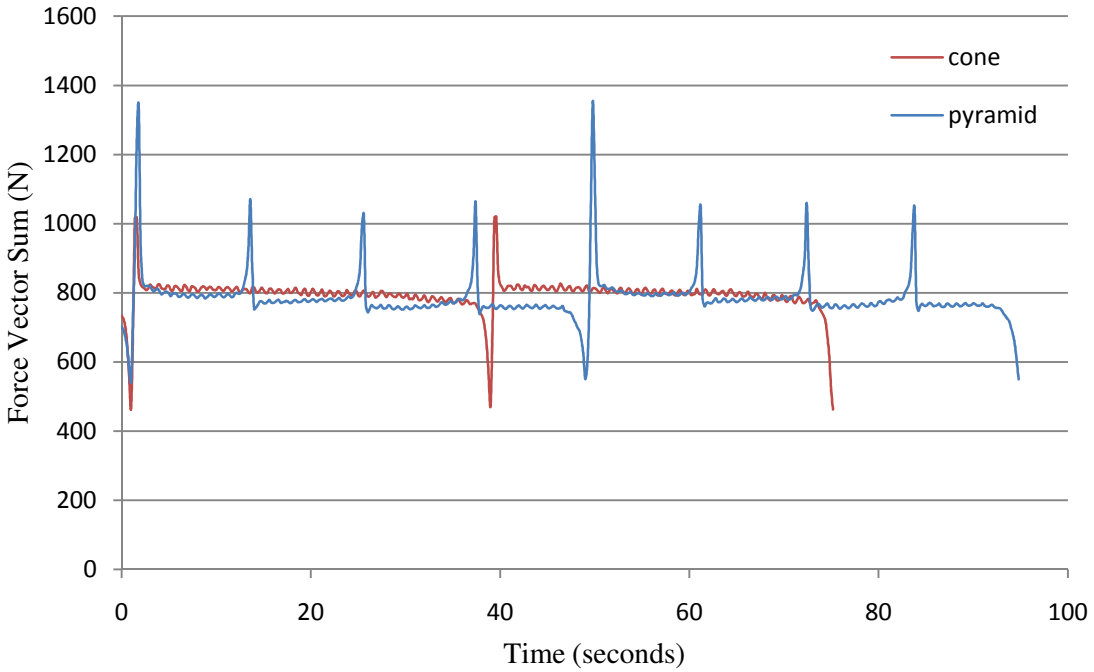

Fig. 39. Comparison of total steady state forming force measured for pyramid and cone shapes having a wall angle of 45 degrees and step size of 1.27 mm, tool radius 6.35 mm.

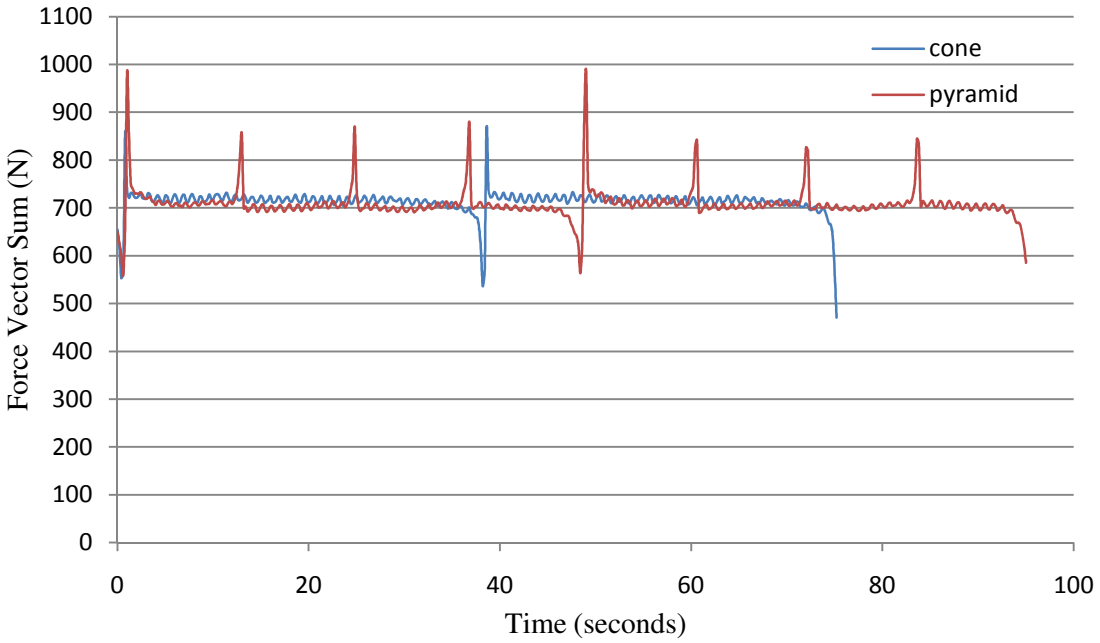

Fig. 40. Comparison of total steady state forming force measured for pyramid and cone shapes having a wall angle of 45 degrees, step size of 0.635 mm, tool radius 6.35 mm.

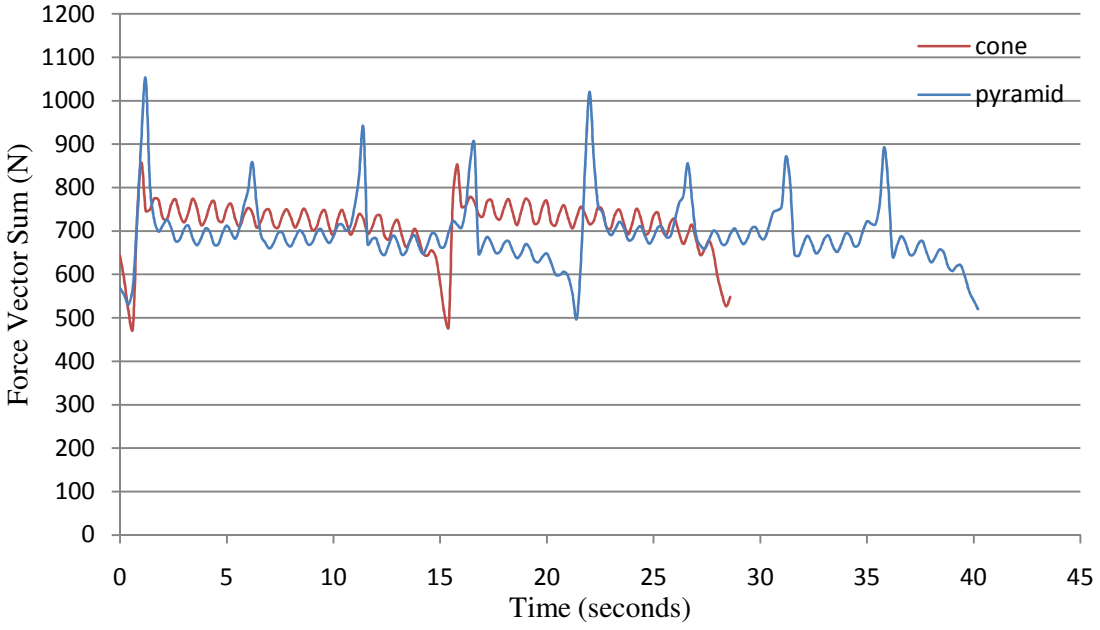

Fig. 41. Comparison of total steady state forming force measured for pyramid and cone shapes having a wall angle of 30 degrees, step size of 0.635 mm, tool radius 9.525 mm.

The above figures showed conclusively that the steady state deformation force required for forming a pyramid and cone which had the same dimensions and input parameters was the same. The path that the tool takes during forming was seen to have no effect on the magnitude of the forming force. The results obtained corroborate the findings in Filice et al. (2002) which mentions that the deformation in incremental sheet forming is restricted to a close vicinity of the contact zone. Due to this nature of deformation, the path taken by the tool does not have influence on the forces generated.

From the experiments conducted, it was seen that the major parameters that influence the force generated during forming were the thickness of the sheet metal blank, the diameter of the tool used for forming, the wall angle of the part being formed and to a certain degree the step size that the tool took after each pass.

4.6. Results of parametric studies obtained from experiments

4.6.1. Pyramid

Several truncated pyramids were formed using different sets of parameters. The steady state forces obtained from these experiments are summarized in Table 1 shown below.

Table 1
Results obtained from pyramid experiments.

Force values obtained during forming of pyramid								
No	Thickness (mm)	Wall angle (degrees)	Step size (mm)	Tool radius (mm)	Force 1 (N)	Force 2 (N)	Force 3 (N)	Force 4 (N)
1	0.8	45	1.27	6.35	1350	750	1000	550
2	0.8	45	0.635	6.35	1000	700	850	550
3	1.27	30	0.635	6.35	1500	1200	1300	800
4	0.8	30	0.635	6.35	800	600	675	450
5	0.8	30	0.635	9.525	1000	700	900	500
6	0.8	30	1.27	6.35	1000	650	800	425
7	0.8	30	1.27	9.525	1200	775	1000	550
8	1.27	30	0.635	9.525	1550	1150	1400	875
9	0.8	45	1.27	9.525	1600	900	1300	700

Sheet thickness, deformation of metal when the tool made a step down, diameter of the tool and the wall angle of the part were found to be the factors that affect the magnitude of the peak force, (number 1). At the corners, the tool was in contact with three surfaces which are the base surface and the inclined surfaces of the pyramid. Due to this, the contact area between the tool and the sheet metal blank and the amount of material required to deform increase thus leading to an increase in the force. Due to all these factors, the highest force was obtained at the corner where the tool made a new

pass. It should also be noted that the corner where the tool makes a step down is the location which was found to fail first during forming. On comparing the difference in the magnitudes of force 1 by changing one parameter at a time, it was seen that the thickness of the sheet is the major factor while the step size had the least significance in determination of the magnitude.

The sheet thickness, wall angle of the part, diameter of the tool and the extra material present in the corners were the major factors that determine the values of the secondary peak forces numbered 2. Again it was noticed that the thickness of the sheet was the major factor which increased the force magnitude followed by the wall angle of the part and the tool diameter.

The force labeled 3, or the deformation force had a constant value due to the fact that the area in contact between the tool and the sheet was constant throughout. The sheet thickness, stiffness of the sheet, wall angle of the part were the major factors influencing the magnitude obtained for this force. The tool diameter was seen to have only a minor effect on the deformation force and the deformation forces were found to be almost the same when different step sizes were used.

The force which was measured just before the tool finished the pass had the lowest value among all forces. The low value of this force was due to the fact that the tool did not deform any metal at this point and the force was solely due to the springback of the metal. The sheet thickness, wall angle and stiffness of the sheet were the major factors that affect the magnitude of this force. It was seen from Table 1 that the step size and tool diameter had a very low influence on this force.

4.6.2. Cone

Steady state forces obtained from the cone forming are summarized in Table 2.

Table 2
Results obtained from cone experiments.

Force values obtained during forming of Cone							
No	Thickness (mm)	Wall angle (degrees)	Step size (mm)	Tool radius (mm)	Force 1 (N)	Force 2 (N)	Force 3 (N)
1	0.8	45	1.27	6.35	1150	800	475
2	0.8	45	0.635	6.35	800	725	500
3	1.27	30	0.635	6.35	1400	1200	720
4	0.8	30	0.635	6.35	7250	650	450
5	0.8	30	0.635	9.525	850	725	500
6	0.8	30	1.27	6.35	900	675	375
7	0.8	30	1.27	9.525	1100	800	550
8	1.27	30	0.635	9.525	1300	1250	850
9	0.8	45	1.27	9.525	1100	950	650

As in the case of the pyramid, the thickness was found to be the major factor which influenced the magnitude of the forces. It was noticed that the peak force for the cone, (force number 1) was much smaller than the peak force for the pyramid. The reason for the higher forces obtained in the pyramid was due to the increased contact area due to the 3 surfaces of the pyramid.

It was seen that the deformation force marked as number 2 for the cone was approximately the same as the deformation force for the pyramid when all parameters were kept the same. This was because these forces depend just on the stiffness of the sheet and the area in contact between the tool and the sheet. This observation confirmed that incremental sheet forming was a localized deformation process where the tool path did not have any bearing on the force generated.

The forces obtained due to the springback of the sheet were also found to be the same for both the pyramid and the cone shape. These forces depend just on the stiffness of the sheet and the area in contact between the tool and the sheet when all other parameters were the same.

It was concluded that the thickness of the sheet was the most important factor which determined the magnitude of the forces generated. The wall angle of the part was also an important criterion followed by the diameter of the tool used. It was seen that the parameter which had the least impact of the measured force was the step size. Incremental sheet forming was confirmed to be a localized deformation process, which meant that the path that the tool took had no relation to the forces developed. This essential information was used to develop a new numerical model in Section 5.

5. NUMERICAL METHOD DEVELOPED TO SIMULATE INCREMENTAL SHEET FORMING

5.1. Introduction

Simulation of the deformation occurring in Incremental sheet forming is a surface based non-linear problem. As the tool moves continuously deforming the sheet metal, the material properties and the boundary conditions keep on changing after each instant. Also large deformations are produced in the sheet metal which adds to the non-linearity of the problem. There are two simulation methods in ABAQUS that could be used to model the contact problem. The first is the implicit method which involves solving non-linear equations iteratively using a global stiffness matrix and the second is the explicit method. An explicit method can produce results quickly. It would take less computational time and converge faster than a standard analysis. The implicit method produces accurate results at a higher computational cost.

For the present thesis work, the standard method of integration was used. The problem of long computational time and memory were tackled by carrying out the incremental sheet forming from a preset depth. Thus, using the numerical model developed, the simulation of only one pass is required to get the steady state force values. This method would greatly reduce the time taken to reduce the time taken to obtain forces numerically.

5.2. Element type

ABAQUS standard has a broad library of elements from which to choose the appropriate element based on the need. Selecting the right element involves choosing between the degree of accuracy desired in the results and the computational time and cost that the user has to incur to run the analysis.

Since the sheet metal thickness is quite small when compared to its length and width, it was decided to use shell elements to represent the sheet metal. Homogenous Continuum shell elements, S4R were used with the shell being the middle layer of the thickness. The default Simpson integration method was selected for the element and it was also decided to have five integration points along the thickness of the sheet. For the shell elements, the shear through the thickness is negligible and some discrepancies can arise in the strain values due to this. Despite this shortcoming it was decided to use shell elements as they converge quite fast and provide accurate results.

The forming tool was modeled as an analytical rigid body having a hemispherical end. Since the force and displacement are the same at all points in the rigid body, a node was chosen as a reference node and the force values can be got at this node in the Visualization module. An analytical rigid body has an in-built mesh which is generated by ABAQUS which can be viewed during the post processing stage.

5.3. Mesh size and density

A good mesh should be refined enough so that the whole model can converge when the tool is deforming the sheet metal. The element mesh should have minimum

density to ensure that the nodes of the master surface (rigid tool) do not get inside through the mesh of the slave surface (sheet) during the simulation as it could create convergence problems. However, using a very dense mesh could mean an increase in the number of elements and thus an increase in the computational time required to do the analysis.

The edges were seeded by specifying a particular number. This method of seeding would give us a uniform mesh size with each element having the same area but the drawback is the increase in the total number of elements as compared to a biased seeding method.

A mesh density study was done to determine the optimum mesh size to be used for the simulation. The equivalent plastic strain (PEEQ) of different mesh densities were found out for a common node and the difference between the maximum and minimum values were plotted. Figure 42 shows the plot of the equivalent plastic strain obtained vs. the total number of elements in the mesh. The mesh density numbered I was chosen to be used for simulation purposes.

The next set of figures show the meshing used for the parts. Figure 43 shows the mesh in the case of the pyramid having wall angle of 30 degrees. 6504 elements were used in the mesh and majority of the elements are concentrated at the base of the pyramid and the sides where the tool makes contact with the sheet. Figure 44 illustrates the meshing pattern used for the pyramid having wall angle of 45 degrees. The part has 8408 elements. The mesh used for the cone is shown in Figure 45. The mesh had 9348 elements. Figure 46 shows the meshing assigned to the analytical rigid tool by the

processor. The element size in the case of the tool had to be much bigger than the sheet, so that the elements of the tool would not get through the elements of the sheet and cause convergence problems.

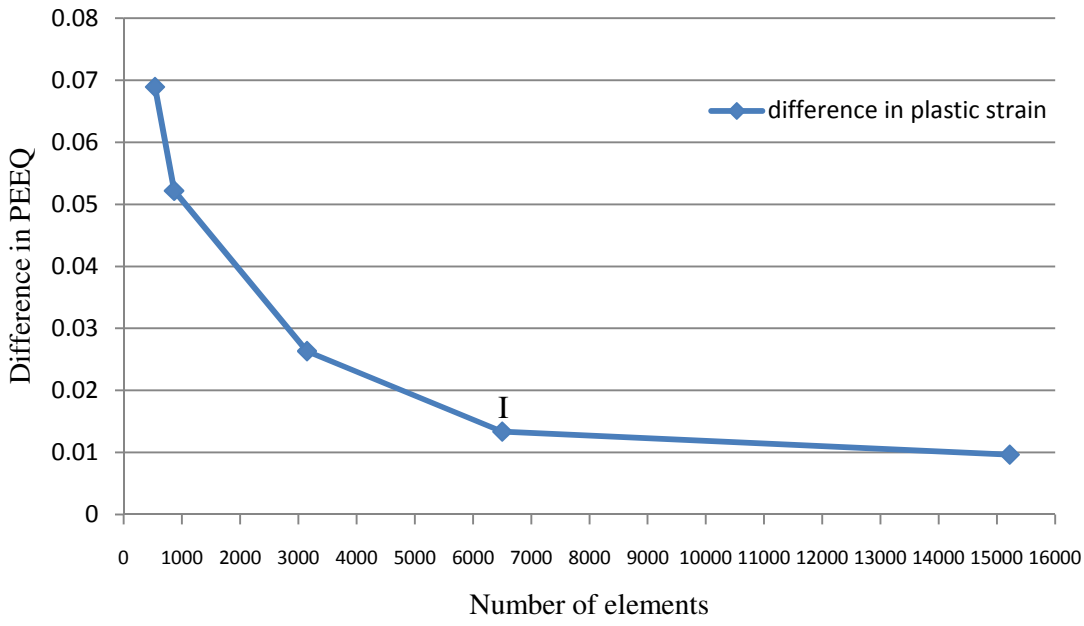

Fig. 42. Mesh density calculation.

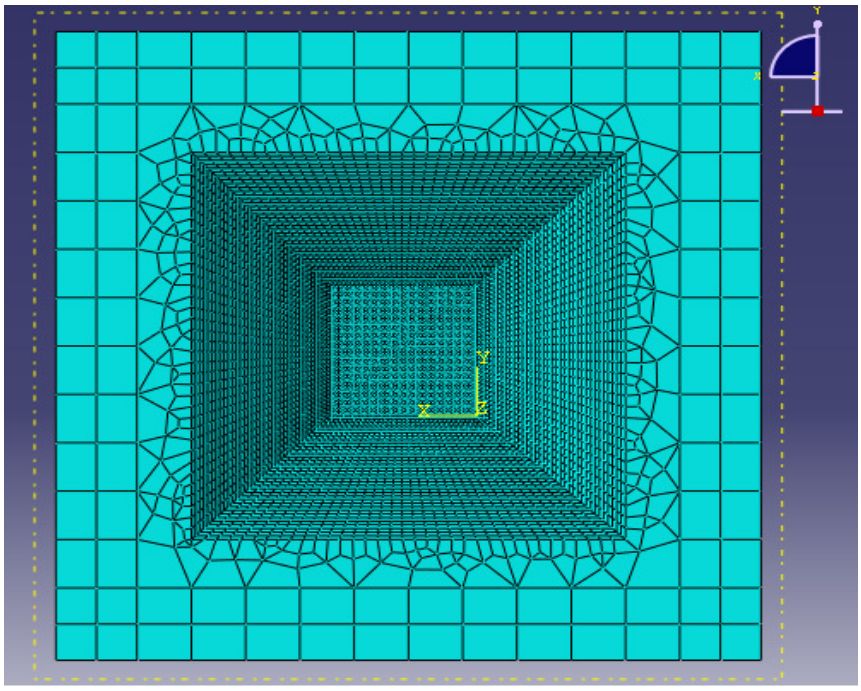

Fig. 43. Mesh used for the pyramid having 30 degrees wall angle.

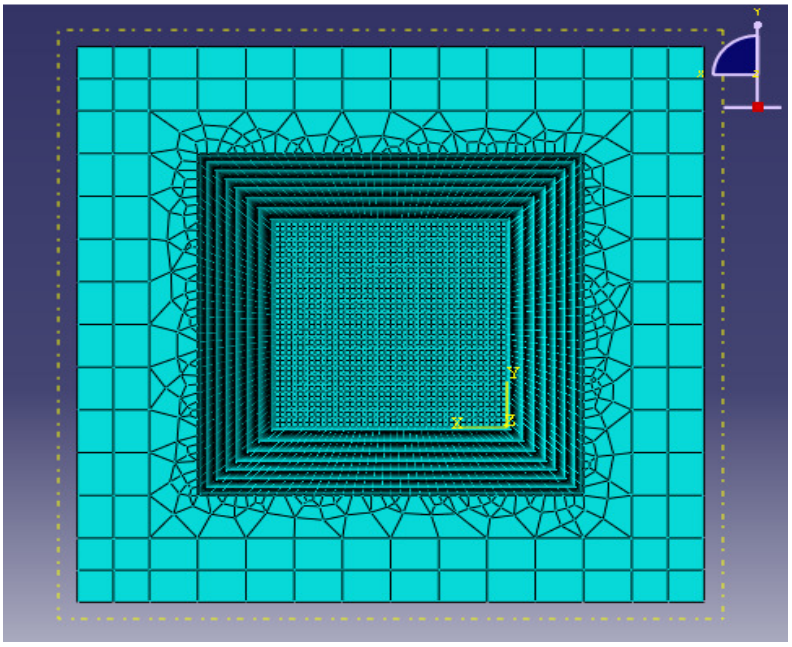

Fig. 44. Mesh used for the pyramid having 45 degrees wall angle.

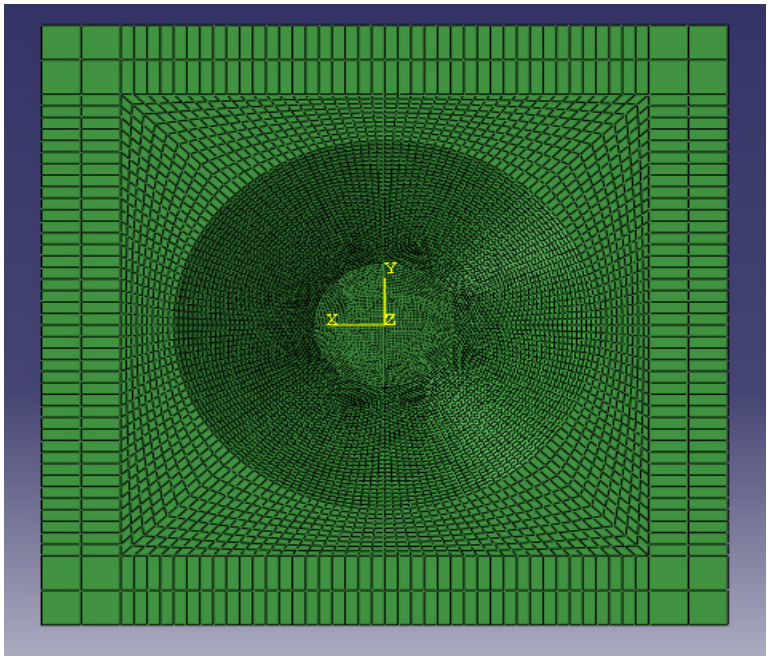

Fig. 45. Mesh used for the cone having 30 degrees wall angle.

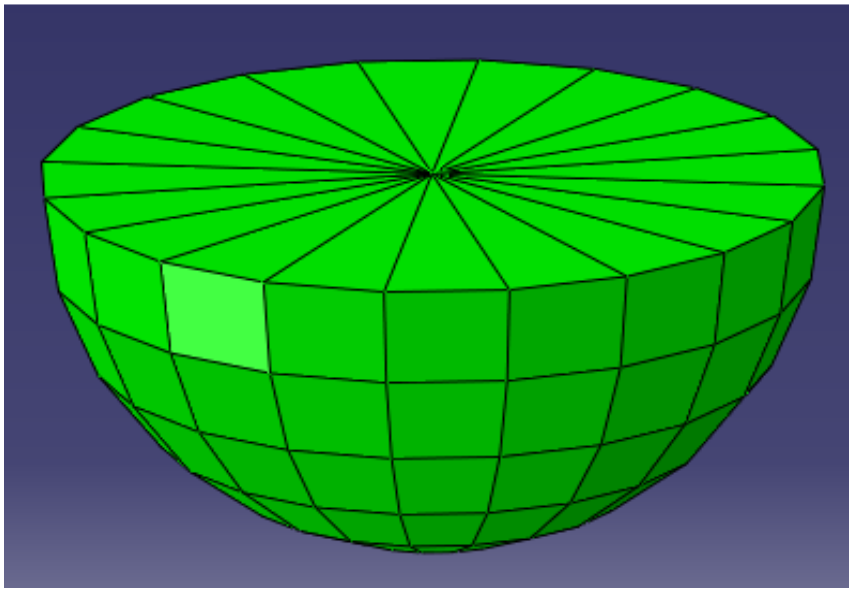

Fig. 46. Mesh used for the tool having radius of 9.525 mm.

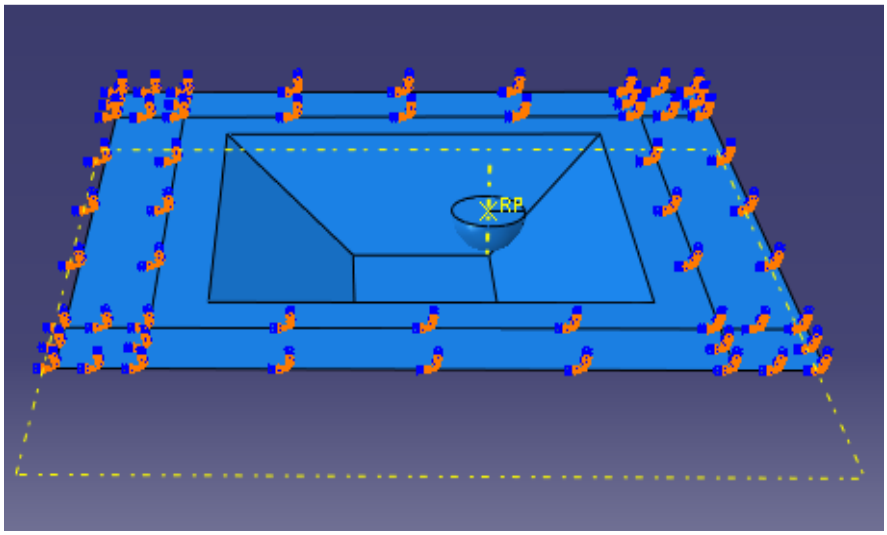

Fig. 47. Boundary conditions applied on the sheet.

The sheet used for the simulation purposes was divided into two main parts. An Encastre boundary condition was assigned to the outside part of the sheet such that the part would have no translational or rotational movement. This boundary condition simulates the clamping effect that the fixture and the frame have on the sheet during the experiments. The boundary condition assigned is illustrated in Figure 47. The tool was given a displacement type boundary condition where the displacement for each step was assigned to the reference point (RP) of the tool. The force acting on the tool during deformation was also calculated at this reference point. The reference point is marked as RP in Figure 47.

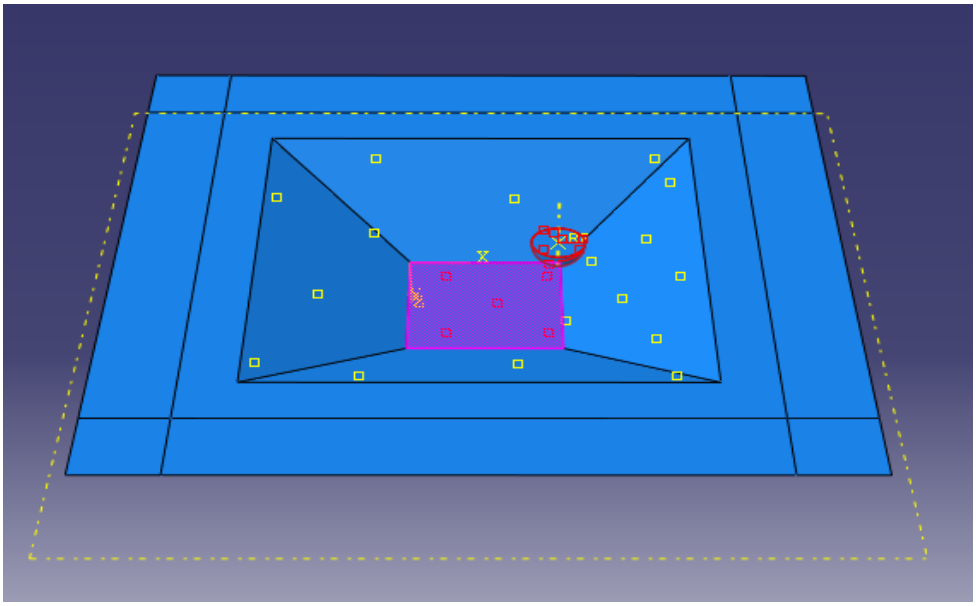

Fig. 48. Contact interaction properties.

Surface to surface contact interaction method was used to describe the interaction between the tool and the sheet. The sheet surface was picked to be the slave surface and the surface of the tool was assigned to be the master surface. The slave surface was defined to be the surface which can move but cannot penetrate the master surface. It was also supposed to be the surface which is supposed to have a higher mesh density. Figure 48 shows the interaction properties used for the numerical model, the master surface is shown in red and the slave surface is shown in violet. Since the deformation obtained is large, finite sliding formulation is used. Node to surface discretization method was used for all the simulations. Four other interactions were also defined with the sides of the pyramids being the slave surface and the tool being the master surface.

The von mises stress plot obtained during the simulation of the pyramid having a wall angle of 45 degrees using a tool having radius of 6.35 mm is shown in Figure 49. It was seen that the maximum stresses occurred at the points where the tool made contact with the sheet metal surface.

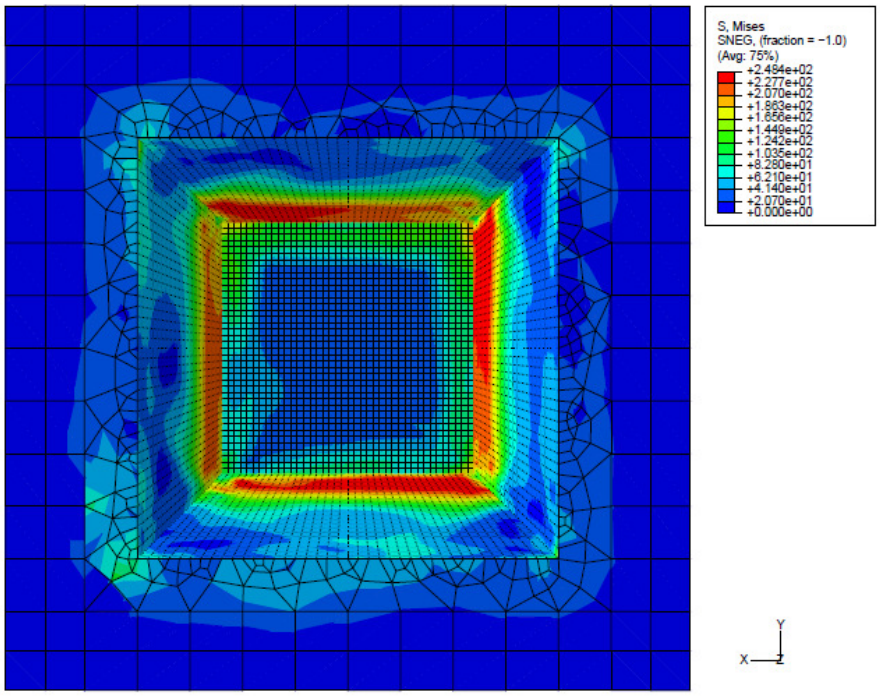

Fig. 49. Stress plot obtained for pyramid having wall angle of 45 degrees.

Figure 50 presents a plot of the maximum principal plastic strain obtained during simulation of the pyramid model. It was noticed that the deformation of the sheet metal was localized and was maximum at the locations where the tool moved over the sheet metal.

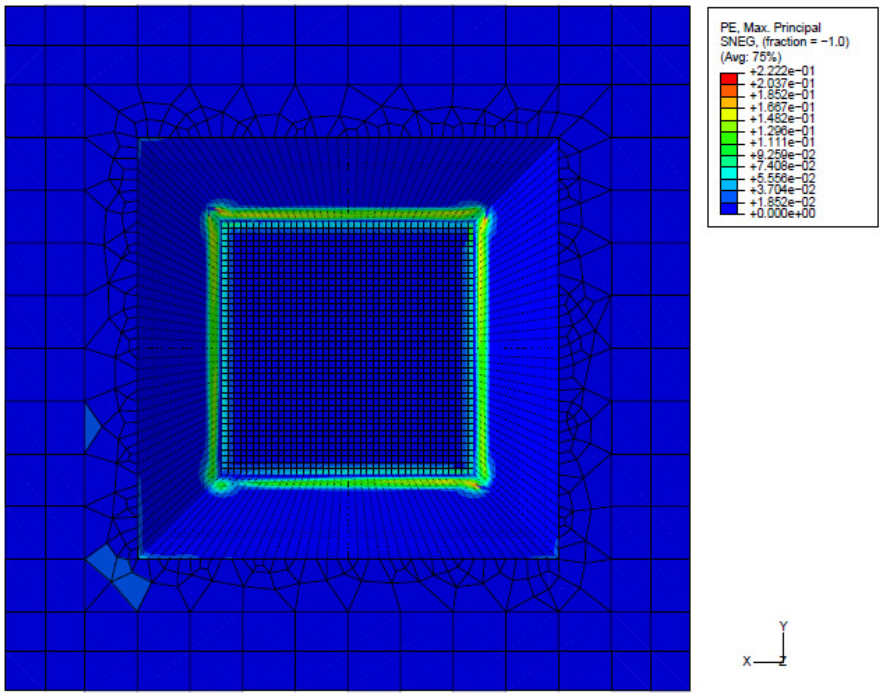

Fig. 50. Plastic strain plot obtained for pyramid having wall angle of 45 degrees.

A plot of the maximum principal plastic strain obtained during simulation of a cone having a wall angle of 30 degrees and a tool using radius of 9.525 mm is presented in Figure 51. The tool travelled only along quarter of the whole cone model. The deformations were again seen to be localized around the locations where the tool made contact with the sheet metal blank.

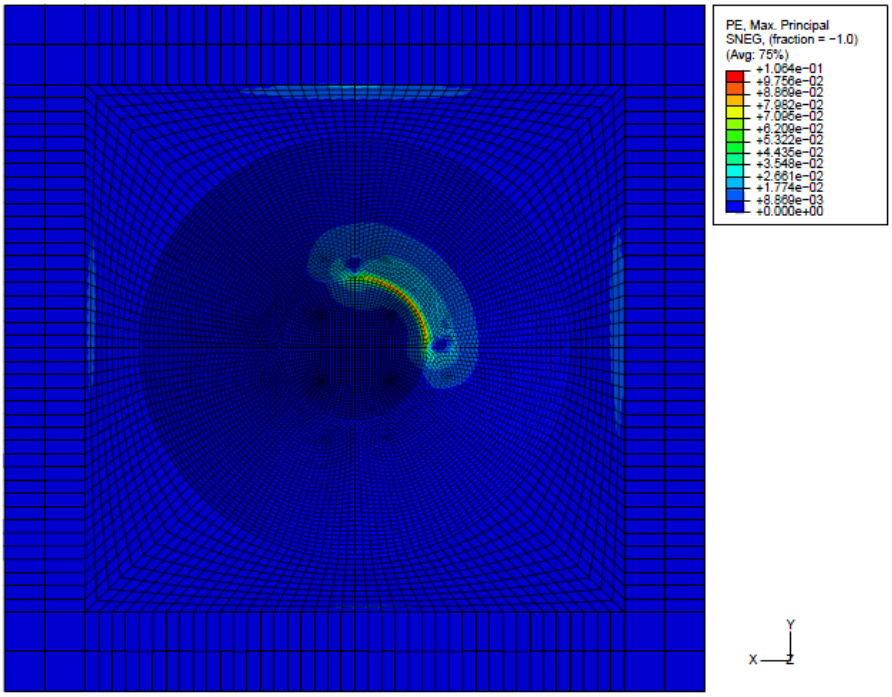

Fig. 51. Plastic strain plot obtained for cone having wall angle of 30 degrees.

5.4. Input parameters used for simulation

The input parameters which are used to define the sheet metal material include the yield strength, the plastic stress and strain and thickness of the sheet. The tensile test data for Al alloy 5052 was taken from Ozturk et al. (2008). The Young's modulus of the aluminum sample used was 70300 MPa and the Poisson's ratio was 0.3. Thickness of the sheet used was measured using ball-tip micrometer and it was found to be 0.815 mm.

Friction between the tool and the sheet surface is another parameter which is necessary for the simulation and since it was difficult to figure out the exact coefficient of friction during the forming, a nominal value of 0.1 was chosen initially. Many

simulations were done for the case of a pyramid having wall angle 30 degrees using a tool having radius of 6.35 mm. The simulations were done changing the friction values and keeping all the other parameters the same. Coefficients of 0.05, 0.1, 0.2 and 0.3 were used and the force values were determined for each. The vector sum of the forces were calculated and this force was compared to the force magnitude obtained from experiments and it was decided to use the friction coefficient which gave the closest steady state value force to the experimental force. The results of the sensitivity of the model to the friction coefficient are presented later. After running the simulations, it was decided to use a friction coefficient of 0.1. The friction value was formulated using the penalty method and an isotropic directionality was assumed.

5.5. Reference model

Incremental sheet forming is a highly non-linear problem and although the stress strain data of the material undergoing deformation can be found out by performing a tensile test, the same properties would not necessarily prevail at the steady state. Also it is quite hard to set up a hardening law for the material.

A pyramid having a wall angle of 30 degrees, formed with a step size of 1.27 mm from a sheet having thickness of 0.815 mm using a tool having a radius of 6.35 mm was chosen as the reference model to set up the numerical simulation. This model was used to fix the coefficient of friction between the tool and the sheet by comparing the forming force obtained by numerical methods and through experiments. Also the sheet thickness which was to be used for all the experiments was fixed using this reference model. The

steady state portion of the force obtained through numerical methods had an error of 7 % but it was considered to be acceptable.

Once the reference model and parameters were set up, all the other simulations were performed keeping the same material parameters as the one used for the reference model. This was to ensure uniformity of the results and to test the effectiveness of the numerical model developed. Figure 52 presents the measured force values for the pyramid having a wall angle of 30 degrees. The force values obtained from the reference model is shown in Figure 53. The force values obtained in both cases are for the pass which the tool makes after it has reached a depth of 19 mm.

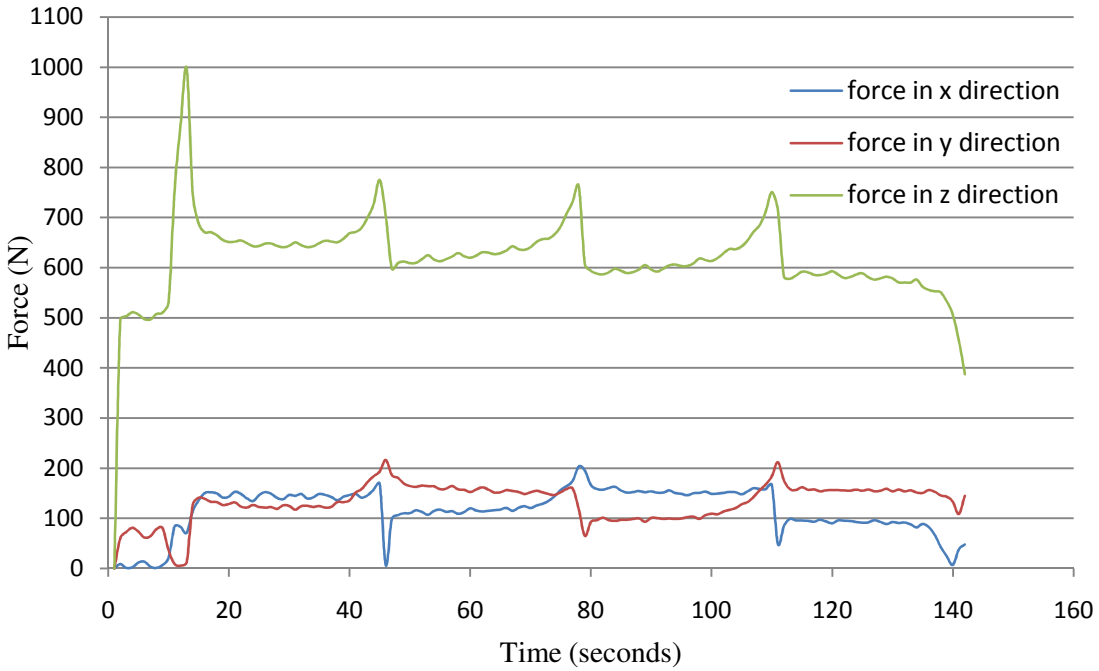

Fig. 52. Experimental forces obtained.

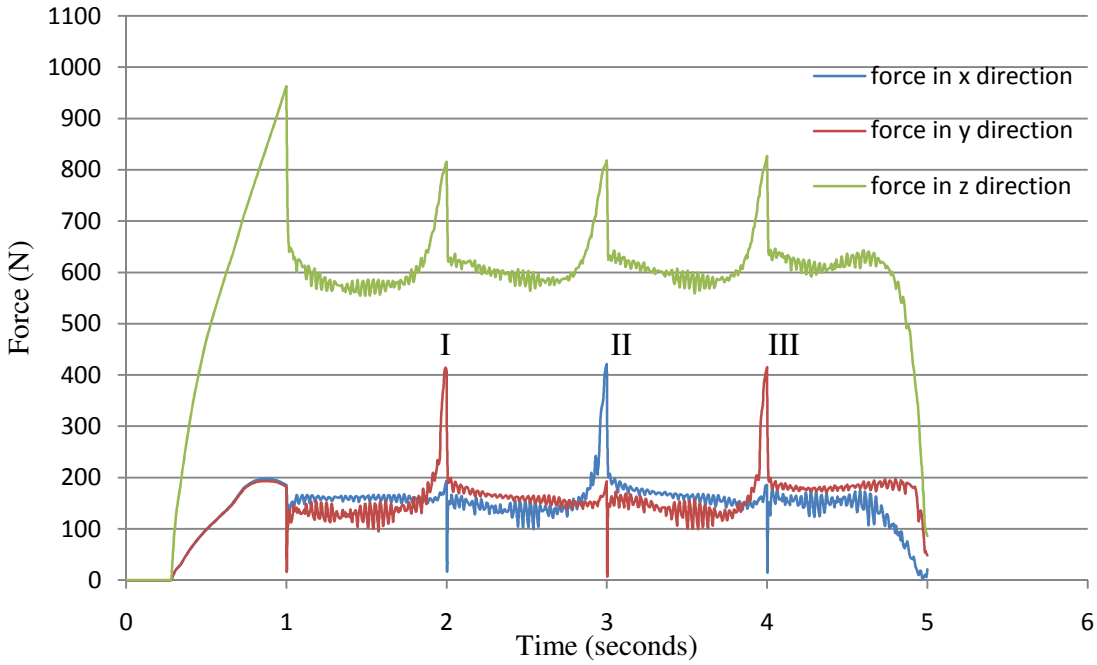

Fig. 53. Force values obtained from reference model.

5.6. Results of simulation

The simulation was carried out to develop a numerical model which could be used to predict the steady state forming force quickly without the need to do any experiments or refer previous literature. Numerical models were developed for the case of the pyramid and the cone and various simulations were done with the same set of material parameters as was used in the experiments.

5.6.1. Results for pyramid shape

Several simulations were carried out changing one or more parameters at a time. The forces obtained are presented in Figures 54 and 55. The comparison of the vector sum between the predicted and measured forces is presented in Section 7 for each case.

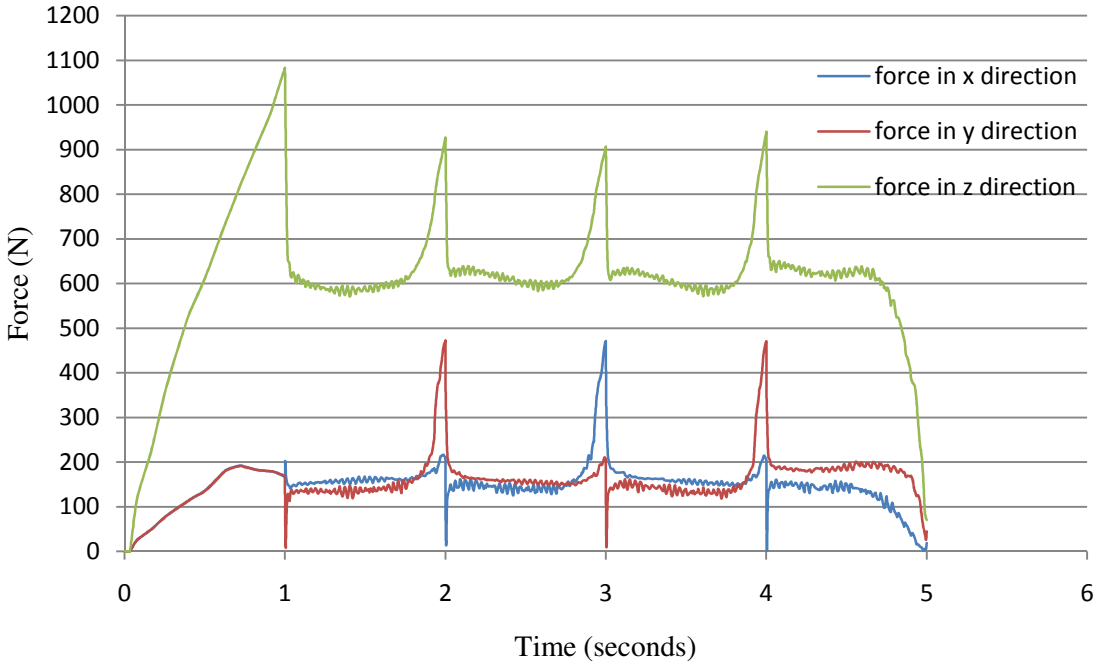

Fig. 54. Force obtained for pyramid having 30 degrees wall angle, tool 9.525 mm radius, step size 1.27 mm, sheet thickness 0.815 mm.

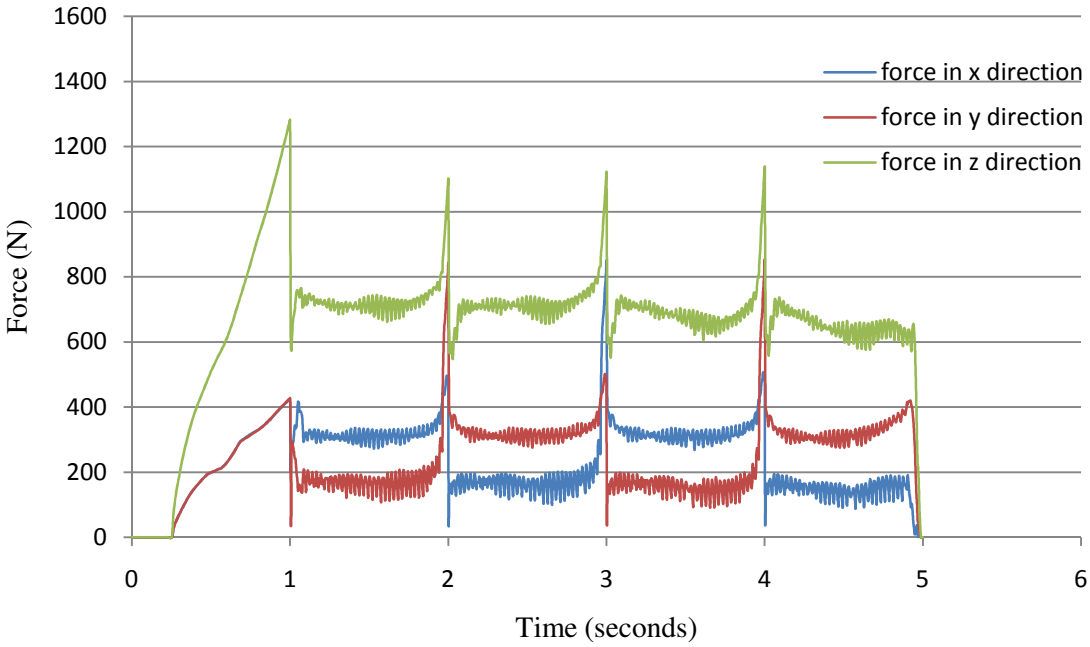

Fig. 55. Force obtained for pyramid having 45 degrees wall angle, tool 6.35 mm radius, step size 1.27 mm, sheet thickness 0.815 mm.

5.6.2. Results for cone shape

Since the cone shape involved a large number of steps, it was decided to restrict the simulation to just 90 degrees i.e. a quarter of the entire pass. A full model of the cone was used for the simulation, however the forming tool was made to go through just 90 degrees. This can be a valid approximation in the case of a cone due to the fact that there are no corners in a cone. Since there are no corners, the area which is in contact with the tool would be the same and hence the force would also be the same. Force would increase in a cone only at the instant the tool is moving down to begin a new pass.

Cone having a wall angle of 30 degrees was used for simulation purposes. Simulations were run for tools having radius of 6.35 and 9.525 mm. The step size used in both cases was 1.27 mm. The sheet used had a thickness of 0.815 mm. Figures 56 and 57 present the forces obtained in the three coordinate directions for the tool having radius of 6.35 and 9.525 mm respectively. The comparison of the vector sum between the predicted and measured forces is presented in Section 7.

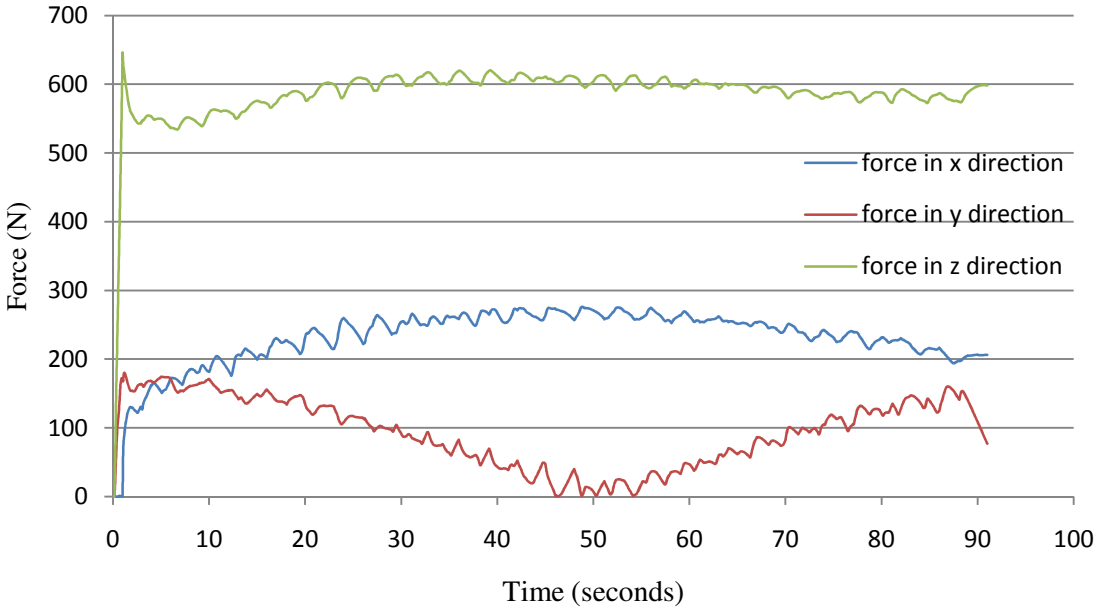

Fig. 56. Force obtained for cone having 30 degrees wall angle, tool 6.35 mm radius, step size 1.27 mm, sheet thickness 0.815 mm.

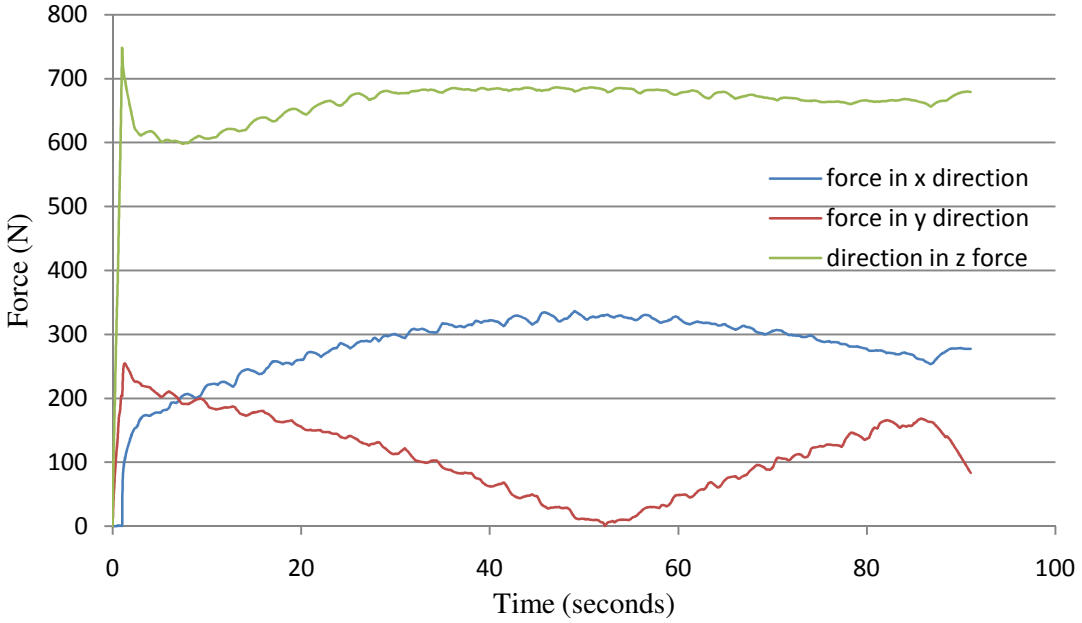

Fig. 57. Force obtained for cone having 30 degrees wall angle, tool 9.525 mm radius, step size 1.27 mm, sheet thickness 0.815 mm.

5.7. Sensitivity study

5.7.1. Friction sensitivity analysis

The sensitivity of the numerical model to friction was analyzed by measuring the forces developed for a pyramid having a wall angle of 30 degrees using different coefficients of friction. Coulomb friction coefficients of 0.05, 0.1, 0.2 and 0.3 were used and all the other input parameters were kept the same. The base dimensions were the wall angle which was 30 degrees and the tool radius which was 6.35 mm. The step size was 1.27 mm in all the cases and the sheet blank had a thickness of 0.815 mm. Figures 58, 59 and 60 present the results of the friction study for the x, y and z directions respectively.

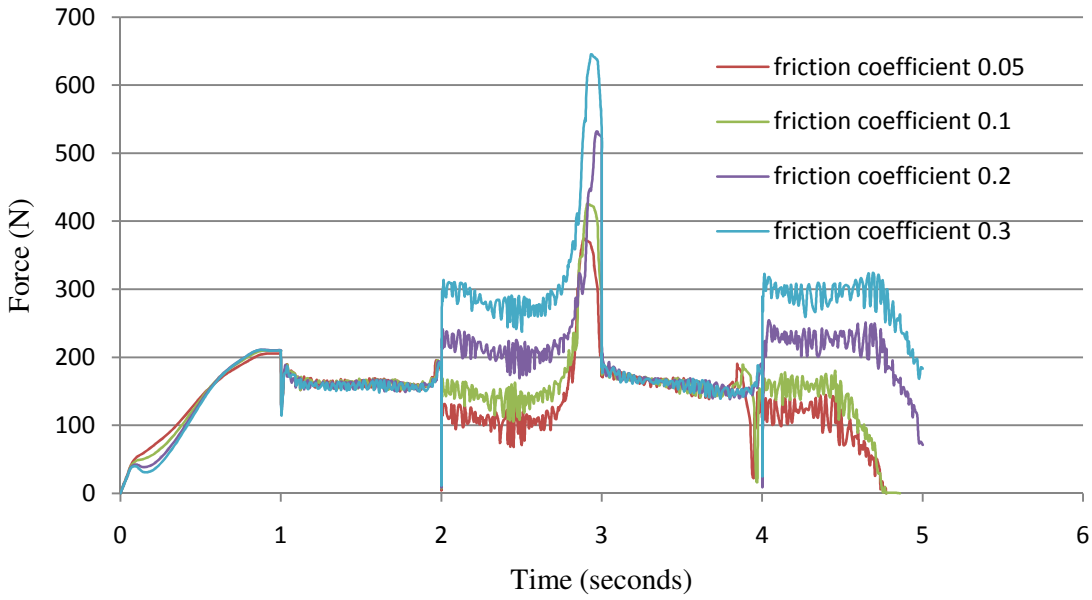

Fig. 58. Force developed in x direction with various coefficients of friction.

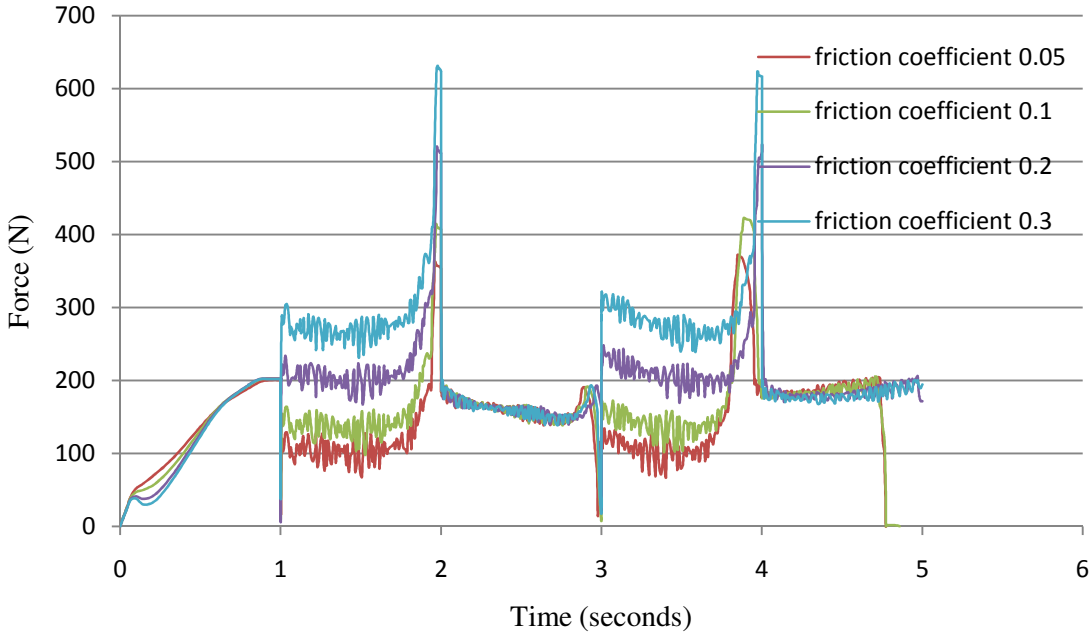

Fig. 59. Force developed in y direction with various coefficients of friction.

A few observations can be noted with reference to Figures 58 and 59. The time between t=0 to t=1 second is the time taken for the tool to take a step down. The tool initially moves along the y direction between t=1 to t=2 seconds. From the above figures, it is seen that the deformation forces vary according to the friction in the y direction but it remained the same in the x direction. At the end of t=2 seconds, the tool reaches a corner and the force also peaks consequently. From t=2 seconds to t=3, the tool changes directions and travels along the x direction. The same phenomenon can be observed, with the effect of friction only influencing the deformation force in the x direction and not in y direction. The reason for this behavior is due to the localized nature of deformation of the sheet during incremental sheet forming. The deformation of

the sheet occurs only at a very small area which is in contact between the tool and the sheet and thus the effect of friction on the deformation force is only along the direction of motion of the tool.

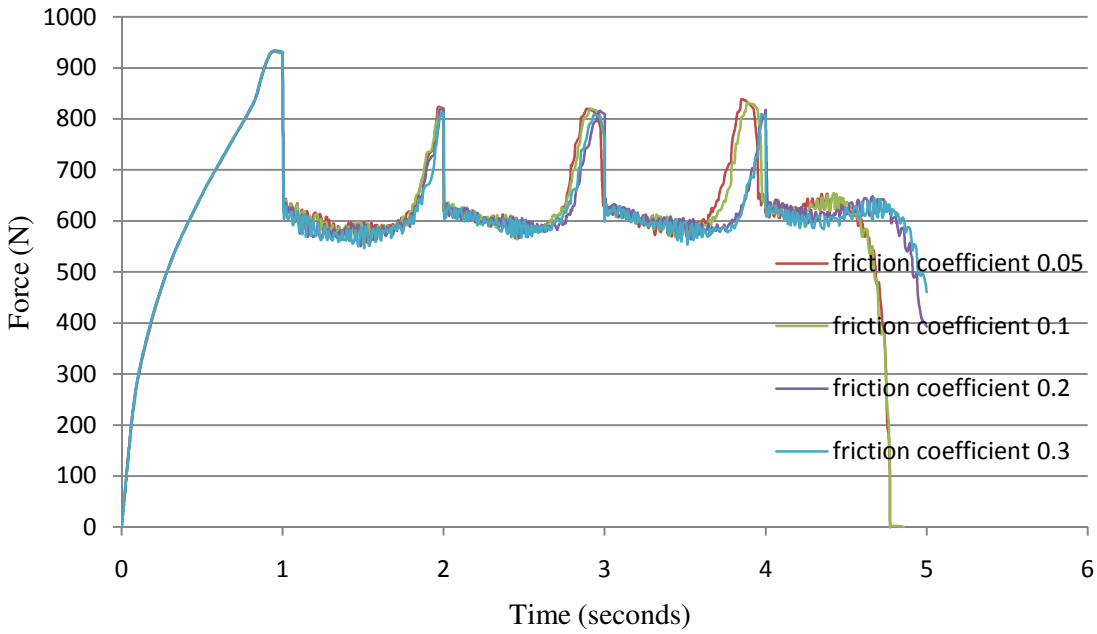

Fig. 60. Force developed in z direction with various coefficients of friction.

It can be seen from Figure 60 that the deformation forces remain the same in the z direction for different values of friction. The friction sensitivity studies confirmed that the force in the z direction just depended only on the amount of metal that is being deformed and not on the friction or the path taken by the tool. However friction has a huge influence on the in-plane forces.

5.7.2. Thickness sensitivity analysis

Thickness of the blank used for forming is a major factor affecting the forces generated during forming. If a thicker sheet is used, the tool has to deform more material and consequently the force acting on the tool increases. The sensitivity of the numerical model to the sheet metal thickness was determined by calculating the forces generated during forming of three sheets having different thickness values. The model was a pyramid having a wall angle of 30 degrees. The tool had a radius of 6.35 mm and a step size of 1.27 mm. The sheets used had thickness values of 0.7493 mm, 0.8128 mm and 0.8763 mm respectively. Figures 61, 62 and 63 present the results of the thickness sensitivity study for the x, y and z directions respectively.

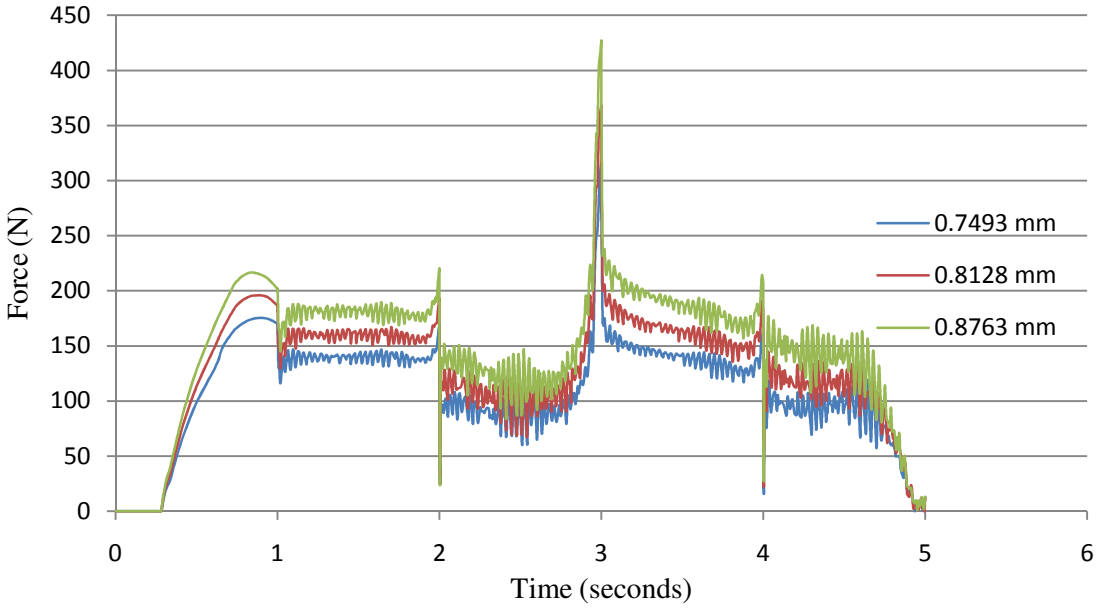

Fig. 61. Force developed in x direction with different thickness.

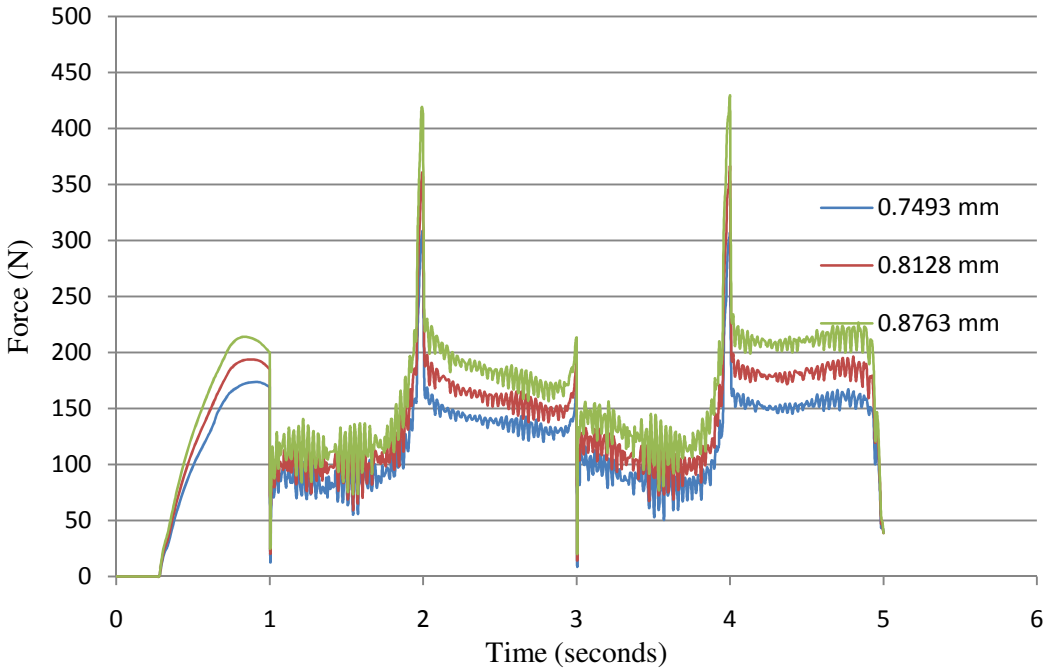

Fig. 62. Force developed in y direction with different thickness.

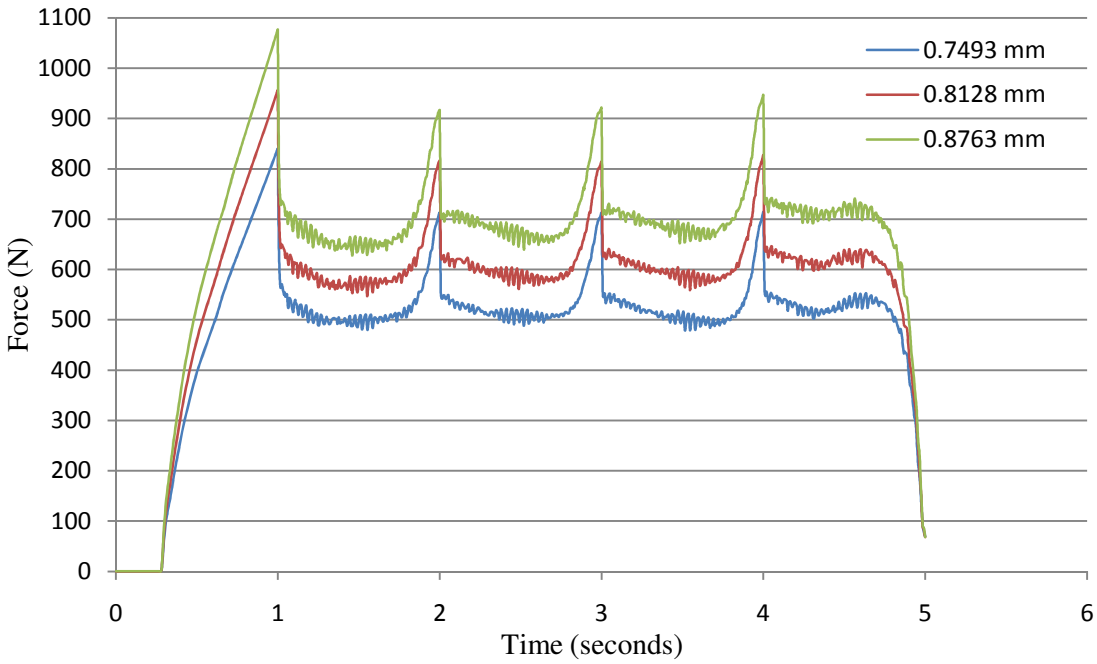

Fig. 63. Force developed in z direction with different thickness.

In pure plastic bending of sheet metal, the force required for deformation is known to be directly proportional to the square of the thickness and the yield strength of the sheet metal. Assuming the same yield strength for the material, a first order analysis was done based on the results obtained from the thickness sensitivity analysis done. It was seen that the ratio of the deformation forces to the square of the thickness of the sheets used was not a constant. This shows us that the deformation of the sheet in incremental sheet forming is not just pure bending but a combination of bending and uni-axial, bi-axial stretching of the sheet Filice et al. (2002), Kim and Park (2002).

6. PREDICTION OF FORMING FORCES

6.1. Introduction

It was seen that the steady state deformation forces for the pyramid, when the tool was between any two corners and the cone were similar. This indicated that the deformation in incremental sheet forming was a heavily localized process where the force depended only on the area in contact between the tool and the sheet metal blank. The force acting on the tool was measured to be the same regardless of the path taken by the tool during forming.

Based on the above knowledge, a new technique to predict the forces generated during forming was established. In this numerical method, the pyramid and cone shapes were preformed to a certain depth. It was assumed that the sheet metal would have been fully stiffened at that depth. The depth was decided based on the experience obtained from running several experiments. At this depth, since the contact area was the same as the contact area between the tool and the sheet during the experiments, it was logical to expect that the force experienced by the tool to further deform the sheet metal would be the same as the experimental force.

The present section deals with the results obtained from the numerical model simulating the deformation of the sheet metal blank after the tool begins to deform it from a point which was sufficiently deep. In the following section, the results obtained from the numerical analysis were compared with the experimental force values obtained from the forming of the cone and pyramid shape. In the second section, arbitrary shapes

were created and the force values obtained for the new shapes were compared with the predicted values as a means to validate the numerical model developed.

6.2. Comparison of forces obtained for pyramid and cone shape

6.2.1. *Comparison for pyramid shape*

The following section compares the vector sum of the forces obtained from the numerical model developed to the vector sum of the forces measured during experiments. Figure 60 presents the force vector sum comparisons of the reference model that was used to decide the value of the coefficient of friction which was to be used for the simulations. The same set of conditions as used in the reference model was used in all the other simulations.

The simulations compared only the forces labeled 2, 3 and 4 in Figure 64. The force labeled 2 was the peak force experienced at the corner where the tool makes a step down to start a new pass. Force numbered 3 was the constant force acting on the tool when the tool was between the corners and the force numbered 4 was the force when the tool reached a corner. The force which is on the left, labeled as 1 was the force acting on the tool just before it completed a pass. This force primarily depends on the stiffness of the sheet and was not modeled.

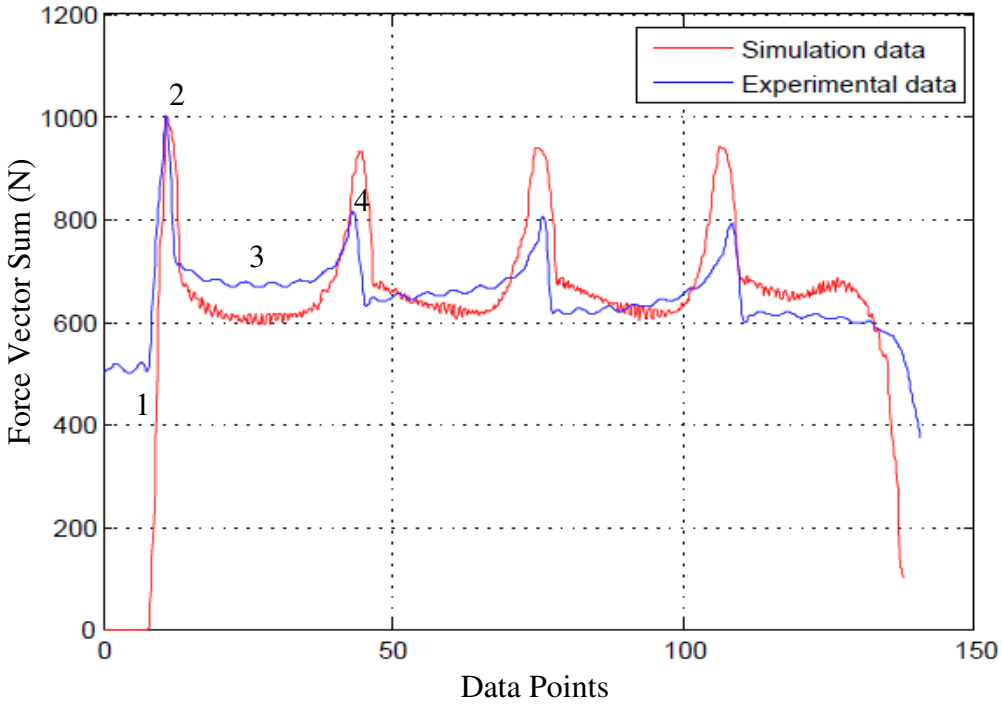

Fig. 64. Force developed for pyramid having wall angle of 30 degrees. Tool has a radius of 6.35 mm and a step size of 1.27 mm. Sheet thickness is 0.815 mm.

It was seen that the error between the numerical and simulation data for the first peak was just 0.2 %. On computing the average of the deformation forces acting on the tool when it was between the peaks, we obtain a force magnitude of 640.045 N for the experimental data and 633.12 N from the calculated data. The error was calculated to be 1.8 %. The average error of the other three peak forces was seen to be 11.5 %.

The comparatively large error in the case of the peak forces was due to the high force values observed at the corners for the x and y forces in the simulation which also increased the magnitude of the force vector sum. The model was seen to predict the

forces values closely for all the other instances except for the case when the tool was at the corner.

The reason for this high value could be due to the difference in the process conditions in the simulation and the actual experiments. The tool was given a low rotation speed of 60 rpm during experiments while it was stationary for the simulation. This could have changed the contact conditions, especially the friction at the corners leading to a higher value. Use of shell elements for the simulation could be another reason for the discrepancy. The other factors responsible for the difference between the measured and predicted force could be the difference in the value of friction, anisotropic effects of the sheet metal blank used, imperfections in the forming tool and thickness variations in the metal blank used for the experiment.

Further force comparisons were made between the experimental values and forces obtained from the numerical model for a number of cases. Figure 65 presents the force comparison between the predicted and experimental force obtained during forming of a pyramid having wall angle of 30 degrees. The tool used had a diameter of 9.525 mm and step size of 1.27 mm. The sheet metal blank used had a thickness of 0.815 mm.

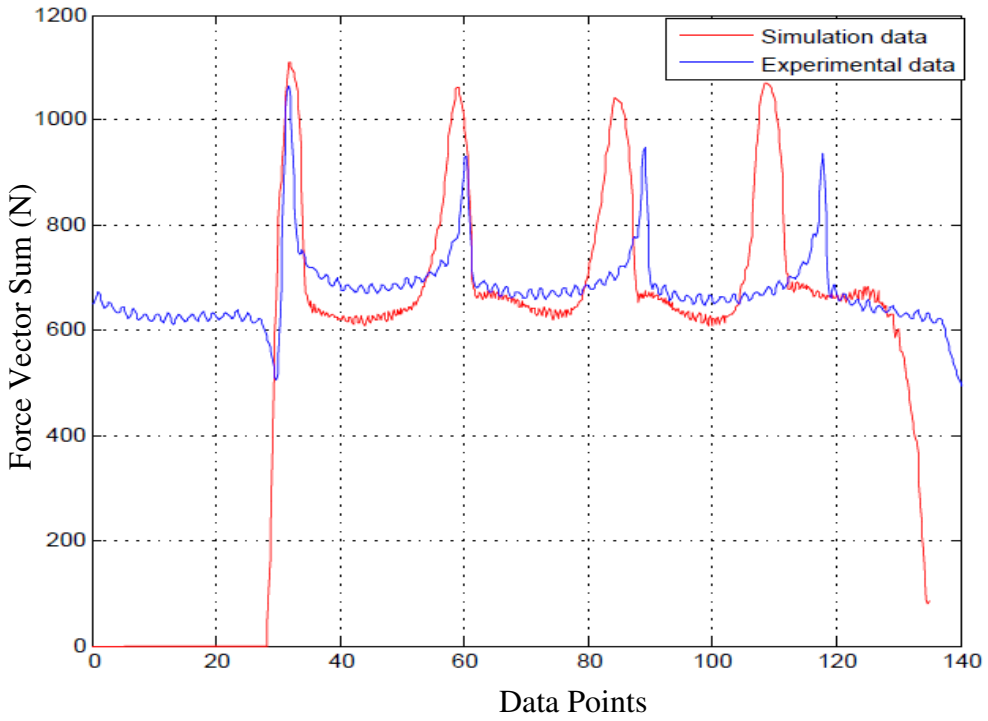

Fig. 65. Force developed for pyramid having wall angle of 30 degrees. Tool has a radius of 9.525 mm and a step size of 1.27 mm. Sheet thickness is 0.815 mm.

The peak force at the start of the pass was observed to have an error of 5 % while the maximum error of the forces when the tool was between the corners was about 1.3 % while the average error between the forces observed at the other three corners was calculated to be 13.2 %. The high error was again to be observed due to the force peaks observed at the corners for the x and y forces.

Figure 66 presents the force comparison between the predicted and experimental force obtained during forming of a pyramid having wall angle of 45 degrees. The tool used had a diameter of 9.525 mm and step size of 1.27 mm. The sheet metal blank used had a thickness of 0.815 mm.

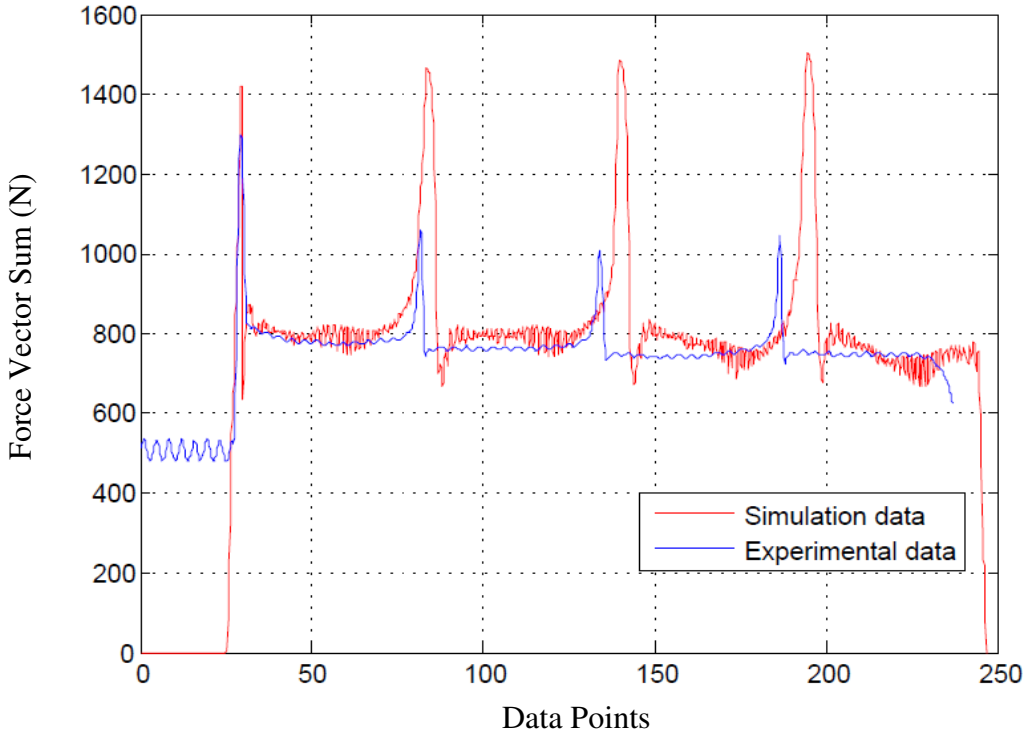

Fig. 66. Force developed for pyramid having wall angle of 45 degrees. Tool has a radius of 9.525 mm and a step size of 1.27 mm. Sheet thickness is 0.815 mm.

For the condition presented in Figure 66, the force values of the first peak and the value between the peaks were seen to match very closely. However an error of approximately 38 % was found between the force values obtained at the other three corners. The reason for this discrepancy was again found to be due to the high force values obtained at these peaks in the x and y direction.

6.2.2. Comparison for cone shape

Figure 67 compares the experimental and numerical forces obtained for a cone having a wall angle of 30 degrees. The tool used had a radius of 6.35 mm. Step size used was 1.27 mm and the sheet metal blank had a thickness of 0.815 mm. The force values

obtained when the tool took a step down and when it was moving along the circular trajectory were compared. Figure 68 compares the experimental and numerical forces obtained for the case of a cone having a wall angle of 30 degrees. The tool used had a radius of 9.525 mm. Step size used was 1.27 mm and the sheet metal blank had a thickness of 0.815 mm. Only 90 degrees of the entire 360 degrees of the circular profile was covered by the cone in the simulations.

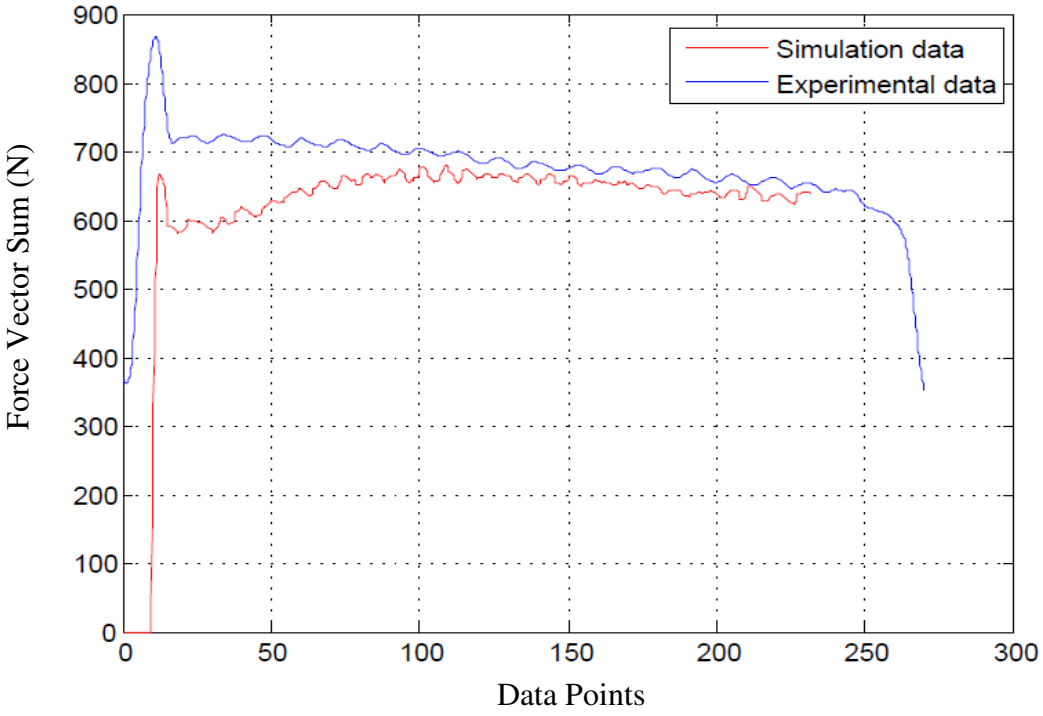

Fig. 67. Force developed for cone having wall angle of 30 degrees. Tool has a radius of 6.35 mm and a step size of 1.27 mm. Sheet thickness is 0.815 mm.

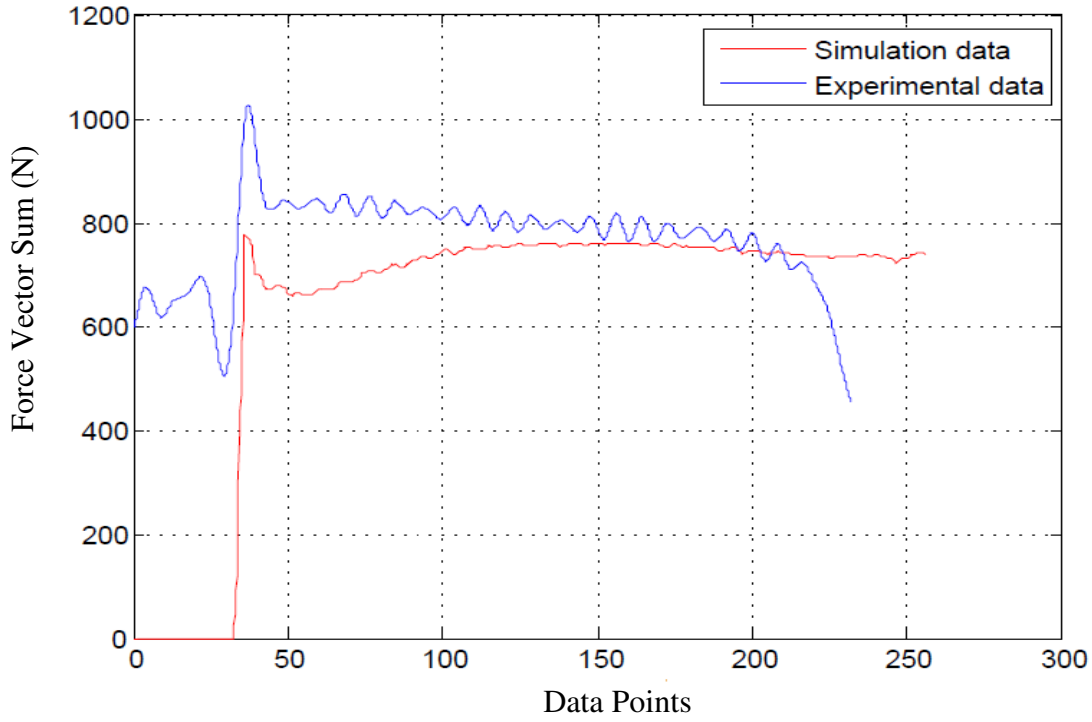

Fig. 68. Force developed for cone having wall angle of 30 degrees. Tool has a radius of 9.525 mm and a step size of 1.27 mm. Sheet thickness is 0.815 mm.

With reference to Figures 67 and 68, it was noticed that the error between the peak forces was found to be around 20 % while the average error between the force values was calculated to be about 7 %.

6.2.3. Discussions

The following conclusions can be made for the model based on the results obtained from simulations:

1) For the case of the pyramid model, the force predicted when the tool was between the corners matched closely with the experimental data.

2) The force acting on the tool when the tool reached a corner and took a step down was accurately predicted by the numerical model in all the cases. Since this is the maximum force obtained during the experiments, the calculated force values could be used to design the machine against failure.
3) The values obtained from the simulation had errors at the other three corners due to the increase in the tool force in the x and y directions at these corners. However since the maximum force is being accurately predicted by the model, the model could be used to predict the forces without performing experiments.
4) The individual force components were seen to match closely with the experimental value for all the forces which confirmed the fact that the deformation in incremental sheet forming is localized and that the area in contact between the tool and the sheet determines the magnitude of the force.
5) The steady state forces were closely predicted by the cone model when compared to the experimental force. The force peak was seen to have been under predicted by the model.
6) The simulations were run on a PC using 4 nodes. Each node had a "IBM Power5+ processor" which ran at 1.9 GHz. The simulation took about 5 hours to solve for the 30 degrees pyramid model, about 9 hours for the 45 degree pyramid model and about 4 hours for the cone model. Previous models offered by Henrard et al. (2005) took around 300 hours using a 8 CPU machine "(MIPS R12000 at 400 MHz)" with the Lagamine code and they were seen to have an error of 30 %. Comparing the accuracy of the forces developed using the model

and the computational cost, the models were seen to be quite useful to predict forces.

6.3. Force prediction for new parts

Arbitrarily shaped designs were created and formed to measure the forces. The main aim of this exercise was to test the effectiveness of the numerical model in predicting the forces that would be generated during forming of the new object. The designs were chosen to have a radial profile and also have corners along which the tool moves. Thus it included both types of tool paths seen in the pyramid and cone.

6.3.1. Three lobed part

Three lobed and four lobed arbitrary shapes were formed. The three lobed part consisted of three circles each of diameter 61 mm. The depth of the three lobed shape was 19 mm. Figure 69 presents the final shape of the three lobed part.

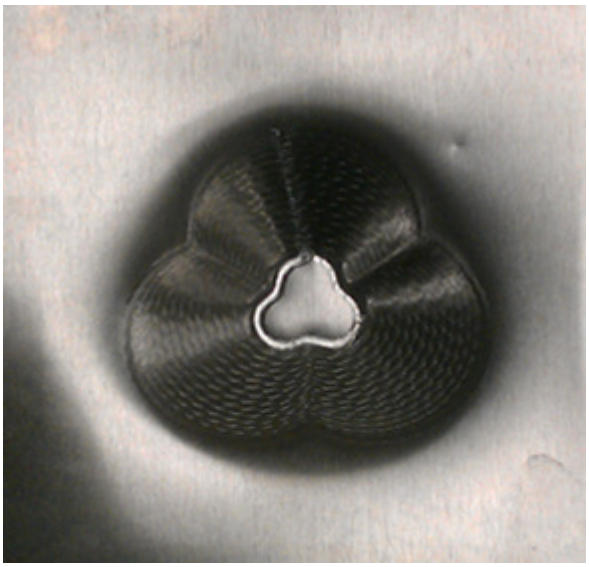

Fig. 69. Three lobed part.

The experimental data collected during the forming of the three lobed shape is shown in Figure 70. The steady state region which was selected for analysis is circled and shown separately in Figure 71. The blank used had a thickness of 0.8 mm, and the step size used was 1.27 mm. The tool used had a radius of 6.35 mm.

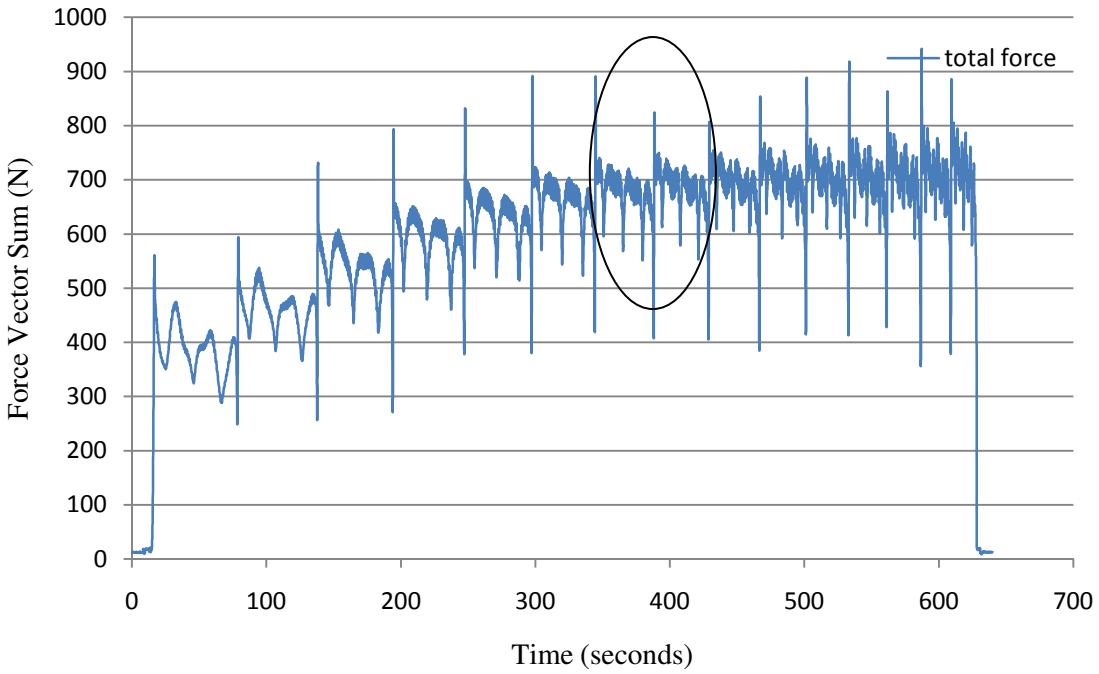

Fig. 70. Force developed for the three lobed part.

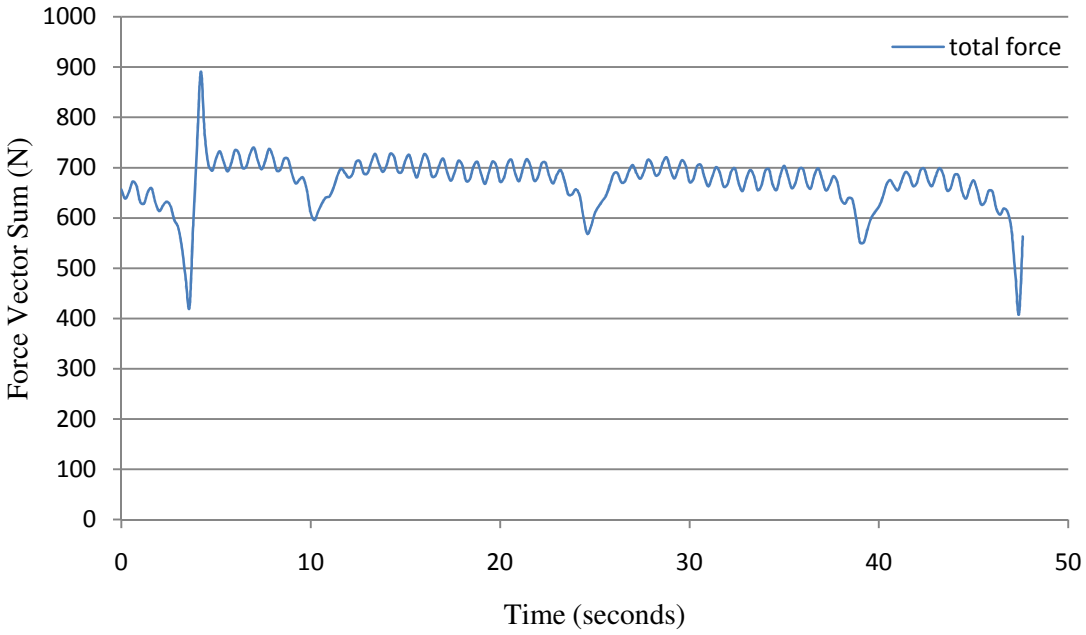

Fig. 71. Steady state force developed for the three lobed part.

The experimental force values obtained during forming of the three lobed part were compared with the force data obtained from the pyramid and cone numerical models having the same parameters and is presented in Figure 72.

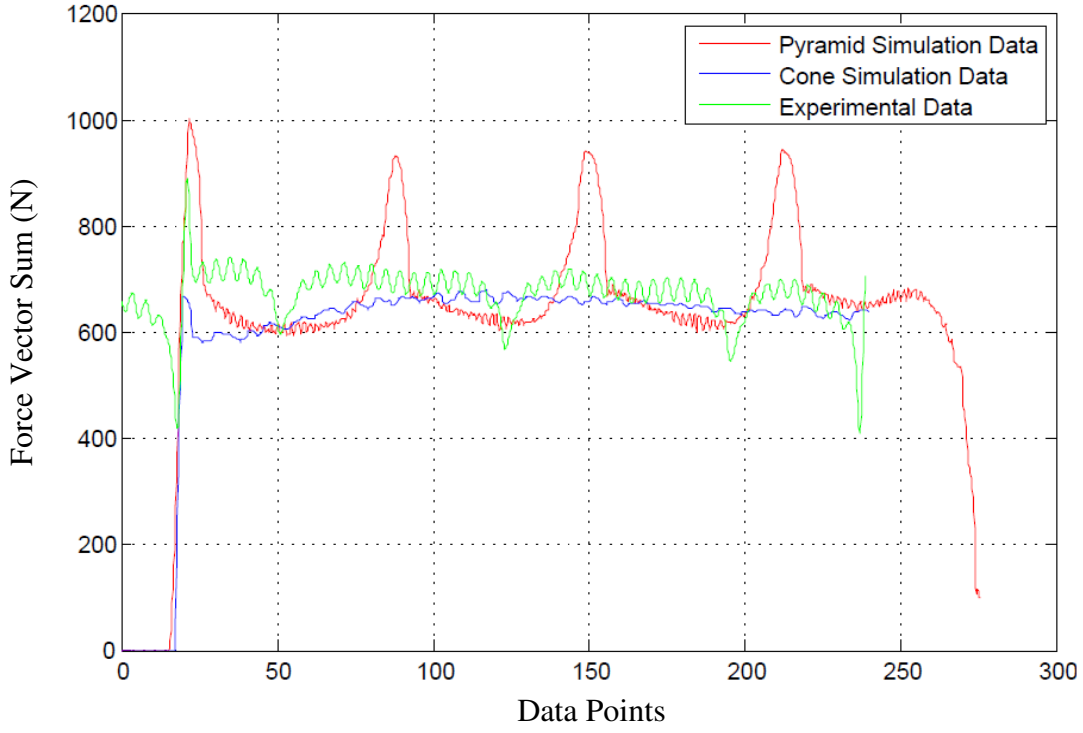

Fig. 72. Comparison between the experimentally obtained force for the three lobed part and the force obtained from the pyramid and cone numerical models for the same conditions.

With reference to Figure 72, it was seen that the error between the experimental and the simulation peak force value was around 10% and the error in the forces at the region after the peak force was about 8 %, which was a good fit.

6.3.2. Four lobed part

The four lobed shape had four circles, each having a diameter of 25 mm. The four lobed model was formed to a depth of 25 mm. Figure 73 shows the final shape of the four lobed part.

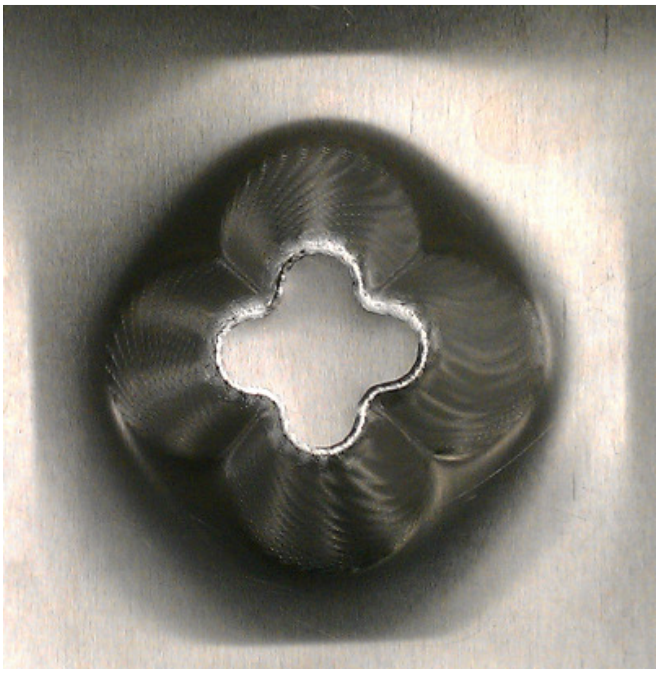

Fig. 73. Four lobed part.

The experimental data collected during the forming of the four lobed part is presented in Figure 74. The steady state region which was selected for analysis is circled and shown separately in Figure 75. The blank used had a thickness of 0.8 mm, and the step size used was 1.27 mm. The tool used had a radius of 6.35 mm. In the case of the

four lobed part, a spiral tool path was used to form the shape. It was mentioned by Duflou and Tunckol (2006) that the spiral tool path and the contour path gave the same deformation force. The experiment was performed using spiral tool path to check if the model could predict deformation forces generated using spiral tool path.

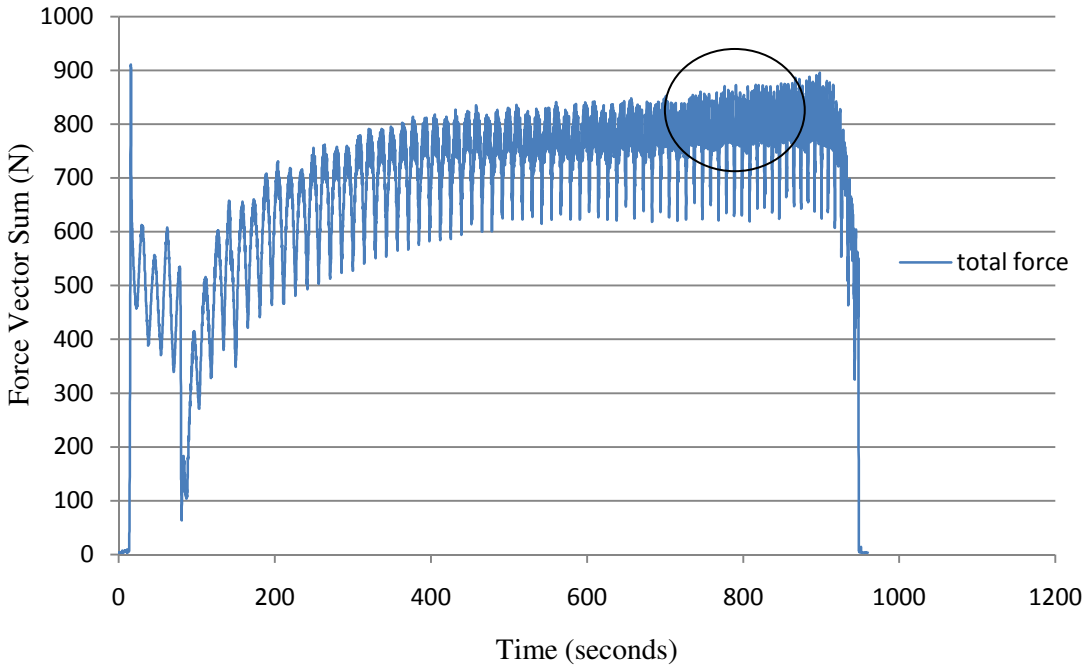

Fig. 74. Force developed for the four lobed part.

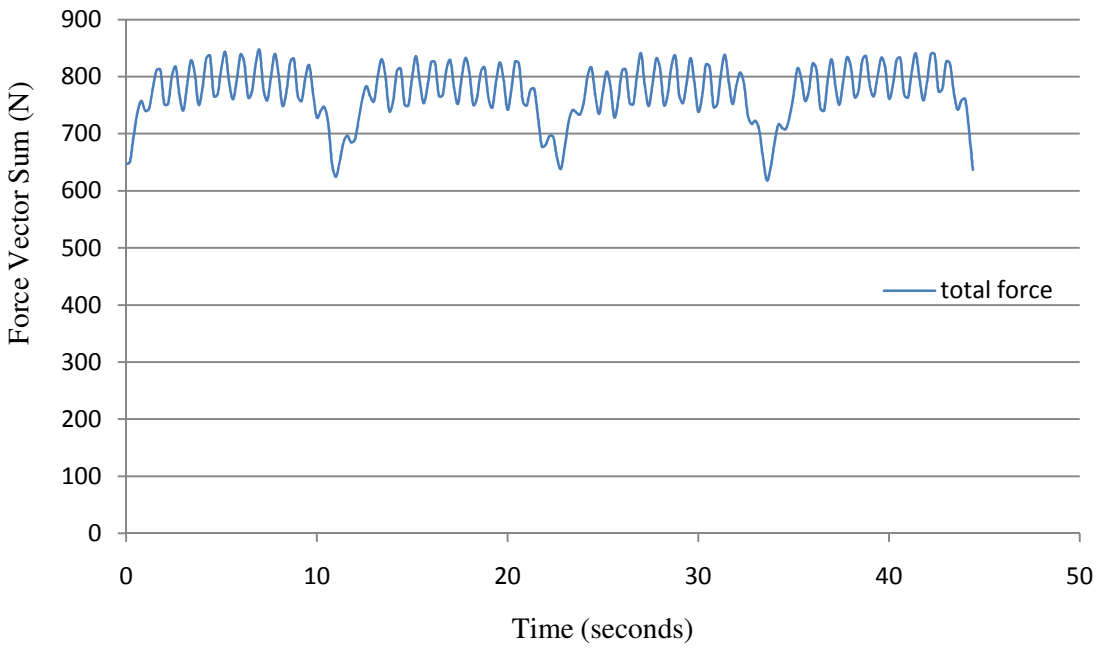

Fig. 75. Steady State force developed for the four lobed part.

The force values measured during forming of the four lobed part were compared with the force data obtained from the pyramid model for the same parameters and is presented in Figure 76.

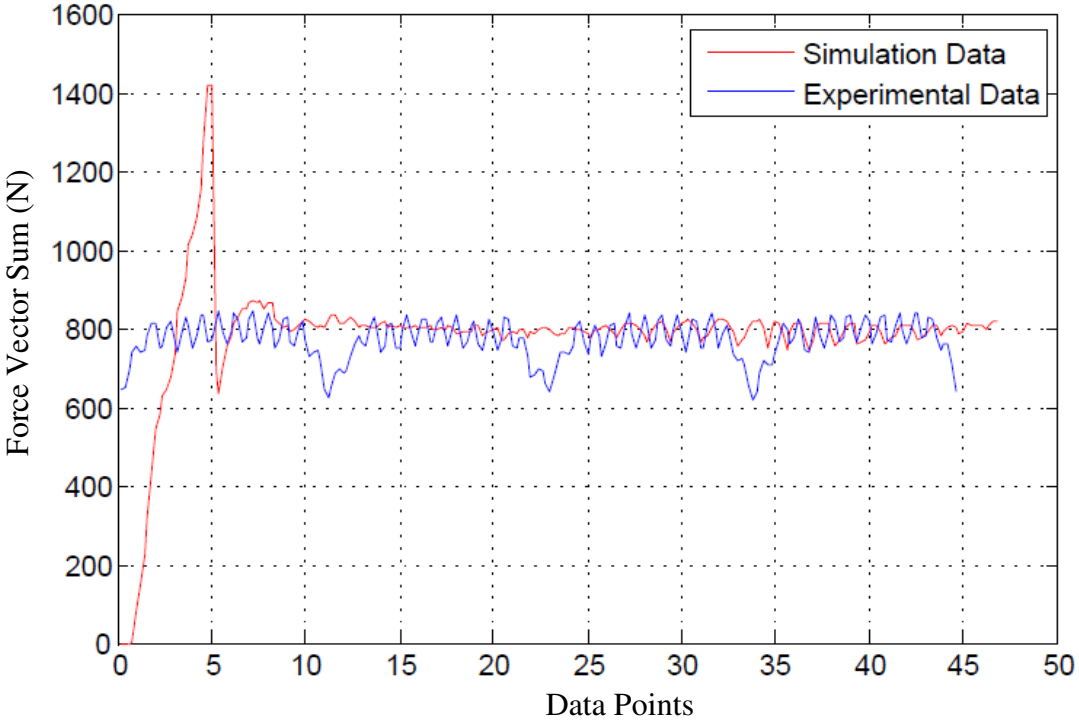

Fig. 76. Comparison between the experimentally obtained force for the four lobed part and the force obtained from the pyramid model for the same conditions.

Since the experimental data had only the flat deformation force due to the spiral tool path, only a straight line was simulated using the pyramid model to save computational time. The simulation took about 2 hours of CPU time using 4 nodes each having the IBM Power5+ processor running at 1. 9 GHz. The force peak shown in the simulation data in Figure 76 was the force on the tool when it took a step down. The rest of the values are the deformation forces acting on the tool as it moved along the sides of the pyramid. Neglecting the force peak and comparing the values, it was seen that the average error was only 6 %, which was quite close to the experimental data.

Based on the results presented above, it was noticed that the numerical models developed could be used to effectively predict forces for any shape with any set of process parameters. The new force modeling technique where the simulation begins at a preset depth was validated by comparing forces measured during forming of new arbitrary shapes. The force models were seen to predict the forces to a reasonable extent provided the radii were not too small. The numerical model developed was seen to predict the steady state forces accurately when both contour and spiral tool paths were used.

7. CONCLUSIONS AND FUTURE WORK

Incremental sheet forming is a novel method of manufacturing which is increasingly gaining attention as a viable manufacturing method in the industry. The ability to predict the forces which would be developed during forming operation could help obtain higher dimensional accuracy during manufacturing and protect the machining set up from failure.

7.1. Conclusion

The work done in the present thesis contributed to the problem of force prediction in incremental sheet forming in the following ways:

1) The vector sum of forces for a pyramid and cone were found to be the same for the same set of input conditions. This meant the incremental sheet forming is a localized process where the force on the tool just depends on the area in contact between the tool and the sheet. The force was seen to not depend on the path taken by the tool.
2) A numerical modeling technique was developed which simulated the deformation of the sheet during forming. The advantages of this technique are the greater accuracy and significantly lesser computational requirements as compared to the presently available models.
3) The numerical simulation of the tool deforming the sheet metal was performed at a prescribed depth. The forces obtained from the simulation were seen to agree

well with the experimental data. The high degree of correspondence between the numerical and measured values verified the initial observation that the force acting on the tool depends just on the contact area and not on the tool path for reasonably large radii.

4) New arbitrary shapes were formed and the forces obtained experimentally were compared to the forces obtained from the simulation and it was seen to have a good match. The numerical model was seen to predict steady state forces accurately for parts made using contour tool path and spiral tool paths.
5) The numerical model developed was thus validated by comparing the results obtained from previous simulations to the results obtained during forming of the new arbitrary shapes.

7.2. Future work

The goal of this research was to provide a numerical method to predict the forces generated during incremental sheet forming. Some of the future research work that could be pursued is listed below:

1) Develop an analytical model which could predict the forces generated during forming as a function of the process and material parameters used.
2) Use the present numerical models developed to study the strain and stresses developed during the forming operation. The stresses can be studied to predict the failure of the metal during the forming operation by setting a failure criterion.
3) Improve the numerical model by including the effects of anisotropy and kinematic hardening of the material.

REFERENCES

Aerens, R., Eyckens, P., Van Bael, A., Duflou, J., 2010. Force prediction for single point incremental forming deduced from experimental and FEM observations. The International Journal of Advanced Manufacturing Technology 46, 969-982.

Ambrogio, G., Duflou, J., Filice, L., Aerens, R., 2007. Some considerations on force trends in Incremental Forming of different materials. In: Proceedings of the 10th ESAFORM conference on material forming, AIP Conference Proceedings, pp. 193-198.

Ambrogio, G., Filice, L., Micari, F., 2006. A force measuring based strategy for failure prevention in incremental forming. Journal of Materials Processing Technology 177, 413-416.

Amino, H., Lu, Y., Maki, T., Osawa, S., Fukuda, K., 2002. Dieless NC forming, prototype of automotive service parts. In: Proceedings of the 2nd International Conference on Rapid Prototyping and Manufacturing, Beijing.

Bouffioux, C., Henrard, C., Eyckens, P., Aerens, R., Van Bael, A., Sol, H., Duflou, J., Habraken, A., 2008. Comparison of the tests chosen for material parameter identification to predict single point incremental forming forces. In: Proceedings of the IDDRG 2008 Conference, Olofström, Sweden, pp. 133-144.

Duflou, J., Callebaut, B., Verbert, J., De Baerdemaeker, H., 2007a. Laser assisted incremental forming: formability and accuracy improvement. CIRP Annals-Manufacturing Technology 56, 273-276.

Duflou, J., Tunckol, Y., 2006. Force modelling for single point incremental forming. In: Proceedings of the 9th ESAFORM Conference on Material Forming, Glasgow, pp. 287-290.

Duflou, J.R., Szekeres, A., Vanherck, P., 2005. Force measurements for single point incremental forming: an experimental study. Advanced Materials Research 6, 441-448.

Duflou, J.R., Tunckol, Y., Aerens, R., 2007b. Force analysis for single point incremental forming. Key Engineering Materials 344, 543-550.

Durante, M., Formisano, A., Langella, A., Capece Minutolo, F.M., 2009. The influence of tool rotation on an incremental forming process. Journal of Materials Processing Technology 209, 4621-4626.

Emmens, W., Van den Boogaard, A., 2009. An overview of stabilizing deformation mechanisms in incremental sheet forming. Journal of Materials Processing Technology 209, 3688-3695.

Eyckens, P., Van Bael, A., Aerens, R., Duflou, J., Van Houtte, P., 2008. Small-scale finite element modelling of the plastic deformation zone in the incremental forming process. International Journal of Material Forming 1, 1159-1162.

Filice, L., Ambrogio, G., Micari, F., 2006. On-line control of single point incremental forming operations through punch force monitoring. CIRP Annals-Manufacturing Technology 55, 245-248.

Filice, L., Fratini, L., Micari, F., 2002. Analysis of material formability in incremental forming. CIRP Annals-Manufacturing Technology 51, 199-202.

Flores, P., Duchene, L., Bouffioux, C., Lelotte, T., Henrard, C., Pernin, N., Van Bael, A., He, S., Duflou, J., Habraken, A., 2007. Model identification and FE simulations: Effect of different yield loci and hardening laws in sheet forming. International journal of plasticity 23, 420-449.

Hagan, E., Jeswiet, J., 2003. A review of conventional and modern single-point sheet metal forming methods. In: Proceedings of the Institution of Mechanical Engineers, Part B: Journal of Engineering Manufacture 217, pp. 213-225.

Ham, M., Jeswiet, J., 2006. Single point incremental forming and the forming criteria for AA3003. CIRP Annals-Manufacturing Technology 55, 241-244.

Ham, M., Jeswiet, J., 2008. Single point incremental forming. International Journal of Materials and Product Technology 32, 374-387.

He, S., Van Bael, A., Van Houtte, P., Duflou, J.R., Szekeres, A., Henrard, C., Habraken, A.M., 2005a. Finite Element Modeling of Incremental Forming of Aluminum Sheets. Advanced Materials Research 6, 525-532.

He, S., Van Bael, A., Van Houtte, P., Tunckol, Y., Duflou, J., Henrard, C., Bouffioux, C., Habraken, A., 2005b. Effect of FEM choices in the modelling of incremental forming of aluminium sheets. In: Proceedings of the 8th ESAFORM Conference on Material Forming, Cluj Napoca, pp. 711-714.

Henrard, C., Habraken, A.M., Szekeres, A., Duflou, J.R., He, S., Van Bael, A., Van Houtte, P., 2005. Comparison of FEM simulations for the incremental forming process. Advanced Materials Research 6, 533-542.

Iseki, H., 2001. An approximate deformation analysis and FEM analysis for the incremental bulging of sheet metal using a spherical roller. Journal of Materials Processing Technology 111, 150-154.

Jackson, K., Allwood, J., 2009. The mechanics of incremental sheet forming. Journal of Materials Processing Technology 209, 1158-1174.

Jackson, K., Allwood, J., Landert, M., 2008. Incremental forming of sandwich panels. Journal of Materials Processing Technology 204, 290-303.

Jeswiet, J., 2005. Asymmetric incremental sheet forming. Advanced Materials Research 6, 35-58.

Jeswiet, J., Ali, A., 2000. Incremental single point forming. In: Proceedings of the ASME, Manufacturing in Engineering Division 11, pp. 509–514.

Jeswiet, J., Duflou, J.R., Szekeres, A., Lefebvre, P., 2005a. Custom manufacture of a solar cooker–a case study. Advanced Materials Research 6, 487-492.

Jeswiet, J., Hagan, E., 2001. Rapid prototyping of a headlight with sheet metal. In: Proceedings of Shelmet, pp. 165-170.

Jeswiet, J., Hagan, E., 2003. Rapid prototyping non-uniform shapes from sheet metal using CNC single point incremental forming. Transactions of North American Manufacturing Research Institute/SME XXXI, 65-69.

Jeswiet, J., Hagan, E., Szekeres, A., 2002. Forming parameters for incremental forming of aluminium alloy sheet metal. In: Proceedings of the Institution of Mechanical Engineers, Part B: Journal of Engineering Manufacture 216, 1367-1371.

Jeswiet, J., Micari, F., Hirt, G., Bramley, A., Duflou, J., Allwood, J., 2005b. Asymmetric single point incremental forming of sheet metal. CIRP Annals-Manufacturing Technology 54, 88-114.

Jeswiet, J., Szekeres, A., 2005. Forces in single point incremental forming. Transactions of North American Manufacturing Research Institute/SME 33, 399-403.

Jeswiet, J., Young, D., 2005. Forming limit diagrams for single-point incremental forming of aluminium sheet. In: Proceedings of the Institution of Mechanical Engineers, Part B: Journal of Engineering Manufacture 219, pp. 359-364.

Kim, Y., Park, J., 2002. Effect of process parameters on formability in incremental forming of sheet metal. Journal of Materials Processing Technology 130, 42-46.

Marciniak, Z., Duncan, J.L., Hu, J., 2002. Combined bending and tension of sheet, Mechanics of sheet metal forming, 2 ed. Butterworth-Heinemann, pp. 136-151.

Ozturk, F., Toros, S., Kilic, S., 2008. Evaluation of tensile properties of 5052 type aluminum-magnesium alloy at warm temperatures. Archives of Materials Science and Engineering 34, 95-98.

Park, J.J., Kim, Y.H., 2003. Fundamental studies on the incremental sheet metal forming technique. Journal of Materials Processing Technology 140, 447-453.

Petek, A., Kuzman, K., Kopac , J., 2009. Deformations and forces analysis of single point incremental sheet metal forming. Archives of Materials Science 35, 107-116.

Pohlak, M., Majak, J., Küttner, R., 2007. Incremental sheet forming process modelling-limitation analysis. Journal of Achievements in Materials and Manufacturing Engineering 22, 67–70.

Reddy, N.V., Cao, J., 2010. Incremental Sheet Metal Forming: A Review. Department of Mechanical Engineering, Indian Institute of Technology Kanpur, Kanpur, India. nvr@ iitk. ac. in; Department of Mechanical Engineering, Northwestern University, Evanston, IL,60208 USA, April 2010.

Shim, M.S., Park, J.J., 2001. The formability of aluminum sheet in incremental forming. Journal of Materials Processing Technology 113, 654-658.

Silva, M., Skjoedt, M., Martins, P.A.F., Bay, N., 2008. Revisiting the fundamentals of single point incremental forming by means of membrane analysis. International Journal of Machine Tools and Manufacture 48, 73-83.

Sortais, H.C., Kobayashi, S., Thomsen, E.G., 1963. Mechanics of conventional spinning. Transactions of the ASME,Series B, Journal of Engineering for Industry 85, 346-350.

APPENDIX A

EXPERIMENTS CONDUCTED

The following section presents the results of experiments done for the pyramid and cone shapes. For the sake of conciseness, only the graph showing all the three steady state force components would be shown for each experiment. The process parameters are mentioned below each figure.

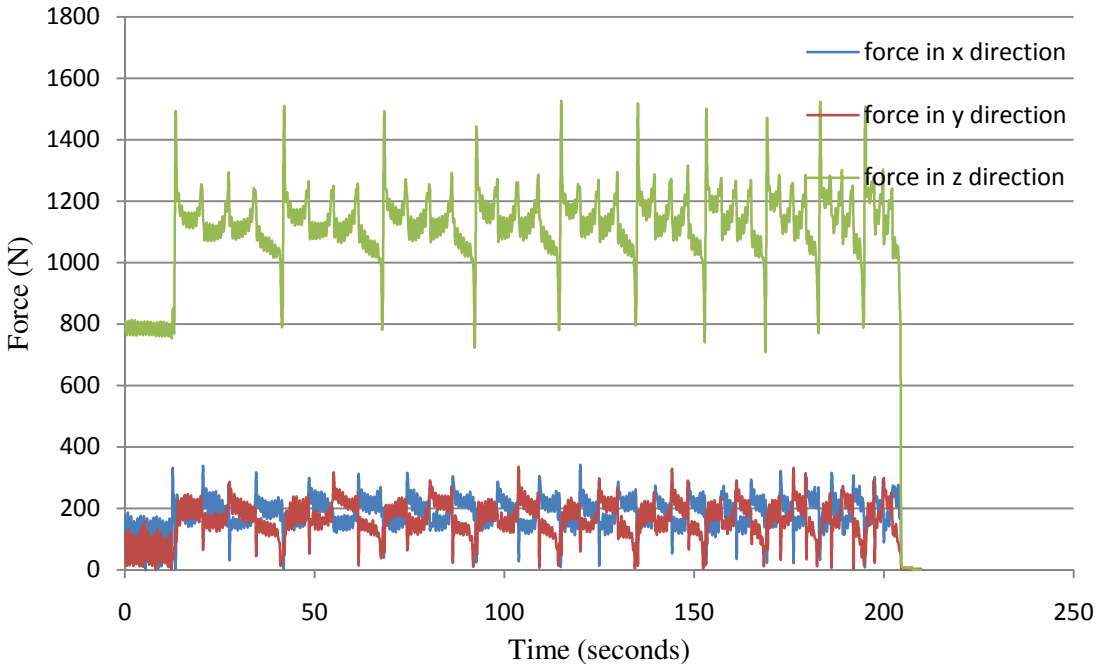

Fig. A1. Force developed for pyramid having wall angle of 30 degrees. Tool has a radius of 6.35 mm and a step size of 0.635 mm. sheet thickness is 1.27 mm.

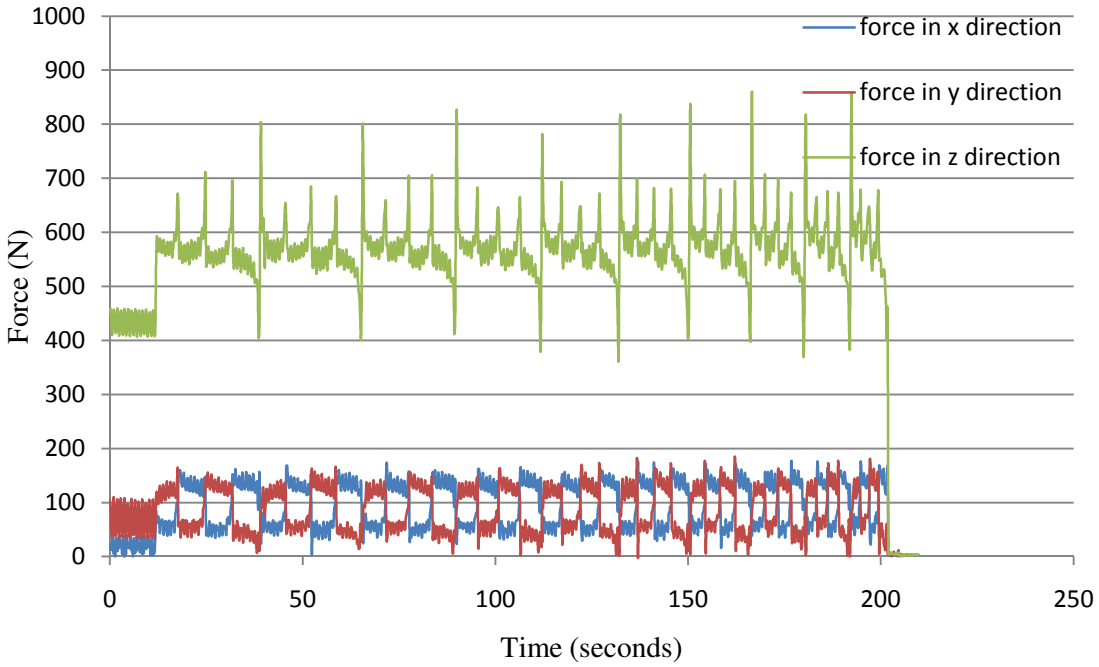

Fig. A2. Force developed for pyramid having wall angle of 30 degrees. Tool has a radius of 6.35 mm and a step size of 0.635 mm. sheet thickness is 0.8 mm.

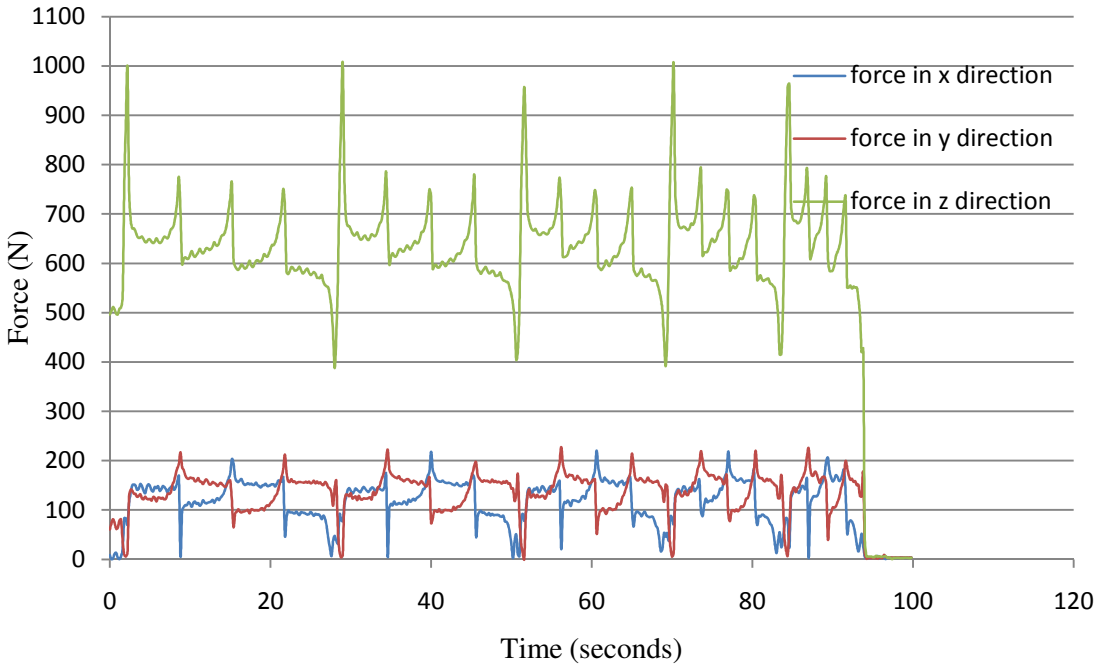

Fig. A3. Force developed for pyramid having wall angle of 30 degrees. Tool has a radius of 6.35 mm and a step size of 1.27 mm. Sheet thickness is 0.8 mm.

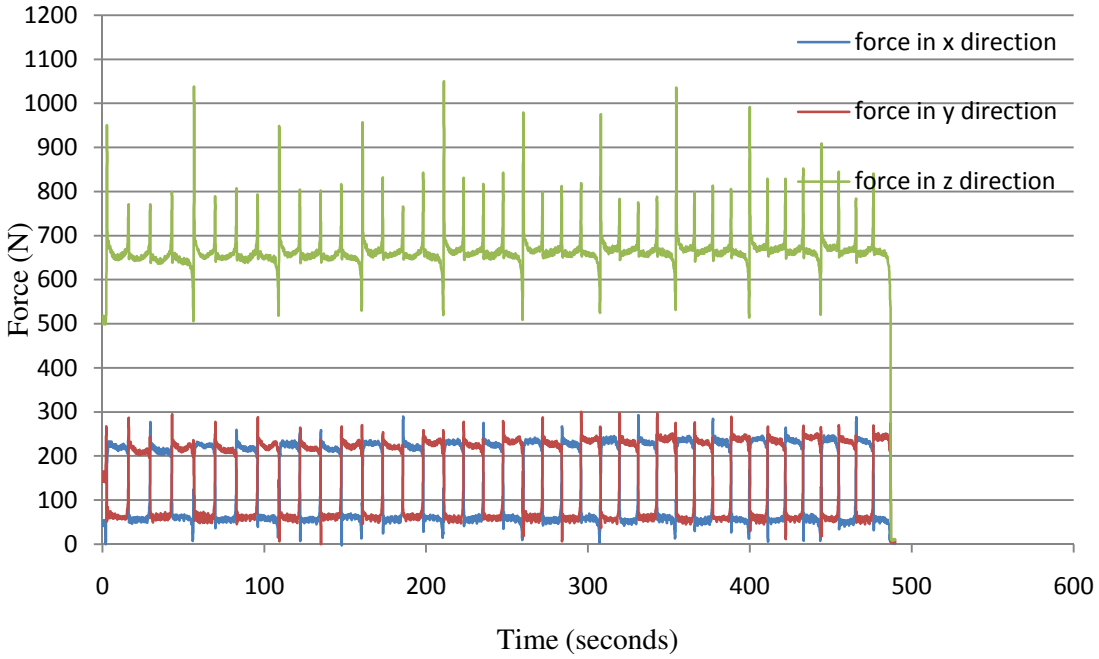

Fig. A4. Force developed for pyramid having wall angle of 45 degrees. Tool has a radius of 6.35 mm and a step size of 0.635 mm. sheet thickness is 0.8 mm.

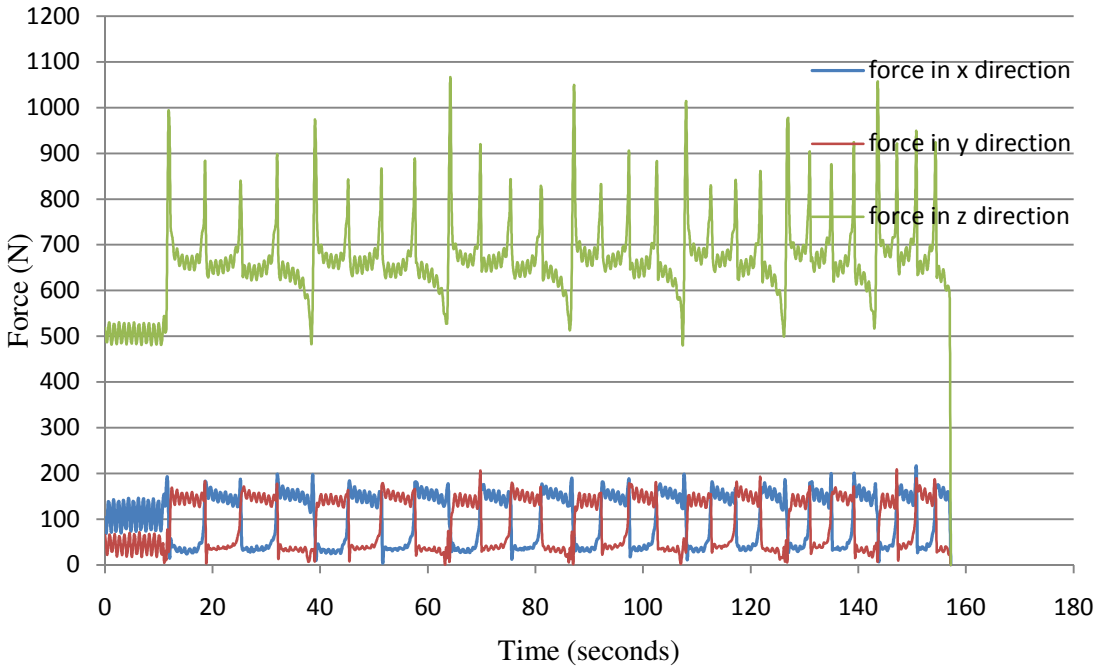

Fig. A5. Force developed for pyramid having wall angle of 30 degrees. Tool has a radius of 9.525 mm and a step size of 0.635 mm. sheet thickness is 0.8 mm.

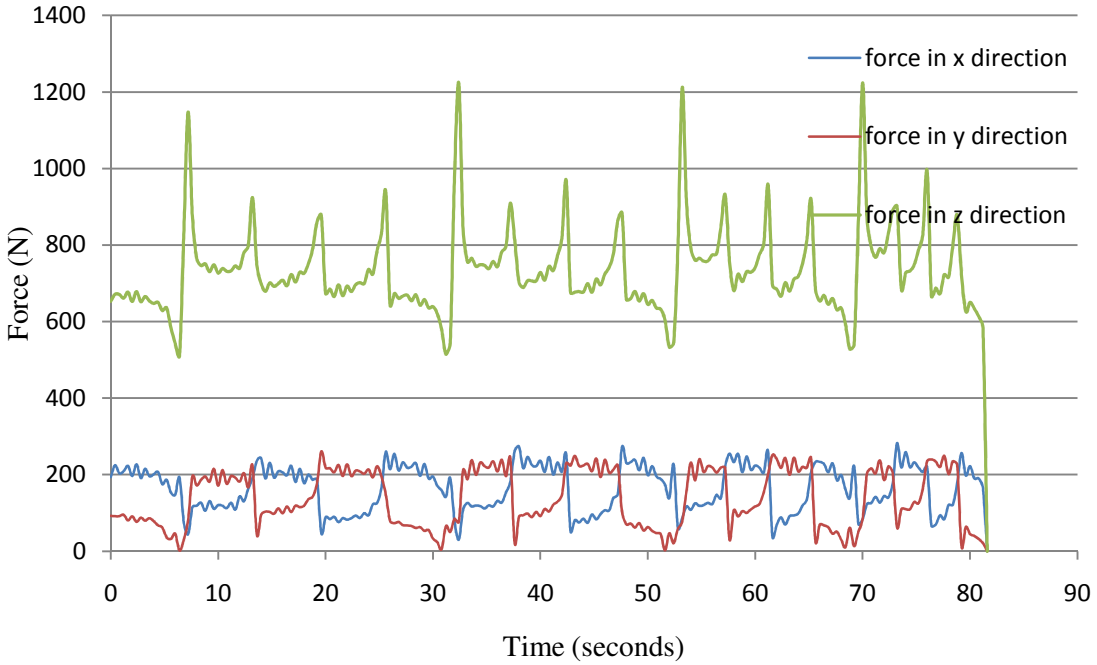

Fig. A6. Force developed for pyramid having wall angle of 30 degrees. Tool has a radius of 9.525 mm and a step size of 1.27 mm. Sheet thickness is 0.8 mm.

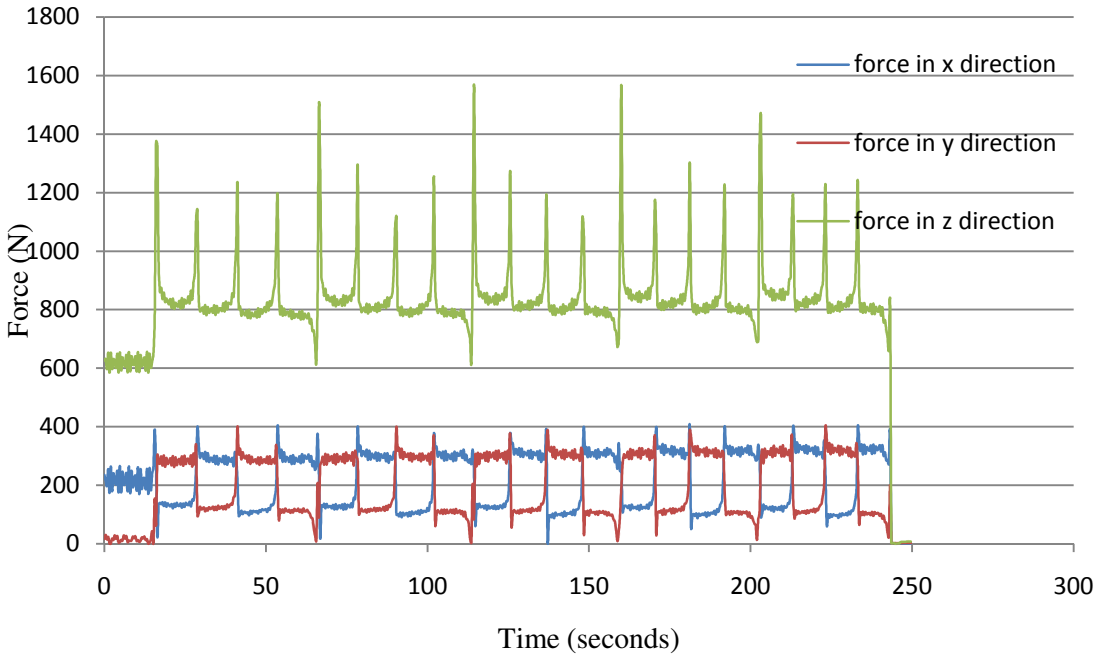

Fig. A7. Force developed for pyramid having wall angle of 45 degrees. Tool has a radius of 9.525 mm and a step size of 1.27 mm. Sheet thickness is 0.8 mm.

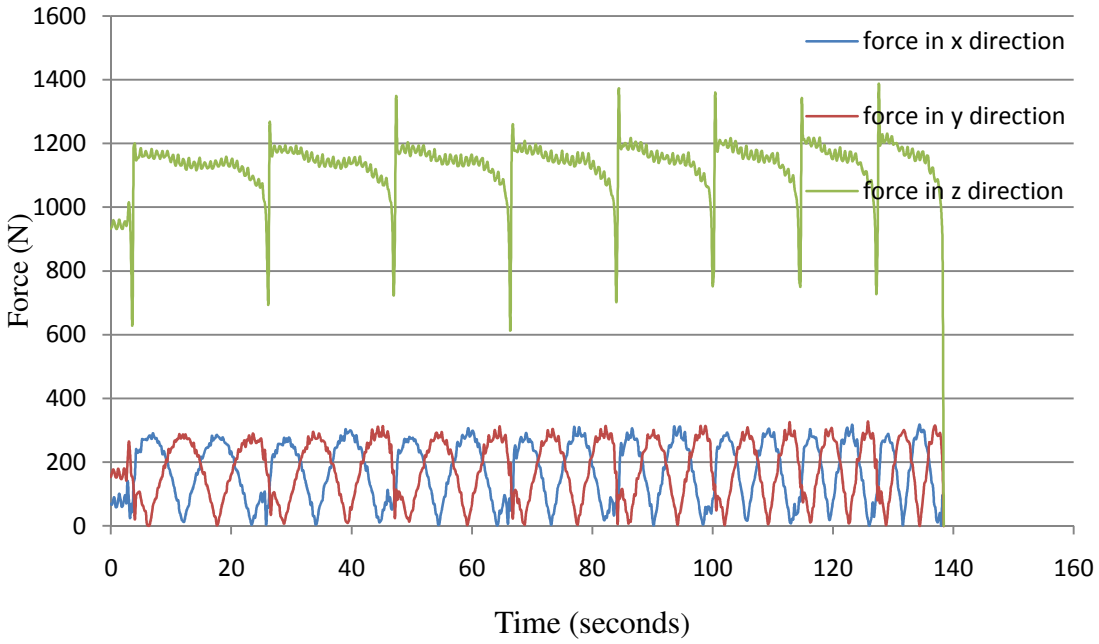

Fig. A8. Force developed for cone having wall angle of 30 degrees. Tool has a radius of 6.35 mm and a step size of 0.635 mm. sheet thickness is 1.27 mm.

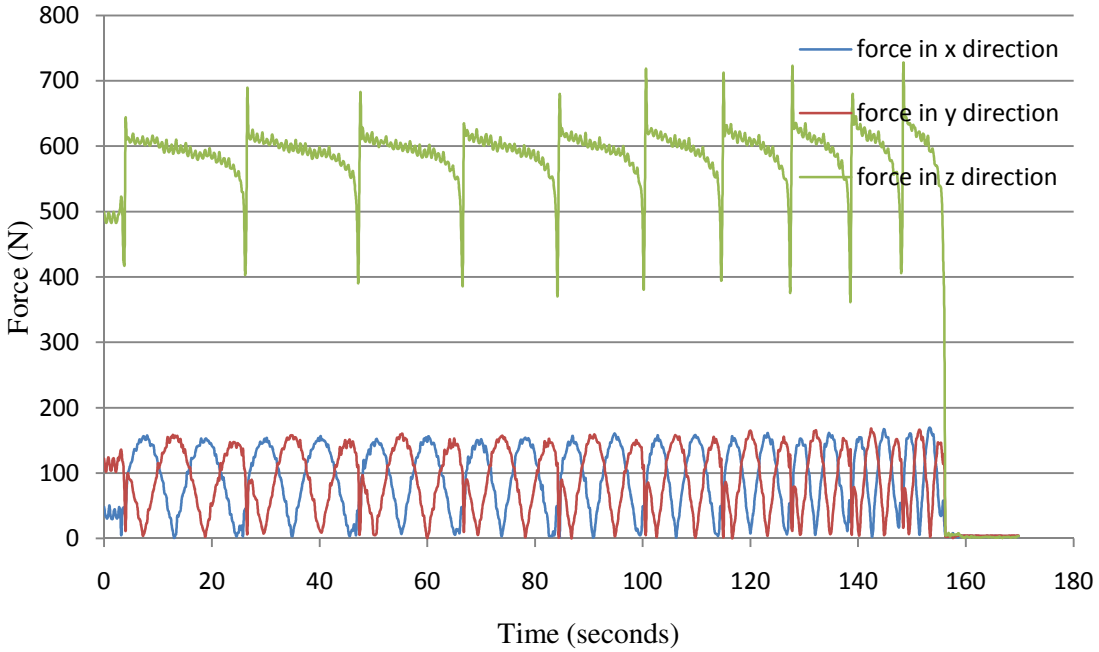

Fig. A9. Force developed for cone having wall angle of 30 degrees. Tool has a radius of 6.35 mm and a step size of 0.635 mm. sheet thickness is 0.8 mm.

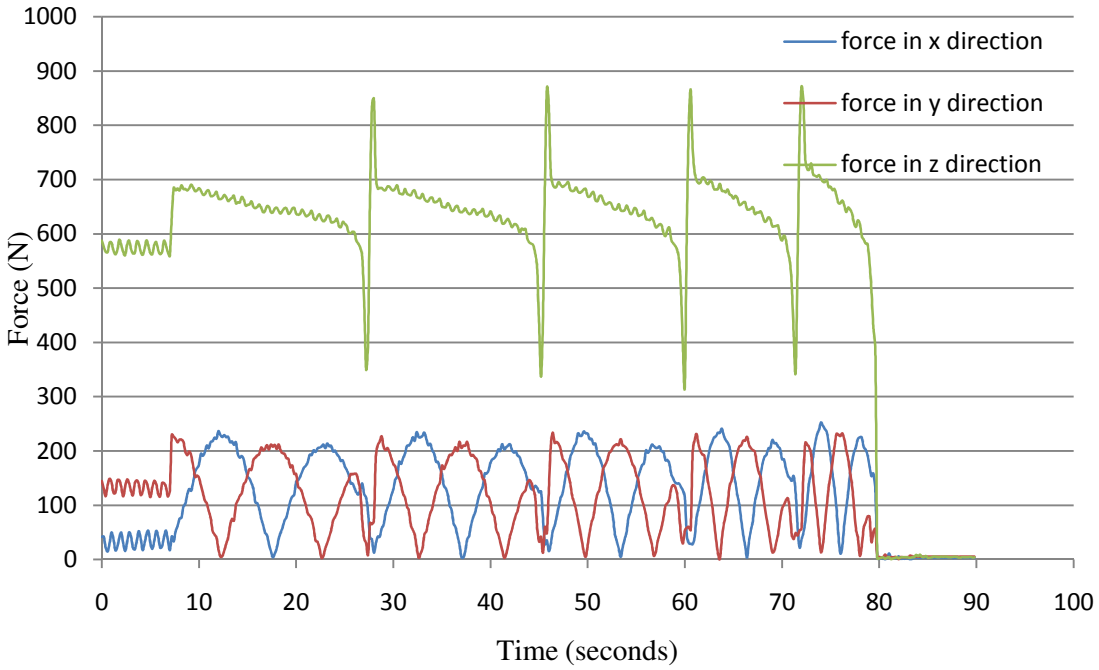

Fig. A10. Force developed for cone having wall angle of 30 degrees. Tool has a radius of 6.35 mm and a step size of 1.27 mm. sheet thickness is 0.8 mm.

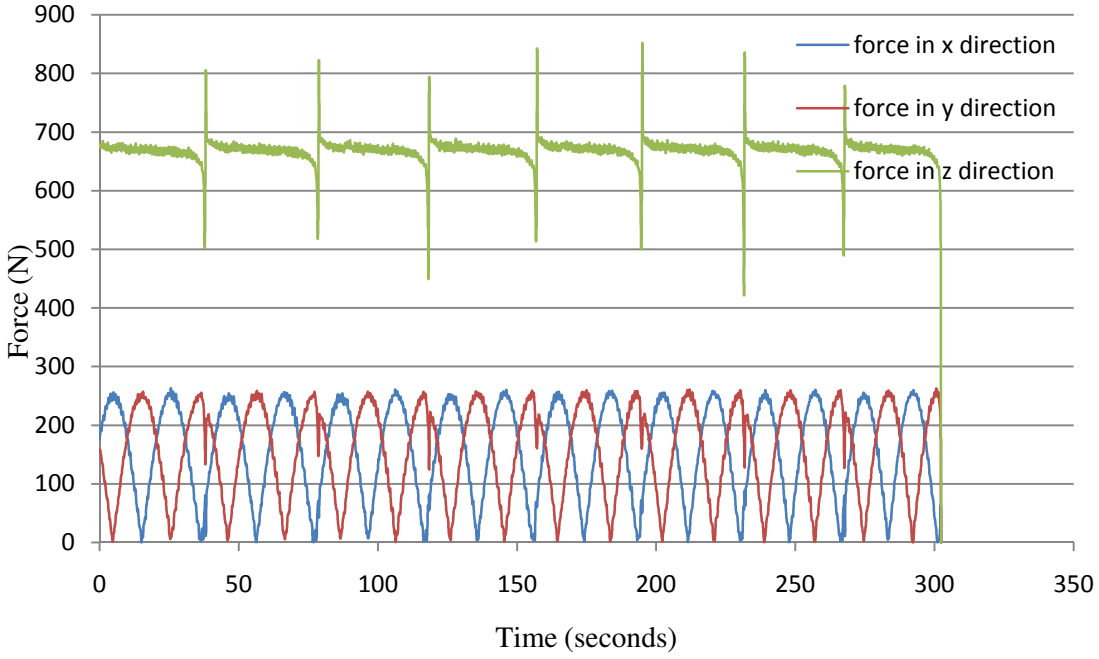

Fig. A11. Force developed for cone having wall angle of 45 degrees. Tool has a radius of 6.35 mm and a step size of 0.635 mm. sheet thickness is 0.8 mm.

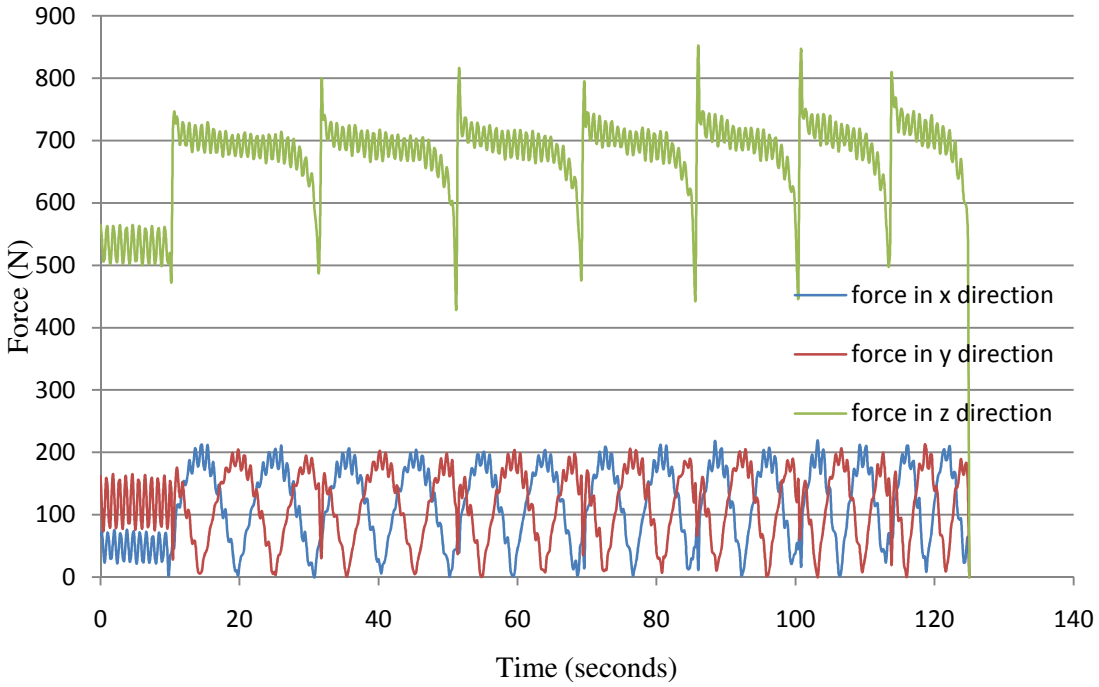

Fig. A12. Force developed for cone having wall angle of 30 degrees. Tool has a radius of 9.525 mm and a step size of 0.635 mm. sheet thickness is 0.8 mm.

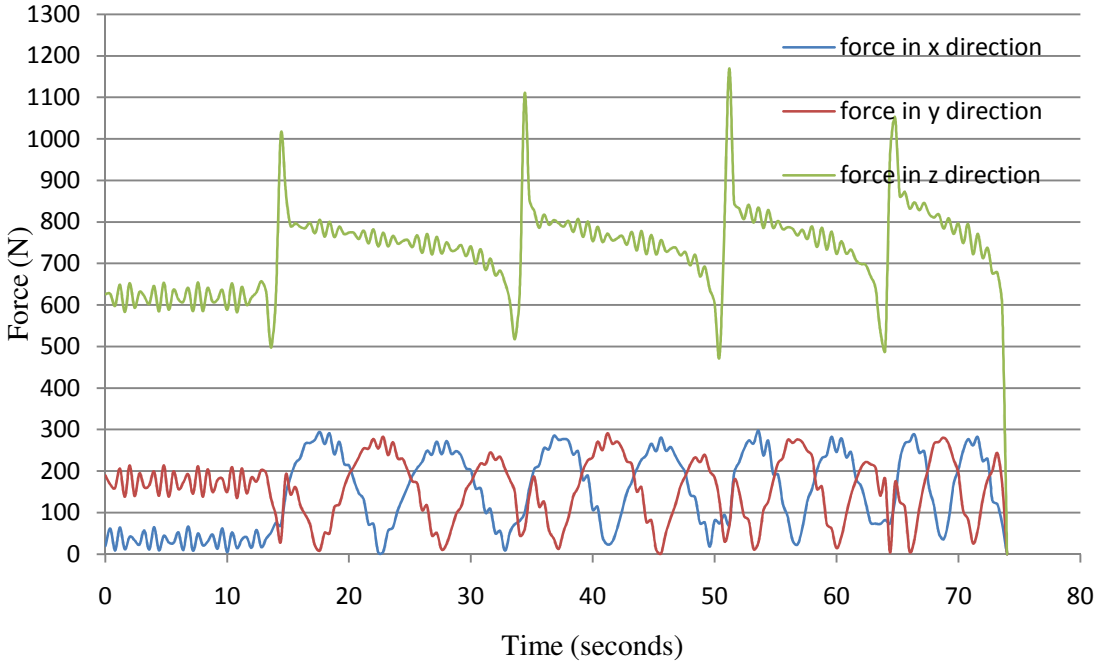

Fig. A13. Force developed for cone having wall angle of 30 degrees. Tool has a radius of 9.525 mm and a step size of 1.27 mm. sheet thickness is 0.8 mm.

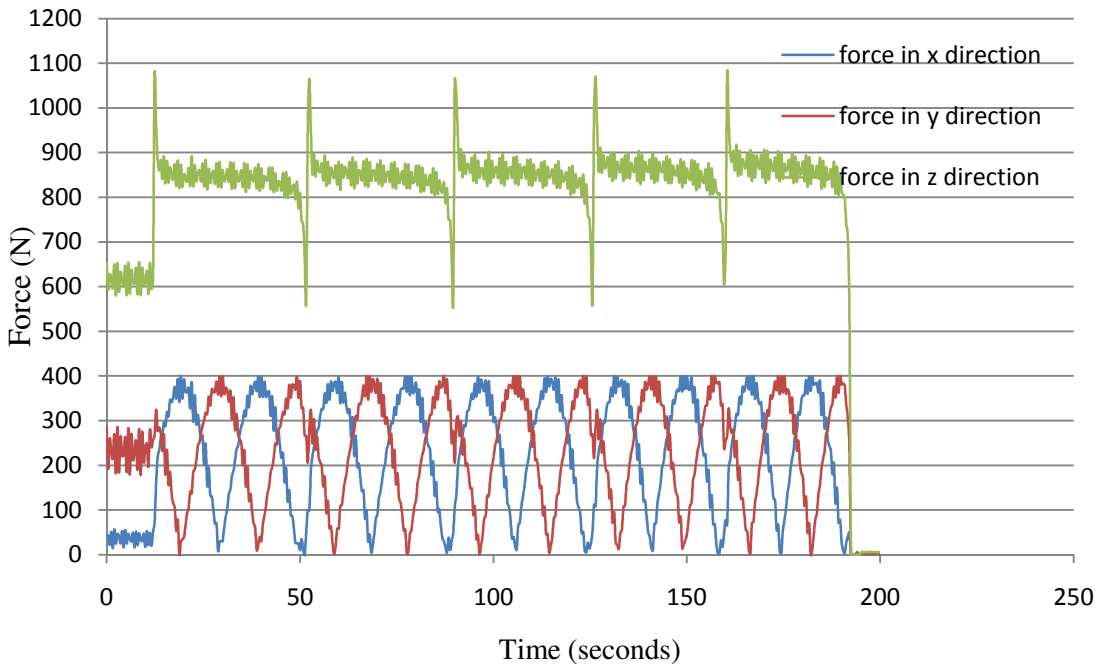

Fig. A14. Force developed for cone having wall angle of 45 degrees. Tool has a radius of 9.525 mm and a step size of 1.27 mm. sheet thickness is 0.8 mm.

APPENDIX B

INPUT FILES USED FOR SIMULATIONS

This section presents the input files generated by ABAQUS used for the simulations. Due to the large size of the files, the information containing the geometry of the shapes and the tool have been removed and presented.

1) Reference model, Pyramid wall angle 30 degrees, tool radius 6.35 mm, 1.27 mm step size, sheet thickness 0.815 mm.

```
*Heading
Pyramid 30 degrees wall angle, tool radius 6.35 mm, 1.27 mm step size,
sheet thickness 0.815 mm
** Job name: friction01
Model name: Model-1
** Generated by: Abaqus/CAE 6.9-EF1
*Preprint, echo=NO, model=NO, history=NO, contact=NO
**
** PARTS
**
*Part, name="pyramid30 005"
*End Part
**
*Part, name=tool
*End Part
**
**
** ASSEMBLY
**
*Assembly, name=Assembly
**
*Instance, name="pyramid30 005-1", part="pyramid30 005"

*Element, type=S4R
1,   1,  25, 521,  28
*Nset, nset=_PickedSet16, internal, generate
    1,  6509,     1
*Elset, elset=_PickedSet16, internal, generate
    1,  6504,     1
** Section: Section-1
*Shell Section, elset=_PickedSet16, material=aluminum
0.815, 5
*End Instance
**
*Instance, name=tool-1, part=tool
```

```
45.370200355962,     -45.3702,    12.628901
45.370200355962,     -45.3702,    12.628901, 44.370200355962,     -
45.3702,    12.628901,          90.
*Node
      1,           0.,  -1.09322062e-16,           0.
*Nset, nset=tool-1-RefPt_, internal
1,
*Surface, type=REVOLUTION, name=RigidSurface_, internal
START,           0.,           0.
 LINE,         6.35,           0.
 CIRCL,           0., -6.42109904378676,           0., -
0.0707054138183594
*Rigid Body, ref node=tool-1-RefPt_, analytical surface=RigidSurface_
*End Instance
*Nset, nset=_PickedSet29, internal, instance="pyramid30 005-1"
*Elset, elset=_PickedSet29, internal, instance="pyramid30 005-1",
generate
  1,  96,   1
*Nset, nset=_PickedSet87, internal, instance=tool-1
 1,
*Elset, elset=__PickedSurf33_SPOS, internal, instance="pyramid30 005-
1", generate
 1322,  2546,     1
*Surface, type=ELEMENT, name=_PickedSurf33, internal
__PickedSurf33_SPOS, SPOS
*Elset, elset=__PickedSurf35_SPOS, internal, instance="pyramid30 005-
1", generate
   97,  1321,     1
*Surface, type=ELEMENT, name=_PickedSurf35, internal
__PickedSurf35_SPOS, SPOS
*Elset, elset=__PickedSurf37_SPOS, internal, instance="pyramid30 005-
1", generate
 3772,  4996,     1
*Surface, type=ELEMENT, name=_PickedSurf37, internal
__PickedSurf37_SPOS, SPOS
*Elset, elset=__PickedSurf39_SPOS, internal, instance="pyramid30 005-
1", generate
 2547,  3771,     1
*Surface, type=ELEMENT, name=_PickedSurf39, internal
__PickedSurf39_SPOS, SPOS
*Elset, elset=__PickedSurf47_SNEG, internal, instance="pyramid30 005-
1", generate
 4997,  6221,     1
*Surface, type=ELEMENT, name=_PickedSurf47, internal
__PickedSurf47_SNEG, SNEG
*End Assembly
**
** MATERIALS
**
*Material, name=aluminum
*Elastic
70300., 0.3
*Plastic
     40.,         0.
```

```
 49.4048, 0.00634851
 66.6667, 0.00866707
 82.7381,  0.0103615
 98.2143,  0.0114234
 131.548,  0.0154365
  161.31,  0.0182182
 169.643,  0.0206638
 177.976,  0.0237504
 185.714,  0.0268454
 192.857,   0.031231
 198.214,   0.035001
 205.952,  0.0393781
 219.643,  0.0462346
 222.619,  0.0506795
 227.976,  0.0538084
 230.952,  0.0569712
 231.548,  0.0614499
   237.5,  0.0652114
   237.5,  0.0684165
 245.238,  0.0721526
 241.071,   0.076699
 247.619,   0.080452
  248.81,  0.0862043
 252.381,  0.0944869
 246.429,   0.102264
**
** INTERACTION PROPERTIES
**
*Surface Interaction, name=_Int-1-Prop
1.,
*Friction, slip tolerance=0.005
 0.1,
*Surface Behavior, pressure-overclosure=HARD
*Surface Interaction, name=_Int-2-Prop
1.,
*Friction, slip tolerance=0.005
 0.1,
*Surface Behavior, pressure-overclosure=HARD
*Surface Interaction, name=_Int-3-Prop
1.,
*Friction, slip tolerance=0.005
 0.1,
*Surface Behavior, pressure-overclosure=HARD
*Surface Interaction, name=_Int-4-Prop
1.,
*Friction, slip tolerance=0.005
 0.1,
*Surface Behavior, pressure-overclosure=HARD
*Surface Interaction, name=_Int-5-Prop
1.,
*Friction, slip tolerance=0.005
 0.1,
*Surface Behavior, pressure-overclosure=HARD
*Surface Interaction, name=friction
```

```
1.,
*Friction, slip tolerance=0.005
 0.1,
*Surface Behavior, pressure-overclosure=HARD
*Surface Interaction, name="friction 01"
1.,
*Friction, slip tolerance=0.005
 0.1,
*Surface Behavior, pressure-overclosure=HARD
*Surface Interaction, name="friction 02"
1.,
*Friction, slip tolerance=0.005
 0.2,
*Surface Behavior, pressure-overclosure=HARD
*Surface Interaction, name=nofric
1.,
*Friction, slip tolerance=0.005
 0.05,
*Surface Behavior, pressure-overclosure=HARD
**
** BOUNDARY CONDITIONS
**
** Name: clamp Type: Symmetry/Antisymmetry/Encastre
*Boundary
_PickedSet29, ENCASTRE
**
** INTERACTIONS
**
** Interaction: Int-1
*Contact Pair, interaction=_Int-1-Prop, adjust=0.0
_PickedSurf47, tool-1.RigidSurface_
** Interaction: Int-2
*Contact Pair, interaction=_Int-2-Prop, adjust=0.0
_PickedSurf33, tool-1.RigidSurface_
** Interaction: Int-3
*Contact Pair, interaction=_Int-3-Prop, adjust=0.0
_PickedSurf35, tool-1.RigidSurface_
** Interaction: Int-4
*Contact Pair, interaction=_Int-4-Prop, adjust=0.0
_PickedSurf37, tool-1.RigidSurface_
** Interaction: Int-5
*Contact Pair, interaction=_Int-5-Prop, adjust=0.0
_PickedSurf39, tool-1.RigidSurface_
** ----------------------------------------------------------------
**
** STEP: move tool down
**
*Step, name="move tool down", nlgeom=YES, inc=1000
tool moves down
*Static
0.001, 1., 1e-05, 1.
**
** BOUNDARY CONDITIONS
**
```

```
** Name: move tool Type: Displacement/Rotation
*Boundary
_PickedSet87, 1, 1
_PickedSet87, 2, 2
_PickedSet87, 3, 3, 2.27
_PickedSet87, 4, 4
_PickedSet87, 5, 5
_PickedSet87, 6, 6
**
** OUTPUT REQUESTS
**
*Restart, write, frequency=0
**
** FIELD OUTPUT: F-Output-1
**
*Output, field
*Node Output
RF, U
*Element Output, directions=YES
E, S
*Contact Output
CFORCE, CNAREA
**
** HISTORY OUTPUT: H-Output-1
**
*Output, history
*Contact Output
CFN1, CFN2, CFN3, CFNM
*End Step
** ----------------------------------------------------------------
**
** STEP: move tool south
**
*Step, name="move tool south", nlgeom=YES, inc=10000
*Static
0.0001, 1., 1e-05, 1.
**
** BOUNDARY CONDITIONS
**
** Name: move tool Type: Displacement/Rotation
*Boundary
_PickedSet87, 2, 2, 33.4204
**
** OUTPUT REQUESTS
**
*Restart, write, frequency=0
**
** FIELD OUTPUT: F-Output-1
**
*Output, field
*Node Output
RF, U
*Element Output, directions=YES
E, S
```

```
*Contact Output
CFORCE, CNAREA
**
** HISTORY OUTPUT: H-Output-1
**
*Output, history
*Contact Output
CFN1, CFN2, CFN3, CFNM
*End Step
** ----------------------------------------------------------------
**
** STEP: move tool left
**
*Step, name="move tool left", nlgeom=YES, inc=10000
*Static
0.0001, 1., 1e-05, 1.
**
** BOUNDARY CONDITIONS
**
** Name: move tool Type: Displacement/Rotation
*Boundary
_PickedSet87, 1, 1, -33.4204
**
** OUTPUT REQUESTS
**
*Restart, write, frequency=0
**
** FIELD OUTPUT: F-Output-1
**
*Output, field
*Node Output
RF, U
*Element Output, directions=YES
E, S
*Contact Output
CFORCE, CNAREA
**
** HISTORY OUTPUT: H-Output-1
**
*Output, history
*Contact Output
CFN1, CFN2, CFN3, CFNM
*End Step
** ----------------------------------------------------------------
**
** STEP: move tool north
**
*Step, name="move tool north", nlgeom=YES, inc=10000
*Static
1e-05, 1., 1e-05, 1.
**
** BOUNDARY CONDITIONS
**
** Name: move tool Type: Displacement/Rotation
```

```
*Boundary
_PickedSet87, 2, 2
** OUTPUT REQUESTS
**
*Restart, write, frequency=0
**
** FIELD OUTPUT: F-Output-1
**
*Output, field
*Node Output
RF, U
*Element Output, directions=YES
E, S
*Contact Output
CFORCE, CNAREA
**
** HISTORY OUTPUT: H-Output-1
**
*Output, history
*Contact Output
CFN1, CFN2, CFN3, CFNM
*End Step
** ----------------------------------------------------------------
** STEP: move tool right and complete the step
**
*Step, name="move tool right and complete the step", nlgeom=YES,
inc=10000
*Static
1e-05, 1., 1e-05, 1.
**
** BOUNDARY CONDITIONS
**
** Name: move tool Type: Displacement/Rotation
*Boundary
_PickedSet87, 1, 1
**
** OUTPUT REQUESTS
**
*Restart, write, frequency=0
**
** FIELD OUTPUT: F-Output-1
**
*Output, field
*Node Output
RF, U
*Element Output, directions=YES
E, S
*Contact Output
CFORCE, CNAREA
**
** HISTORY OUTPUT: H-Output-1
**
*Output, history
*Contact Output
```

CFN1, CFN2, CFN3, CFNM
*End Step

2) Pyramid wall angle 45 degrees, tool radius 6.35 mm, 1.27 mm step size, sheet thickness 0.815 mm.

```
*Heading
Pyramid 45 degrees wall angle, tool radius 6.35 mm, 1.27 mm step size,
sheet thickness 0.815 mm.
** Job name: py45smalltool Model name: smalltool
** Generated by: Abaqus/CAE 6.9-EF1
*Preprint, echo=NO, model=NO, history=NO, contact=NO
**
** PARTS
**
*Part, name=pyramid45
*End Part
**
*Part, name="tool smaller"
*End Part
**
**
** ASSEMBLY
**
*Assembly, name=Assembly
**
*Instance, name=pyramid45-1, part=pyramid45
          0.,           0.,           1.
*Node
*Element, type=S4R
*Nset, nset=_PickedSet16, internal, generate
    1,  8407,     1
*Elset, elset=_PickedSet16, internal, generate
    1,  8408,     1
** Section: Section-1
*Shell Section, elset=_PickedSet16, material=aluminum
0.815, 5
*End Instance
**
*Instance, name="tool smaller-1", part="tool smaller"
*Nset, nset="tool smaller-1-RefPt_", internal
1,
*Surface, type=REVOLUTION, name=RigidSurface_, internal
START,           0.,           0.
 LINE,         6.35,           0.
 CIRCL,           0., -6.27968444392684,           0.,
0.070709228515625
*Rigid Body, ref node="tool smaller-1-RefPt_", analytical
surface=RigidSurface_
*End Instance
**
*Nset, nset=_PickedSet29, internal, instance=pyramid45-1
```

```
*Elset, elset=_PickedSet29, internal, instance=pyramid45-1, generate
  1,  96,   1
*Nset, nset=_PickedSet95, internal, instance="tool smaller-1"
 1,
*Elset, elset=__PickedSurf33_SPOS, internal, instance=pyramid45-1,
generate
 1697,  3296,     1
*Surface, type=ELEMENT, name=_PickedSurf33, internal
__PickedSurf33_SPOS, SPOS
*Elset, elset=__PickedSurf35_SPOS, internal, instance=pyramid45-1,
generate
   97,  1696,     1
*Surface, type=ELEMENT, name=_PickedSurf35, internal
__PickedSurf35_SPOS, SPOS
*Elset, elset=__PickedSurf37_SPOS, internal, instance=pyramid45-1,
generate
 4897,  6496,     1
*Surface, type=ELEMENT, name=_PickedSurf37, internal
__PickedSurf37_SPOS, SPOS
*Elset, elset=__PickedSurf39_SPOS, internal, instance=pyramid45-1,
generate
 3297,  4896,     1
*Surface, type=ELEMENT, name=_PickedSurf39, internal
__PickedSurf39_SPOS, SPOS
*Elset, elset=__PickedSurf88_SNEG, internal, instance=pyramid45-1,
generate
 6497,  8096,     1
*Surface, type=ELEMENT, name=_PickedSurf88, internal
__PickedSurf88_SNEG, SNEG
*End Assembly
**
** MATERIALS
**
*Material, name=aluminum
*Elastic
70300., 0.3
*Plastic
     40.,          0.
 49.4048, 0.00634851
 66.6667, 0.00866707
 82.7381,  0.0103615
 98.2143,  0.0114234
 131.548,  0.0154365
  161.31,  0.0182182
 169.643,  0.0206638
 177.976,  0.0237504
 185.714,  0.0268454
 192.857,   0.031231
 198.214,   0.035001
 205.952,  0.0393781
 219.643,  0.0462346
 222.619,  0.0506795
 227.976,  0.0538084
 230.952,  0.0569712
```

```
 231.548,  0.0614499
   237.5,  0.0652114
   237.5,  0.0684165
 245.238,  0.0721526
 241.071,   0.076699
 247.619,   0.080452
  248.81,  0.0862043
 252.381,  0.0944869
 246.429,   0.102264
**
** INTERACTION PROPERTIES
**
*Surface Interaction, name=_Int-1-Prop
1.,
*Friction, slip tolerance=0.005
 0.1,
*Surface Behavior, pressure-overclosure=HARD
*Surface Interaction, name=_Int-2-Prop
1.,
*Friction, slip tolerance=0.005
 0.1,
*Surface Behavior, pressure-overclosure=HARD
*Surface Interaction, name=_Int-3-Prop
1.,
*Friction, slip tolerance=0.005
 0.1,
*Surface Behavior, pressure-overclosure=HARD
*Surface Interaction, name=_Int-4-Prop
1.,
*Friction, slip tolerance=0.005
 0.1,
*Surface Behavior, pressure-overclosure=HARD
*Surface Interaction, name=_Int-5-Prop
1.,
*Friction, slip tolerance=0.005
 0.1,
*Surface Behavior, pressure-overclosure=HARD
*Surface Interaction, name="friction 01"
1.,
*Friction, slip tolerance=0.005
 0.1,
*Surface Behavior, pressure-overclosure=HARD
*Surface Interaction, name=nofric
1.,
*Friction
0.,
**
** BOUNDARY CONDITIONS
**
** Name: clamp Type: Symmetry/Antisymmetry/Encastre
*Boundary
_PickedSet29, ENCASTRE
**
** INTERACTIONS
```

```
**
** Interaction: Int-1
*Contact Pair, interaction=_Int-1-Prop, adjust=0.0
_PickedSurf88, "tool smaller-1".RigidSurface_
** Interaction: Int-2
*Contact Pair, interaction=_Int-2-Prop, adjust=0.0
_PickedSurf33, "tool smaller-1".RigidSurface_
** Interaction: Int-3
*Contact Pair, interaction=_Int-3-Prop, adjust=0.0
_PickedSurf35, "tool smaller-1".RigidSurface_
** Interaction: Int-4
*Contact Pair, interaction=_Int-4-Prop, adjust=0.0
_PickedSurf37, "tool smaller-1".RigidSurface_
** Interaction: Int-5
*Contact Pair, interaction=_Int-5-Prop, adjust=0.0
_PickedSurf39, "tool smaller-1".RigidSurface_
** ----------------------------------------------------------------
**
** STEP: move tool down
**
*Step, name="move tool down", nlgeom=YES, inc=10000
tool moves down
*Static
1e-05, 1., 1e-05, 1.
**
** BOUNDARY CONDITIONS
**
** Name: move tool Type: Displacement/Rotation
*Boundary
_PickedSet95, 1, 1
_PickedSet95, 2, 2
_PickedSet95, 3, 3, 3.27
_PickedSet95, 4, 4
_PickedSet95, 5, 5
_PickedSet95, 6, 6
**
** OUTPUT REQUESTS
**
*Restart, write, frequency=0
**
** FIELD OUTPUT: F-Output-1
**
*Output, field
*Node Output
RF, U
*Element Output, directions=YES
E, S
*Contact Output
CFORCE, CNAREA
**
** HISTORY OUTPUT: H-Output-1
**
*Output, history
*Contact Output
```

```
CFN1, CFN2, CFN3, CFNM
*End Step
** ----------------------------------------------------------------
**
** STEP: move tool south
**
*Step, name="move tool south", nlgeom=YES, inc=10000
*Static
1e-05, 1., 1e-05, 1.
**
** BOUNDARY CONDITIONS
**
** Name: move tool Type: Displacement/Rotation
*Boundary
_PickedSet95, 2, 2, 62.25
**
** OUTPUT REQUESTS
**
*Restart, write, frequency=0
**
** FIELD OUTPUT: F-Output-1
**
*Output, field
*Node Output
RF, U
*Element Output, directions=YES
E, S
*Contact Output
CFORCE, CNAREA
**
** HISTORY OUTPUT: H-Output-1
**
*Output, history
*Contact Output
CFN1, CFN2, CFN3, CFNM
*End Step
** ----------------------------------------------------------------
**
** STEP: move tool left
**
*Step, name="move tool left", nlgeom=YES, inc=10000
*Static
1e-05, 1., 1e-05, 1.
**
** BOUNDARY CONDITIONS
**
** Name: move tool Type: Displacement/Rotation
*Boundary
_PickedSet95, 1, 1, -62.25
**
** OUTPUT REQUESTS
**
*Restart, write, frequency=0
**
```

```
** FIELD OUTPUT: F-Output-1
**
*Output, field
*Node Output
RF, U
*Element Output, directions=YES
E, S
*Contact Output
CFORCE, CNAREA
**
** HISTORY OUTPUT: H-Output-1
**
*Output, history
*Contact Output
CFN1, CFN2, CFN3, CFNM
*End Step
** ----------------------------------------------------------------
**
** STEP: move tool north
**
*Step, name="move tool north", nlgeom=YES, inc=10000
*Static
1e-05, 1., 1e-05, 1.
**
** BOUNDARY CONDITIONS
**
** Name: move tool Type: Displacement/Rotation
*Boundary
_PickedSet95, 2, 2
**
** OUTPUT REQUESTS
**
*Restart, write, frequency=0
**
** FIELD OUTPUT: F-Output-1
**
*Output, field
*Node Output
RF, U
*Element Output, directions=YES
E, S
*Contact Output
CFORCE, CNAREA
**
** HISTORY OUTPUT: H-Output-1
**
*Output, history
*Contact Output
CFN1, CFN2, CFN3, CFNM
*End Step
** ----------------------------------------------------------------
**
** STEP: move tool right and complete the step
**
```

```
*Step, name="move tool right and complete the step", nlgeom=YES,
inc=10000
*Static
1e-05, 1., 1e-05, 1.
**
** BOUNDARY CONDITIONS
**
** Name: move tool Type: Displacement/Rotation
*Boundary
_PickedSet95, 1, 1
_PickedSet95, 3, 3, 3.27
**
** OUTPUT REQUESTS
**
*Restart, write, frequency=0
**
** FIELD OUTPUT: F-Output-1
**
*Output, field
*Node Output
RF, U
*Element Output, directions=YES
E, S
*Contact Output
CFORCE, CNAREA
**
** HISTORY OUTPUT: H-Output-1
**
*Output, history
*Contact Output
CFN1, CFN2, CFN3, CFNM
*End Step
```

3) Pyramid wall angle 30 degrees, tool radius 9.525 mm, 1.27 mm step size, sheet thickness 0.815 mm.

```
*Heading
Pyramid 30 degrees wall angle, tool radius 9.525 mm, 1.27 mm step size,
sheet thickness 0.815 mm
** Job name: bigtoolfriction01 Model name: big tool 005 depth
** Generated by: Abaqus/CAE 6.9-EF1
*Preprint, echo=NO, model=NO, history=NO, contact=NO
**
** PARTS
**
*Part, name="pyramid30 005"
*End Part
**
*Part, name="tool large"
*End Part
**
**
** ASSEMBLY
**
*Assembly, name=Assembly
**
*Instance, name="pyramid30 005-1", part="pyramid30 005"
          0.,           0.,           1.
*Node
*Element, type=S4R
*Nset, nset=_PickedSet16, internal, generate
    1,  6509,     1
*Elset, elset=_PickedSet16, internal, generate
    1,  6504,     1
** Section: Section-1
*Shell Section, elset=_PickedSet16, material=aluminum
0.815, 5
*End Instance
**
*Instance, name="tool large-1", part="tool large"
     45.3702,     -45.3702,        9.525
     45.3702,     -45.3702,        9.525,      44.3702,     -45.3702,
9.525,          90.
*Node
      1,           0.,           0.,           0.
*Nset, nset="tool large-1-RefPt_", internal
1,
*Surface, type=REVOLUTION, name=RigidSurface_, internal
START,           0.,           0.
 LINE,        9.525,           0.
 CIRCL,           0.,       -9.525,           0.,           0.
*Rigid Body, ref node="tool large-1-RefPt_", analytical
surface=RigidSurface_
*End Instance
```

```
**
*Nset, nset=_PickedSet29, internal, instance="pyramid30 005-1"

*Elset, elset=_PickedSet29, internal, instance="pyramid30 005-1",
generate
  1,  96,   1
*Nset, nset=_PickedSet99, internal, instance="tool large-1"
 1,
*Elset, elset=__PickedSurf33_SPOS, internal, instance="pyramid30 005-
1", generate
 1322,  2546,     1
*Surface, type=ELEMENT, name=_PickedSurf33, internal
__PickedSurf33_SPOS, SPOS
*Elset, elset=__PickedSurf35_SPOS, internal, instance="pyramid30 005-
1", generate
   97,  1321,     1
*Surface, type=ELEMENT, name=_PickedSurf35, internal
__PickedSurf35_SPOS, SPOS
*Elset, elset=__PickedSurf37_SPOS, internal, instance="pyramid30 005-
1", generate
 3772,  4996,     1
*Surface, type=ELEMENT, name=_PickedSurf37, internal
__PickedSurf37_SPOS, SPOS
*Elset, elset=__PickedSurf39_SPOS, internal, instance="pyramid30 005-
1", generate
 2547,  3771,     1
*Surface, type=ELEMENT, name=_PickedSurf39, internal
__PickedSurf39_SPOS, SPOS
*Elset, elset=__PickedSurf47_SNEG, internal, instance="pyramid30 005-
1", generate
 4997,  6221,     1
*Surface, type=ELEMENT, name=_PickedSurf47, internal
__PickedSurf47_SNEG, SNEG
*End Assembly
**
** MATERIALS
**
*Material, name=aluminum
*Elastic
70300., 0.3
*Plastic
     40.,         0.
 49.4048, 0.00634851
 66.6667, 0.00866707
 82.7381,  0.0103615
 98.2143,  0.0114234
 131.548,  0.0154365
  161.31,  0.0182182
 169.643,  0.0206638
 177.976,  0.0237504
 185.714,  0.0268454
 192.857,   0.031231
 198.214,   0.035001
 205.952,  0.0393781
```

```
 219.643,  0.0462346
 222.619,  0.0506795
 227.976,  0.0538084
 230.952,  0.0569712
 231.548,  0.0614499
   237.5,  0.0652114
   237.5,  0.0684165
 245.238,  0.0721526
 241.071,   0.076699
 247.619,   0.080452
  248.81,  0.0862043
 252.381,  0.0944869
 246.429,   0.102264
**
** INTERACTION PROPERTIES
**
*Surface Interaction, name=_Int-1-Prop
1.,
*Friction, slip tolerance=0.005
 0.1,
*Surface Behavior, pressure-overclosure=HARD
*Surface Interaction, name=_Int-2-Prop
1.,
*Friction, slip tolerance=0.005
 0.1,
*Surface Behavior, pressure-overclosure=HARD
*Surface Interaction, name=_Int-3-Prop
1.,
*Friction, slip tolerance=0.005
 0.1,
*Surface Behavior, pressure-overclosure=HARD
*Surface Interaction, name=_Int-4-Prop
1.,
*Friction, slip tolerance=0.005
 0.1,
*Surface Behavior, pressure-overclosure=HARD
*Surface Interaction, name=_Int-5-Prop
1.,
*Friction, slip tolerance=0.005
 0.1,
*Surface Behavior, pressure-overclosure=HARD
*Surface Interaction, name=friction
1.,
*Friction, slip tolerance=0.005
 0.1,
*Surface Behavior, pressure-overclosure=HARD
*Surface Interaction, name="friction 01"
1.,
*Friction, slip tolerance=0.005
 0.1,
*Surface Behavior, pressure-overclosure=HARD
*Surface Interaction, name="friction 02"
1.,
*Friction, slip tolerance=0.005
```

```
 0.2,
*Surface Behavior, pressure-overclosure=HARD
*Surface Interaction, name=nofric
1.,
*Friction, slip tolerance=0.005
 0.05,
*Surface Behavior, pressure-overclosure=HARD
**
** BOUNDARY CONDITIONS
**
** Name: clamp Type: Symmetry/Antisymmetry/Encastre
*Boundary
_PickedSet29, ENCASTRE
**
** INTERACTIONS
**
** Interaction: Int-1
*Contact Pair, interaction=_Int-1-Prop, adjust=0.0
_PickedSurf47, "tool large-1".RigidSurface_
** Interaction: Int-2
*Contact Pair, interaction=_Int-2-Prop, adjust=0.0
_PickedSurf33, "tool large-1".RigidSurface_
** Interaction: Int-3
*Contact Pair, interaction=_Int-3-Prop, adjust=0.0
_PickedSurf35, "tool large-1".RigidSurface_
** Interaction: Int-4
*Contact Pair, interaction=_Int-4-Prop, adjust=0.0
_PickedSurf37, "tool large-1".RigidSurface_
** Interaction: Int-5
*Contact Pair, interaction=_Int-5-Prop, adjust=0.0
_PickedSurf39, "tool large-1".RigidSurface_
** ----------------------------------------------------------------
**
** STEP: move tool down
**
*Step, name="move tool down", nlgeom=YES, inc=1000
tool moves down
*Static
0.001, 1., 1e-05, 1.
**
** BOUNDARY CONDITIONS
**
** Name: move tool Type: Displacement/Rotation
*Boundary
_PickedSet99, 1, 1
_PickedSet99, 2, 2
_PickedSet99, 3, 3, 2.27
_PickedSet99, 4, 4
_PickedSet99, 5, 5
_PickedSet99, 6, 6
**
** OUTPUT REQUESTS
**
*Restart, write, frequency=0
```

```
**
** FIELD OUTPUT: F-Output-1
**
*Output, field
*Node Output
RF, U
*Element Output, directions=YES
E, S
*Contact Output
CFORCE, CNAREA
**
** HISTORY OUTPUT: H-Output-1
**
*Output, history
*Contact Output
CFN1, CFN2, CFN3, CFNM
*End Step
** ----------------------------------------------------------------
**
** STEP: move tool south
**
*Step, name="move tool south", nlgeom=YES, inc=10000
*Static
0.0001, 1., 1e-05, 1.
**
** BOUNDARY CONDITIONS
**
** Name: move tool Type: Displacement/Rotation
*Boundary
_PickedSet99, 2, 2, 33.4204
**
** OUTPUT REQUESTS
**
*Restart, write, frequency=0
**
** FIELD OUTPUT: F-Output-1
**
*Output, field
*Node Output
RF, U
*Element Output, directions=YES
E, S
*Contact Output
CFORCE, CNAREA
**
** HISTORY OUTPUT: H-Output-1
**
*Output, history
*Contact Output
CFN1, CFN2, CFN3, CFNM
*End Step
** ----------------------------------------------------------------
**
** STEP: move tool left
```

```
**
*Step, name="move tool left", nlgeom=YES, inc=10000
*Static
0.0001, 1., 1e-05, 1.
**
** BOUNDARY CONDITIONS
**
** Name: move tool Type: Displacement/Rotation
*Boundary
_PickedSet99, 1, 1, -33.4204
**
** OUTPUT REQUESTS
**
*Restart, write, frequency=0
**
** FIELD OUTPUT: F-Output-1
**
*Output, field
*Node Output
RF, U
*Element Output, directions=YES
E, S
*Contact Output
CFORCE, CNAREA
**
** HISTORY OUTPUT: H-Output-1
**
*Output, history
*Contact Output
CFN1, CFN2, CFN3, CFNM
*End Step
** ----------------------------------------------------------------
**
** STEP: move tool north
**
*Step, name="move tool north", nlgeom=YES, inc=10000
*Static
1e-05, 1., 1e-05, 1.
**
** BOUNDARY CONDITIONS
**
** Name: move tool Type: Displacement/Rotation
*Boundary
_PickedSet99, 2, 2
**
** OUTPUT REQUESTS
**
*Restart, write, frequency=0
**
** FIELD OUTPUT: F-Output-1
**
*Output, field
*Node Output
RF, U
```

```
*Element Output, directions=YES
E, S
*Contact Output
CFORCE, CNAREA
**
** HISTORY OUTPUT: H-Output-1
**
*Output, history
*Contact Output
CFN1, CFN2, CFN3, CFNM
*End Step
** ----------------------------------------------------------------
**
** STEP: move tool right and complete the step
**
*Step, name="move tool right and complete the step", nlgeom=YES,
inc=10000
*Static
1e-05, 1., 1e-05, 1.
**
** BOUNDARY CONDITIONS
**
** Name: move tool Type: Displacement/Rotation
*Boundary
_PickedSet99, 1, 1
**
** OUTPUT REQUESTS
**
*Restart, write, frequency=0
**
** FIELD OUTPUT: F-Output-1
**
*Output, field
*Node Output
RF, U
*Element Output, directions=YES
E, S
*Contact Output
CFORCE, CNAREA
**
** HISTORY OUTPUT: H-Output-1
**
*Output, history
*Contact Output
CFN1, CFN2, CFN3, CFNM
*End Step
```

The cone models have 90 steps in the simulation. For the sake of conciseness, only the first 10 and the last steps have been mentioned in the following input files.

4) Cone 30 degrees wall angle, tool radius 6.35 mm, 1.27 mm step size, sheet thickness 0.815 mm

```
*Heading
Cone 30 degrees wall angle, tool radius 6.35 mm, 1.27 mm step size,
sheet thickness 0.815 mm
** Job name: c Model name: 07239-copy2
** Generated by: Abaqus/CAE 6.9-EF1
*Preprint, echo=NO, model=NO, history=NO, contact=NO
**
** PARTS
**
*Part, name=cone
*End Part
**
*Part, name=tool
*End Part
**
**

*Element, type=S4R

*Element, type=S3

*Nset, nset=_PickedSet26, internal, generate
    1,  9435,     1
*Elset, elset=_PickedSet26, internal, generate
    1,  9348,     1
** Section: Section-1
*Shell Section, elset=_PickedSet26, material=aluminum
0.815, 5
*End Instance
**
*Instance, name=tool-1, part=tool

*End Assembly
**
** MATERIALS
**
*Material, name=aluminum
*Elastic
70300., 0.3
*Plastic
     40.,          0.
 49.4048, 0.00634851
 66.6667, 0.00866707
 82.7381,  0.0103615
 98.2143,  0.0114234
```

```
 131.548,  0.0154365
  161.31,  0.0182182
 169.643,  0.0206638
 177.976,  0.0237504
 185.714,  0.0268454
 192.857,   0.031231
 198.214,   0.035001
 205.952,  0.0393781
 219.643,  0.0462346
 222.619,  0.0506795
 227.976,  0.0538084
 230.952,  0.0569712
 231.548,  0.0614499
   237.5,  0.0652114
   237.5,  0.0684165
 245.238,  0.0721526
 241.071,   0.076699
 247.619,   0.080452
  248.81,  0.0862043
 252.381,  0.0944869
 246.429,   0.102264
**
** INTERACTION PROPERTIES
**
*Surface Interaction, name=friction
1.,
*Friction, slip tolerance=0.005
 0.1,
*Surface Behavior, pressure-overclosure=HARD
**
** BOUNDARY CONDITIONS
**
** Name: clamp the ends Type: Symmetry/Antisymmetry/Encastre
*Boundary
_PickedSet79, ENCASTRE
**
** INTERACTIONS
**
** Interaction: Int-1
*Contact Pair, interaction=friction, adjust=0.0
_PickedSurf21, tool-1.RigidSurface_
** Interaction: Int-4
*Contact Pair, interaction=friction, adjust=0.0
_PickedSurf27, tool-1.RigidSurface_
** Interaction: Int-5
*Contact Pair, interaction=friction, adjust=0.
_PickedSurf29, tool-1.RigidSurface_
** Interaction: Int-8
*Contact Pair, interaction=friction, adjust=0.0
_PickedSurf35, tool-1.RigidSurface_
** ----------------------------------------------------------------
**
** STEP: move tool down
**
```

```
*Step, name="move tool down", nlgeom=YES, inc=1000
*Static
0.01, 1., 1e-05, 1.
**
** BOUNDARY CONDITIONS
**
** Name: move tool down Type: Displacement/Rotation
*Boundary
_PickedSet80, 1, 1
_PickedSet80, 2, 2
_PickedSet80, 3, 3, 2.27
_PickedSet80, 4, 4
_PickedSet80, 5, 5
_PickedSet80, 6, 6
**
** OUTPUT REQUESTS
**
*Restart, write, frequency=0
**
** FIELD OUTPUT: F-Output-1
**
*Output, field
*Node Output
RF, U
*Element Output, directions=YES
E, S
*Contact Output
CFORCE,
**
** HISTORY OUTPUT: H-Output-1
**
*Output, history
*Contact Output
CFN1, CFN2, CFN3
*End Step
** ----------------------------------------------------------------
**
** STEP: angle1
**
*Step, name=angle1, nlgeom=YES, inc=10000
*Static
0.002, 1., 1e-09, 1.
**
** BOUNDARY CONDITIONS
**
** Name: move tool down Type: Displacement/Rotation
*Boundary
_PickedSet80, 1, 1, -0.298096
_PickedSet80, 2, 2, -0.00260145
_PickedSet80, 3, 3, 2.27
**
** OUTPUT REQUESTS
**
*Restart, write, frequency=0
```

```
**
** FIELD OUTPUT: F-Output-1
**
*Output, field
*Node Output
RF, U
*Element Output, directions=YES
E, S
*Contact Output
CFORCE,
**
** HISTORY OUTPUT: H-Output-1
**
*Output, history
*Contact Output
CFN1, CFN2, CFN3
*End Step
** ----------------------------------------------------------------
**
** STEP: angle2
**
*Step, name=angle2, nlgeom=YES, inc=1000
*Static
0.001, 1., 1e-09, 1.
**
** BOUNDARY CONDITIONS
**
** Name: move tool down Type: Displacement/Rotation
*Boundary
_PickedSet80, 1, 1, -0.596102
_PickedSet80, 2, 2, -0.010405
**
** OUTPUT REQUESTS
**
*Restart, write, frequency=0
**
** FIELD OUTPUT: F-Output-1
**
*Output, field
*Node Output
RF, U
*Element Output, directions=YES
E, S
*Contact Output
CFORCE,
**
** HISTORY OUTPUT: H-Output-1
**
*Output, history
*Contact Output
CFN1, CFN2, CFN3
*End Step
** ----------------------------------------------------------------
**
```

```
** STEP: angle3
**
*Step, name=angle3, nlgeom=YES, inc=1000
*Static
0.001, 1., 1e-09, 1.
**
** BOUNDARY CONDITIONS
**
** Name: move tool down Type: Displacement/Rotation
*Boundary
_PickedSet80, 1, 1, -0.893926
_PickedSet80, 2, 2, -0.0234083
**
** OUTPUT REQUESTS
**
*Restart, write, frequency=0
**
** FIELD OUTPUT: F-Output-1
**
*Output, field
*Node Output
RF, U
*Element Output, directions=YES
E, S
*Contact Output
CFORCE,
**
** HISTORY OUTPUT: H-Output-1
**
*Output, history
*Contact Output
CFN1, CFN2, CFN3
*End Step
** ----------------------------------------------------------------
**
** STEP: angle4
**
*Step, name=angle4, nlgeom=YES, inc=1000
*Static
0.001, 1., 1e-09, 1.
**
** BOUNDARY CONDITIONS
**
** Name: move tool down Type: Displacement/Rotation
*Boundary
_PickedSet80, 1, 1, -1.19148
_PickedSet80, 2, 2, -0.0416073
**
** OUTPUT REQUESTS
**
*Restart, write, frequency=0
**
** FIELD OUTPUT: F-Output-1
**
```

```
*Output, field
*Node Output
RF, U
*Element Output, directions=YES
E, S
*Contact Output
CFORCE,
**
** HISTORY OUTPUT: H-Output-1
**
*Output, history
*Contact Output
CFN1, CFN2, CFN3
*End Step
** ----------------------------------------------------------------
**
** STEP: angle5
**
*Step, name=angle5, nlgeom=YES, inc=1000
*Static
0.01, 1., 1e-12, 1.
**
** BOUNDARY CONDITIONS
**
** Name: move tool down Type: Displacement/Rotation
*Boundary
_PickedSet80, 1, 1, -1.48867
_PickedSet80, 2, 2, -0.0649966
_PickedSet80, 3, 3, 2.27
**
** OUTPUT REQUESTS
**
*Restart, write, frequency=0
**
** FIELD OUTPUT: F-Output-1
**
*Output, field
*Node Output
RF, U
*Element Output, directions=YES
E, S
*Contact Output
CFORCE,
**
** HISTORY OUTPUT: H-Output-1
**
*Output, history
*Contact Output
CFN1, CFN2, CFN3
*End Step
** ----------------------------------------------------------------
**
** STEP: angle6
**
```

```
*Step, name=angle6, nlgeom=YES, inc=1000
*Static
0.01, 1., 1e-12, 1.
**
** BOUNDARY CONDITIONS
**
** Name: move tool down Type: Displacement/Rotation
*Boundary
_PickedSet80, 1, 1, -1.7854
_PickedSet80, 2, 2, -0.0935689
**
** OUTPUT REQUESTS
**
*Restart, write, frequency=0
**
** FIELD OUTPUT: F-Output-1
**
*Output, field
*Node Output
RF, U
*Element Output, directions=YES
E, S
*Contact Output
CFORCE,
**
** HISTORY OUTPUT: H-Output-1
**
*Output, history
*Contact Output
CFN1, CFN2, CFN3
*End Step
** ----------------------------------------------------------------
**
** STEP: a7
**
*Step, name=a7, nlgeom=YES, inc=1000
*Static
0.01, 1., 1e-12, 1.
**
** BOUNDARY CONDITIONS
**
** Name: move tool down Type: Displacement/Rotation
*Boundary
_PickedSet80, 1, 1, -2.08159
_PickedSet80, 2, 2, -0.127316
**
** OUTPUT REQUESTS
**
*Restart, write, frequency=0
**
** FIELD OUTPUT: F-Output-1
**
*Output, field
*Node Output
```

```
RF, U
*Element Output, directions=YES
E, S
*Contact Output
CFORCE,
**
** HISTORY OUTPUT: H-Output-1
**
*Output, history
*Contact Output
CFN1, CFN2, CFN3
*End Step
** ----------------------------------------------------------------
**
** STEP: a8
**
*Step, name=a8, nlgeom=YES, inc=1000
*Static
0.01, 1., 1e-12, 1.
**
** BOUNDARY CONDITIONS
**
** Name: move tool down Type: Displacement/Rotation
*Boundary
_PickedSet80, 1, 1, -2.37715
_PickedSet80, 2, 2, -0.166227
**
** OUTPUT REQUESTS
**
*Restart, write, frequency=0
**
** FIELD OUTPUT: F-Output-1
**
*Output, field
*Node Output
RF, U
*Element Output, directions=YES
E, S
*Contact Output
CFORCE,
**
** HISTORY OUTPUT: H-Output-1
**
*Output, history
*Contact Output
CFN1, CFN2, CFN3
*End Step
** ----------------------------------------------------------------
**
** STEP: a9
**
*Step, name=a9, nlgeom=YES, inc=1000
*Static
0.01, 1., 1e-12, 1.
```

```
**
** BOUNDARY CONDITIONS
**
** Name: move tool down Type: Displacement/Rotation
*Boundary
_PickedSet80, 1, 1, -2.67198
_PickedSet80, 2, 2, -0.21029
**
** OUTPUT REQUESTS
**
*Restart, write, frequency=0
**
** FIELD OUTPUT: F-Output-1
**
*Output, field
*Node Output
RF, U
*Element Output, directions=YES
E, S
*Contact Output
CFORCE,
**
** HISTORY OUTPUT: H-Output-1
**
*Output, history
*Contact Output
CFN1, CFN2, CFN3
*End Step
** ----------------------------------------------------------------
**
** STEP: a10
**
*Step, name=a10, nlgeom=YES, inc=1000
*Static
0.01, 1., 1e-12, 1.
**
** BOUNDARY CONDITIONS
**
** Name: move tool down Type: Displacement/Rotation
*Boundary
_PickedSet80, 1, 1, -2.966
_PickedSet80, 2, 2, -0.259492
_PickedSet80, 3, 3, 2.27
**
** OUTPUT REQUESTS
**
*Restart, write, frequency=0
**
** FIELD OUTPUT: F-Output-1
**
*Output, field
*Node Output
RF, U
*Element Output, directions=YES
```

```
E, S
*Contact Output
CFORCE,
**
** HISTORY OUTPUT: H-Output-1
**
*Output, history
*Contact Output
CFN1, CFN2, CFN3
*End Step
** ----------------------------------------------------------------
** STEP: a90
**
*Step, name=a90, nlgeom=YES, inc=1000
*Static
0.01, 1., 1e-12, 1.
**
** BOUNDARY CONDITIONS
**
** Name: move tool down Type: Displacement/Rotation
*Boundary
_PickedSet80, 1, 1, -17.0805
_PickedSet80, 2, 2, -17.0805
**
** OUTPUT REQUESTS
**
*Restart, write, frequency=0
**
** FIELD OUTPUT: F-Output-1
**
*Output, field
*Node Output
RF, U
*Element Output, directions=YES
E, S
*Contact Output
CFORCE,
**
** HISTORY OUTPUT: H-Output-1
**
*Output, history
*Contact Output
CFN1, CFN2, CFN3
*End Step
```

5) Cone 30 degrees wall angle, tool radius 9.525 mm, 1.27 mm step size, sheet thickness 0.815 mm

```
*Heading
Cone 30 degrees wall angle, tool radius 9.525 mm, 1.27 mm step size,
sheet thickness 0.815 mm
** Job name: conelargetool Model name: 07239-copy2
** Generated by: Abaqus/CAE 6.9-EF1
*Preprint, echo=NO, model=NO, history=NO, contact=NO
**
** PARTS
**
*Part, name=cone
*End Part
**
*Part, name=toollarge
*End Part
**
** ASSEMBLY
**
*Assembly, name=Assembly
**
*Instance, name=cone-1, part=cone
*Element, type=S4R
*Element, type=S3
4233, 4480, 4504, 4503
6090, 6236, 6260, 6259
7491, 7572, 7596, 7595
8888, 8907, 8931, 8930
*Nset, nset=_PickedSet26, internal, generate
    1,  9435,     1
*Elset, elset=_PickedSet26, internal, generate
    1,  9348,     1
** Section: Section-1
*Shell Section, elset=_PickedSet26, material=aluminum
0.815, 5
*End Instance
**
*Instance, name=toollarge-1, part=toollarge
*Node
      1,           0.,           0.,           0.
*Nset, nset=toollarge-1-RefPt_, internal
1,
*Surface, type=REVOLUTION, name=RigidSurface_, internal
START,           0.,           0.
 LINE,        9.525,           0.
 CIRCL,           0.,       -9.525,           0.,           0.
*Rigid Body, ref node=toollarge-1-RefPt_, analytical
surface=RigidSurface_
*End Instance
**
*Nset, nset=_PickedSet79, internal, instance=cone-1
*Nset, nset=_PickedSet84, internal, instance=toollarge-1
```

```
 1,
*Elset, elset=__PickedSurf21_SNEG, internal, instance=cone-1, generate
 6095,  7491,     1
*Surface, type=ELEMENT, name=_PickedSurf21, internal
__PickedSurf21_SNEG, SNEG
*Elset, elset=__PickedSurf23_SNEG, internal, instance=cone-1, generate
 4694,  6090,     1
*Surface, type=ELEMENT, name=_PickedSurf23, internal
__PickedSurf23_SNEG, SNEG
*Elset, elset=__PickedSurf25_SNEG, internal, instance=cone-1, generate
 2837,  4233,     1
*Surface, type=ELEMENT, name=_PickedSurf25, internal
__PickedSurf25_SNEG, SNEG
*Elset, elset=__PickedSurf27_SNEG, internal, instance=cone-1, generate
 7492,  8888,     1
*Surface, type=ELEMENT, name=_PickedSurf27, internal
__PickedSurf27_SNEG, SNEG
*Elset, elset=__PickedSurf29_SNEG, internal, instance=cone-1, generate
 8889,  9344,     1
*Surface, type=ELEMENT, name=_PickedSurf29, internal
__PickedSurf29_SNEG, SNEG
*Elset, elset=__PickedSurf31_SNEG, internal, instance=cone-1, generate
 2181,  2636,     1
*Surface, type=ELEMENT, name=_PickedSurf31, internal
__PickedSurf31_SNEG, SNEG
*Elset, elset=__PickedSurf33_SNEG, internal, instance=cone-1, generate
 4234,  4689,     1
*Surface, type=ELEMENT, name=_PickedSurf33, internal
__PickedSurf33_SNEG, SNEG
*Elset, elset=__PickedSurf35_SNEG, internal, instance=cone-1, generate
 1725,  2180,     1
*Surface, type=ELEMENT, name=_PickedSurf35, internal
__PickedSurf35_SNEG, SNEG
*End Assembly
**
** MATERIALS
**
*Material, name=aluminum
*Elastic
70300., 0.3
*Plastic
     40.,         0.
 49.4048, 0.00634851
 66.6667, 0.00866707
 82.7381,  0.0103615
 98.2143,  0.0114234
 131.548,  0.0154365
  161.31,  0.0182182
 169.643,  0.0206638
 177.976,  0.0237504
 185.714,  0.0268454
 192.857,   0.031231
 198.214,   0.035001
 205.952,  0.0393781
```

```
 219.643,  0.0462346
 222.619,  0.0506795
 227.976,  0.0538084
 230.952,  0.0569712
 231.548,  0.0614499
   237.5,  0.0652114
   237.5,  0.0684165
 245.238,  0.0721526
 241.071,   0.076699
 247.619,   0.080452
  248.81,  0.0862043
 252.381,  0.0944869
 246.429,   0.102264
**
** INTERACTION PROPERTIES
**
*Surface Interaction, name=friction
1.,
*Friction, slip tolerance=0.005
 0.1,
*Surface Behavior, pressure-overclosure=HARD
**
** BOUNDARY CONDITIONS
**
** Name: clamp the ends Type: Symmetry/Antisymmetry/Encastre
*Boundary
_PickedSet79, ENCASTRE
**
** INTERACTIONS
**
** Interaction: Int-1
*Contact Pair, interaction=friction, adjust=0.0
_PickedSurf21, toollarge-1.RigidSurface_
** Interaction: Int-4
*Contact Pair, interaction=friction, adjust=0.0
_PickedSurf27, toollarge-1.RigidSurface_
** Interaction: Int-5
*Contact Pair, interaction=friction, adjust=0.
_PickedSurf29, toollarge-1.RigidSurface_
** Interaction: Int-8
*Contact Pair, interaction=friction, adjust=0.0
_PickedSurf35, toollarge-1.RigidSurface_
** ----------------------------------------------------------------
**
** STEP: move tool down
**
*Step, name="move tool down", nlgeom=YES, inc=1000
*Static
0.01, 1., 1e-05, 1.
**
** BOUNDARY CONDITIONS
**
** Name: move tool down Type: Displacement/Rotation
*Boundary
```

```
_PickedSet84, 1, 1
_PickedSet84, 2, 2
_PickedSet84, 3, 3, 2.27
_PickedSet84, 4, 4
_PickedSet84, 5, 5
_PickedSet84, 6, 6
**
** OUTPUT REQUESTS
**
*Restart, write, frequency=0
**
** FIELD OUTPUT: F-Output-1
**
*Output, field
*Node Output
RF, U
*Element Output, directions=YES
E, S
*Contact Output
CFORCE,
**
** HISTORY OUTPUT: H-Output-1
**
*Output, history
*Contact Output
CFN1, CFN2, CFN3
*End Step
** ----------------------------------------------------------------
**
** STEP: angle1
**
*Step, name=angle1, nlgeom=YES, inc=10000
*Static
0.002, 1., 1e-09, 1.
**
** BOUNDARY CONDITIONS
**
** Name: move tool down Type: Displacement/Rotation
*Boundary
_PickedSet84, 1, 1, -0.298096
_PickedSet84, 2, 2, -0.00260145
_PickedSet84, 3, 3, 2.27
**
** OUTPUT REQUESTS
**
*Restart, write, frequency=0
**
** FIELD OUTPUT: F-Output-1
**
*Output, field
*Node Output
RF, U
*Element Output, directions=YES
E, S
```

```
*Contact Output
CFORCE,
**
** HISTORY OUTPUT: H-Output-1
**
*Output, history
*Contact Output
CFN1, CFN2, CFN3
*End Step
** ----------------------------------------------------------------
**
** STEP: angle2
**
*Step, name=angle2, nlgeom=YES, inc=1000
*Static
0.001, 1., 1e-09, 1.
**
** BOUNDARY CONDITIONS
**
** Name: move tool down Type: Displacement/Rotation
*Boundary
_PickedSet84, 1, 1, -0.596102
_PickedSet84, 2, 2, -0.010405
**
** OUTPUT REQUESTS
**
*Restart, write, frequency=0
**
** FIELD OUTPUT: F-Output-1
**
*Output, field
*Node Output
RF, U
*Element Output, directions=YES
E, S
*Contact Output
CFORCE,
**
** HISTORY OUTPUT: H-Output-1
**
*Output, history
*Contact Output
CFN1, CFN2, CFN3
*End Step
** ----------------------------------------------------------------**
** STEP: angle3
**
*Step, name=angle3, nlgeom=YES, inc=1000
*Static
0.001, 1., 1e-09, 1.
**
** BOUNDARY CONDITIONS
**
** Name: move tool down Type: Displacement/Rotation
```

```
*Boundary
_PickedSet84, 1, 1, -0.893926
_PickedSet84, 2, 2, -0.0234083
**
** OUTPUT REQUESTS
**
*Restart, write, frequency=0
**
** FIELD OUTPUT: F-Output-1
**
*Output, field
*Node Output
RF, U
*Element Output, directions=YES
E, S
*Contact Output
CFORCE,
**
** HISTORY OUTPUT: H-Output-1
**
*Output, history
*Contact Output
CFN1, CFN2, CFN3
*End Step
** ----------------------------------------------------------------
**
** STEP: angle4
**
*Step, name=angle4, nlgeom=YES, inc=1000
*Static
0.001, 1., 1e-09, 1.
**
** BOUNDARY CONDITIONS
**
** Name: move tool down Type: Displacement/Rotation
*Boundary
_PickedSet84, 1, 1, -1.19148
_PickedSet84, 2, 2, -0.0416073
**
** OUTPUT REQUESTS
**
*Restart, write, frequency=0
**
** FIELD OUTPUT: F-Output-1
**
*Output, field
*Node Output
RF, U
*Element Output, directions=YES
E, S
*Contact Output
CFORCE,
**
** HISTORY OUTPUT: H-Output-1
```

```
**
*Output, history
*Contact Output
CFN1, CFN2, CFN3
*End Step
** ----------------------------------------------------------------
**
** STEP: angle5
**
*Step, name=angle5, nlgeom=YES, inc=1000
*Static
0.01, 1., 1e-12, 1.
**
** BOUNDARY CONDITIONS
**
** Name: move tool down Type: Displacement/Rotation
*Boundary
_PickedSet84, 1, 1, -1.48867
_PickedSet84, 2, 2, -0.0649966
_PickedSet84, 3, 3, 2.27
**
** OUTPUT REQUESTS
**
*Restart, write, frequency=0
**
** FIELD OUTPUT: F-Output-1
**
*Output, field
*Node Output
RF, U
*Element Output, directions=YES
E, S
*Contact Output
CFORCE,
**
** HISTORY OUTPUT: H-Output-1
**
*Output, history
*Contact Output
CFN1, CFN2, CFN3
*End Step
** ----------------------------------------------------------------
**
** STEP: angle6
**
*Step, name=angle6, nlgeom=YES, inc=1000
*Static
0.01, 1., 1e-12, 1.
**
** BOUNDARY CONDITIONS
**
** Name: move tool down Type: Displacement/Rotation
*Boundary
_PickedSet84, 1, 1, -1.7854
```

```
_PickedSet84, 2, 2, -0.0935689
**
** OUTPUT REQUESTS
**
*Restart, write, frequency=0
**
** FIELD OUTPUT: F-Output-1
**
*Output, field
*Node Output
RF, U
*Element Output, directions=YES
E, S
*Contact Output
CFORCE,
**
** HISTORY OUTPUT: H-Output-1
**
*Output, history
*Contact Output
CFN1, CFN2, CFN3
*End Step
** ----------------------------------------------------------------
**
** STEP: a7
**
*Step, name=a7, nlgeom=YES, inc=1000
*Static
0.01, 1., 1e-12, 1.
**
** BOUNDARY CONDITIONS
**
** Name: move tool down Type: Displacement/Rotation
*Boundary
_PickedSet84, 1, 1, -2.08159
_PickedSet84, 2, 2, -0.127316
**
** OUTPUT REQUESTS
**
*Restart, write, frequency=0
**
** FIELD OUTPUT: F-Output-1
**
*Output, field
*Node Output
RF, U
*Element Output, directions=YES
E, S
*Contact Output
CFORCE,
**
** HISTORY OUTPUT: H-Output-1
**
*Output, history
```

```
*Contact Output
CFN1, CFN2, CFN3
*End Step
** ----------------------------------------------------------------
**
** STEP: a8
**
*Step, name=a8, nlgeom=YES, inc=1000
*Static
0.01, 1., 1e-12, 1.
**
** BOUNDARY CONDITIONS
**
** Name: move tool down Type: Displacement/Rotation
*Boundary
_PickedSet84, 1, 1, -2.37715
_PickedSet84, 2, 2, -0.166227
**
** OUTPUT REQUESTS
**
*Restart, write, frequency=0
**
** FIELD OUTPUT: F-Output-1
**
*Output, field
*Node Output
RF, U
*Element Output, directions=YES
E, S
*Contact Output
CFORCE,
**
** HISTORY OUTPUT: H-Output-1
**
*Output, history
*Contact Output
CFN1, CFN2, CFN3
*End Step
** ----------------------------------------------------------------
**
** STEP: a9
**
*Step, name=a9, nlgeom=YES, inc=1000
*Static
0.01, 1., 1e-12, 1.
**
** BOUNDARY CONDITIONS
**
** Name: move tool down Type: Displacement/Rotation
*Boundary
_PickedSet84, 1, 1, -2.67198
_PickedSet84, 2, 2, -0.21029
**
** OUTPUT REQUESTS
```

```
**
*Restart, write, frequency=0
**
** FIELD OUTPUT: F-Output-1
**
*Output, field
*Node Output
RF, U
*Element Output, directions=YES
E, S
*Contact Output
CFORCE,
**
** HISTORY OUTPUT: H-Output-1
**
*Output, history
*Contact Output
CFN1, CFN2, CFN3
*End Step
** ----------------------------------------------------------------
**
** STEP: a10
**
*Step, name=a10, nlgeom=YES, inc=1000
*Static
0.01, 1., 1e-12, 1.
**
** BOUNDARY CONDITIONS
**
** Name: move tool down Type: Displacement/Rotation
*Boundary
_PickedSet84, 1, 1, -2.966
_PickedSet84, 2, 2, -0.259492
_PickedSet84, 3, 3, 2.27
**
** OUTPUT REQUESTS
*Restart, write, frequency=0
**
** FIELD OUTPUT: F-Output-1
**
*Output, field
*Node Output
RF, U
*Element Output, directions=YES
E, S
*Contact Output
CFORCE,
**
** HISTORY OUTPUT: H-Output-1
**
*Output, history
*Contact Output
CFN1, CFN2, CFN3
*End Step
```

```
** ----------------------------------------------------------------
** STEP: a90
**
*Step, name=a90, nlgeom=YES, inc=1000
*Static
0.01, 1., 1e-12, 1.
**
** BOUNDARY CONDITIONS
**
** Name: move tool down Type: Displacement/Rotation
*Boundary
_PickedSet84, 1, 1, -17.0805
_PickedSet84, 2, 2, -17.0805
**
** OUTPUT REQUESTS
**
*Restart, write, frequency=0
**
** FIELD OUTPUT: F-Output-1
**
*Output, field
*Node Output
RF, U
*Element Output, directions=YES
E, S
*Contact Output
CFORCE,
**
** HISTORY OUTPUT: H-Output-1
**
*Output, history
*Contact Output
CFN1, CFN2, CFN3
*End Step
```

APPENDIX C

CNC CODES GENERATED

The following appendix presents some of the CNC codes that were generated by FeatureCAM which was used to form the parts.

1) Pyramid wall angle 30 degrees, tool radius 6.35 mm, 1.27 mm step size, sheet thickness 0.815 mm.

```
.N10G70G94G75G90
'30 degree pyramid 1.27 mm step size   3-20-2011'
'SRF_MILL2'
'TOOL NUMBER:1'
'SPINDLE RPM:60'
N35G0X0.Y0.T1M6
N40S60
N45X4.3464Y0.6806
N50Z0.1
N55G1Z-0.05F5.0
N60Y4.3214F10.0
N65G3X4.3214Y4.3464I4.3214J4.3214
N70G1X0.6786
N75G3X0.6536Y4.3214I0.6786J4.3214
N80G1Y0.6786
N85G3X0.6786Y0.6536I0.6786J0.6786
N90G1X4.3214
N95G3X4.3464Y0.6786I4.3214J0.6786
N100G1Y0.6806
N105X4.2548Y0.7502Z-0.1
N110G3X4.2598Y0.7652I4.2348J0.7652
N115G1Y0.7699
N120Y4.2348
N125G3X4.2348Y4.2598I4.2348J4.2348
N130G1X0.7652
N135G3X0.7402Y4.2348I0.7652J4.2348
N140G1Y0.7652
N145G3X0.7652Y0.7402I0.7652J0.7652
N150G1X4.2348
N155G3X4.2548Y0.7502I4.2348J0.7652
N160G1X4.1663Y0.8346Z-0.15
N165G3X4.1732Y0.8518I4.1482J0.8518
N170G1Y0.8591
N175Y4.1482
N180G3X4.1482Y4.1732I4.1482J4.1482
N185G1X0.8518
N190G3X0.8268Y4.1482I0.8518J4.1482
N195G1Y0.8518
N200G3X0.8518Y0.8268I0.8518J0.8518
```

N205G1X4.1482
N210G3X4.1663Y0.8346I4.1482J0.8518
N215G1X4.0794Y0.9208Z-0.2
N220G3X4.0866Y0.9384I4.0616J0.9384
N225G1Y0.9484
N230Y4.0616
N235G3X4.0616Y4.0866I4.0616J4.0616
N240G1X0.9384
N245G3X0.9134Y4.0616I0.9384J4.0616
N250G1Y0.9384
N255G3X0.9384Y0.9134I0.9384J0.9384
N260G1X4.0616
N265G3X4.0794Y0.9208I4.0616J0.9384
N270G1X3.9927Y1.0074Z-0.25
N275G3X4.0Y1.025I3.975J1.025
N280G1Y1.0376
N285Y3.975
N290G3X3.975Y4.0I3.975J3.975
N295G1X1.025
N300G3X1.0Y3.975I1.025J3.975
N305G1Y1.025
N310G3X1.025Y1.0I1.025J1.025
N315G1X3.975
N320G3X3.9927Y1.0074I3.975J1.025
N325G1X3.9061Y1.0939Z-0.3
N330G3X3.9134Y1.1116I3.8884J1.1116
N335G1Y1.1269
N340Y3.8884
N345G3X3.8884Y3.9134I3.8884J3.8884
N350G1X1.1116
N355G3X1.0866Y3.8884I1.1116J3.8884
N360G1Y1.1116
N365G3X1.1116Y1.0866I1.1116J1.1116
N370G1X3.8884
N375G3X3.9061Y1.0939I3.8884J1.1116
N380G1X3.8194Y1.1805Z-0.35
N385G3X3.8268Y1.1982I3.8018J1.1982
N390G1Y1.2162
N395Y3.8018
N400G3X3.8018Y3.8268I3.8018J3.8018
N405G1X1.1982
N410G3X1.1732Y3.8018I1.1982J3.8018
N415G1Y1.1982
N420G3X1.1982Y1.1732I1.1982J1.1982
N425G1X3.8018
N430G3X3.8194Y1.1805I3.8018J1.1982
N435G1X3.7329Y1.2671Z-0.4
N440G3X3.7402Y1.2848I3.7152J1.2848
N445G1Y3.7152
N450G3X3.7152Y3.7402I3.7152J3.7152
N455G1X1.2848
N460G3X1.2598Y3.7152I1.2848J3.7152
N465G1Y1.2848

N470G3X1.2848Y1.2598I1.2848J1.2848
N475G1X3.7152
N480G3X3.7329Y1.2671I3.7152J1.2848
N485G1X3.6462Y1.3538Z-0.45
N490G3X3.6536Y1.3714I3.6286J1.3714
N495G1Y3.6286
N500G3X3.6286Y3.6536I3.6286J3.6286
N505G1X1.3714
N510G3X1.3464Y3.6286I1.3714J3.6286
N515G1Y1.3714
N520G3X1.3714Y1.3464I1.3714J1.3714
N525G1X3.6286
N530G3X3.6462Y1.3538I3.6286J1.3714
N535G1X3.5596Y1.4404Z-0.5
N540G3X3.567Y1.458I3.542J1.458
N545G1Y3.542
N550G3X3.542Y3.567I3.542J3.542
N555G1X1.458
N560G3X1.433Y3.542I1.458J3.542
N565G1Y1.458
N570G3X1.458Y1.433I1.458J1.458
N575G1X3.542
N580G3X3.5596Y1.4404I3.542J1.458
N585G1X3.473Y1.527Z-0.55
N590G3X3.4804Y1.5446I3.4554J1.5446
N595G1Y3.4554
N600G3X3.4554Y3.4804I3.4554J3.4554
N605G1X1.5446
N610G3X1.5196Y3.4554I1.5446J3.4554
N615G1Y1.5446
N620G3X1.5446Y1.5196I1.5446J1.5446
N625G1X3.4554
N630G3X3.473Y1.527I3.4554J1.5446
N635G1X3.3864Y1.6136Z-0.6
N640G3X3.3938Y1.6313I3.3688J1.6313
N645G1Y3.3688
N650G3X3.3688Y3.3938I3.3688J3.3688
N655G1X1.6312
N660G3X1.6062Y3.3688I1.6312J3.3688
N665G1Y1.6312
N670G3X1.6312Y1.6062I1.6312J1.6312
N675G1X3.3688Y1.6063
N680G3X3.3864Y1.6136I3.3688J1.6313
N685G1X3.2998Y1.7002Z-0.65
N690G3X3.3071Y1.7179I3.2821J1.7179
N695G1Y3.2821
N700G3X3.2821Y3.3071I3.2821J3.2821
N705G1X1.7179
N710G3X1.6929Y3.2821I1.7179J3.2821
N715G1Y1.7179
N720G3X1.7179Y1.6929I1.7179J1.7179
N725G1X3.2821
N730G3X3.2998Y1.7002I3.2821J1.7179

N735G1X3.2132Y1.7868Z-0.7
N740G3X3.2205Y1.8045I3.1955J1.8045
N745G1Y3.1955
N750G3X3.1955Y3.2205I3.1955J3.1955
N755G1X1.8045
N760G3X1.7795Y3.1955I1.8045J3.1955
N765G1Y1.8045
N770G3X1.8045Y1.7795I1.8045J1.8045
N775G1X3.1955
N780G3X3.2132Y1.7868I3.1955J1.8045
N785G1X3.1266Y1.8734Z-0.75
N790G3X3.1339Y1.8911I3.1089J1.8911
N795G1Y3.1089
N800G3X3.1089Y3.1339I3.1089J3.1089
N805G1X1.8911
N810G3X1.8661Y3.1089I1.8911J3.1089
N815G1Y1.8911
N820G3X1.8911Y1.8661I1.8911J1.8911
N825G1X3.1089
N830G3X3.1266Y1.8734I3.1089J1.8911
N835G1X3.04Y1.96Z-0.8
N840G3X3.0473Y1.9777I3.0223J1.9777
N845G1Y3.0223
N850G3X3.0223Y3.0473I3.0223J3.0223
N855G1X1.9777
N860G3X1.9527Y3.0223I1.9777J3.0223
N865G1Y1.9777
N870G3X1.9777Y1.9527I1.9777J1.9777
N875G1X3.0223
N880G3X3.04Y1.96I3.0223J1.9777
N885G1X2.9534Y2.0466Z-0.85
N890G3X2.9607Y2.0643I2.9357J2.0643
N895G1Y2.9357
N900G3X2.9357Y2.9607I2.9357J2.9357
N905G1X2.0643
N910G3X2.0393Y2.9357I2.0643J2.9357
N915G1Y2.0643
N920G3X2.0643Y2.0393I2.0643J2.0643
N925G1X2.9357
N930G3X2.9534Y2.0466I2.9357J2.0643
N935G1X2.8668Y2.1332Z-0.9
N940G3X2.8741Y2.1509I2.8491J2.1509
N945G1Y2.1534
N950Y2.8491
N955G3X2.8491Y2.8741I2.8491J2.8491
N960G1X2.1509
N965G3X2.1259Y2.8491I2.1509J2.8491
N970G1Y2.1509
N975G3X2.1509Y2.1259I2.1509J2.1509
N980G1X2.8491
N985G3X2.8668Y2.1332I2.8491J2.1509
N990G1X2.7802Y2.2198Z-0.95
N995G3X2.7875Y2.2375I2.7625J2.2375

```
N1000G1Y2.2427
N1005Y2.7625
N1010G3X2.7625Y2.7875I2.7625J2.7625
N1015G1X2.2375
N1020G3X2.2125Y2.7625I2.2375J2.7625
N1025G1Y2.2375
N1030G3X2.2375Y2.2125I2.2375J2.2375
N1035G1X2.7625
N1040G3X2.7802Y2.2198I2.7625J2.2375
N1045G1X2.6939Y2.3061Z-0.9998
N1050G3X2.7012Y2.3237I2.6762J2.3238
N1055G1Y2.332
N1060Y2.6762
N1065G3X2.6762Y2.7012I2.6762J2.6762
N1070G1X2.3238
N1075G3X2.2988Y2.6762I2.3238J2.6762
N1080G1Y2.3238
N1085G3X2.3238Y2.2988I2.3238J2.3238
N1090G1X2.6762
N1095G3X2.6939Y2.3061I2.6762J2.3238
N1100G0Z1.0
N1105X0.Y0.M2
```

2) Pyramid wall angle 45 degrees, tool radius 6.35 mm, 1.27 mm step size, sheet thickness 0.815 mm.

```
.N10G70G94G75G90
'45 degree pyramid 1.27 mm step size   3-20-2011'
'SRF_MILL2'
'TOOL NUMBER:1'
'SPINDLE RPM:60'
N35G0X0.Y0.T1M6
N40S60
N45X4.2964Y4.2714
N50Z0.1
N55G1Z-0.1F5.0
N60G3X4.2714Y4.2964I4.2714J4.2714F10.0
N65G1X0.7286
N70G3X0.7036Y4.2714I0.7286J4.2714
N75G1Y0.7286
N80G3X0.7286Y0.7036I0.7286J0.7286
N85G1X4.2714
N90G3X4.2964Y0.7286I4.2714J0.7286
N95G1Y4.2714
N100X4.2424Y4.2351Z-0.15
N105G3X4.2214Y4.2464I4.2214J4.2214
N110G1X0.7786
N115G3X0.7536Y4.2214I0.7786J4.2214
N120G1Y0.7786
N125G3X0.7786Y0.7536I0.7786J0.7786
N130G1X4.2215
N135G3X4.2465Y0.7786I4.2215J0.7786
N140G1Y0.7831
N145X4.2464Y4.2214
N150G3X4.2424Y4.2351I4.2214J4.2214
N155G1X4.1901Y4.1881Z-0.2
N160G3X4.1714Y4.1964I4.1714J4.1714
N165G1X0.8286
N170G3X0.8036Y4.1714I0.8286J4.1714
N175G1Y0.8286
N180G3X0.8286Y0.8036I0.8286J0.8286
N185G1X4.1714
N190G3X4.1964Y0.8286I4.1714J0.8286
N195G1Y4.1714
N200G3X4.1901Y4.1881I4.1714J4.1714
N205G1X4.1394Y4.1388Z-0.25
N210G3X4.1214Y4.1464I4.1214J4.1214
N215G1X0.8786
N220G3X0.8536Y4.1214I0.8786J4.1214
N225G1Y0.8786
N230G3X0.8786Y0.8536I0.8786J0.8786
N235G1X4.1215
N240G3X4.1465Y0.8786I4.1215J0.8786
N245G1X4.1464Y4.1214
N250G3X4.1394Y4.1388I4.1214J4.1214
```

N255G1X4.0892Y4.089Z-0.3
N260G3X4.0714Y4.0964I4.0714J4.0714
N265G1X0.9286
N270G3X0.9036Y4.0714I0.9286J4.0714
N275G1Y0.9286
N280G3X0.9286Y0.9036I0.9286J0.9286
N285G1X4.0714
N290G3X4.0964Y0.9286I4.0714J0.9286
N295G1Y4.0714
N300G3X4.0892Y4.089I4.0714J4.0714
N305G1X4.0391Y4.0391Z-0.35
N310G3X4.0214Y4.0464I4.0214J4.0214
N315G1X0.9786
N320G3X0.9536Y4.0214I0.9786J4.0214
N325G1Y0.9786
N330G3X0.9786Y0.9536I0.9786J0.9786
N335G1X4.0214
N340G3X4.0464Y0.9786I4.0214J0.9786
N345G1Y4.0214
N350G3X4.0391Y4.0391I4.0214J4.0214
N355G1X3.9891Y3.9891Z-0.4
N360G3X3.9714Y3.9964I3.9714J3.9714
N365G1X1.0286
N370G3X1.0036Y3.9714I1.0286J3.9714
N375G1Y1.0286
N380G3X1.0286Y1.0036I1.0286J1.0286
N385G1X3.9714
N390G3X3.9964Y1.0286I3.9714J1.0286
N395G1Y3.9714
N400G3X3.9891Y3.9891I3.9714J3.9714
N405G1X3.9391Y3.9391Z-0.45
N410G3X3.9214Y3.9464I3.9214J3.9214
N415G1X1.0786
N420G3X1.0536Y3.9214I1.0786J3.9214
N425G1Y1.0786
N430G3X1.0786Y1.0536I1.0786J1.0786
N435G1X3.9214
N440G3X3.9464Y1.0786I3.9214J1.0786
N445G1Y3.9214
N450G3X3.9391Y3.9391I3.9214J3.9214
N455G1X3.8891Y3.8891Z-0.5
N460G3X3.8714Y3.8964I3.8714J3.8714
N465G1X1.1286
N470G3X1.1036Y3.8714I1.1286J3.8714
N475G1Y1.1286
N480G3X1.1286Y1.1036I1.1286J1.1286
N485G1X3.8714
N490G3X3.8964Y1.1285I3.8714J1.1286
N495G1Y1.1306
N500Y3.8714
N505G3X3.8891Y3.8891I3.8714J3.8714
N510G1X3.8391Y3.8391Z-0.55
N515G3X3.8214Y3.8464I3.8214J3.8214

N520G1X1.1786
N525G3X1.1536Y3.8214I1.1786J3.8214
N530G1Y1.1786
N535G3X1.1786Y1.1536I1.1786J1.1786
N540G1X3.8214
N545G3X3.8464Y1.1786I3.8214J1.1786
N550G1Y3.8214
N555G3X3.8391Y3.8391I3.8214J3.8214
N560G1X3.7891Y3.7891Z-0.6
N565G3X3.7714Y3.7964I3.7714J3.7714
N570G1X1.2286
N575G3X1.2036Y3.7714I1.2286J3.7714
N580G1Y1.2286
N585G3X1.2286Y1.2036I1.2286J1.2286
N590G1X3.7714
N595G3X3.7964Y1.2286I3.7714J1.2286
N600G1Y3.7714
N605G3X3.7891Y3.7891I3.7714J3.7714
N610G1X3.7391Y3.7391Z-0.65
N615G3X3.7214Y3.7464I3.7214J3.7214
N620G1X1.2786
N625G3X1.2536Y3.7214I1.2786J3.7214
N630G1Y1.2786
N635G3X1.2786Y1.2536I1.2786J1.2786
N640G1X3.7214
N645G3X3.7464Y1.2786I3.7214J1.2786
N650G1Y3.7214
N655G3X3.7391Y3.7391I3.7214J3.7214
N660G1X3.6891Y3.6891Z-0.7
N665G3X3.6714Y3.6964I3.6714J3.6714
N670G1X1.3286
N675G3X1.3036Y3.6714I1.3286J3.6714
N680G1Y1.3286
N685G3X1.3286Y1.3036I1.3286J1.3286
N690G1X3.6714
N695G3X3.6964Y1.3286I3.6714J1.3286
N700G1Y3.6714
N705G3X3.6891Y3.6891I3.6714J3.6714
N710G1X3.6391Y3.6391Z-0.75
N715G3X3.6214Y3.6464I3.6214J3.6214
N720G1X1.3786
N725G3X1.3536Y3.6214I1.3786J3.6214
N730G1Y1.3786
N735G3X1.3786Y1.3536I1.3786J1.3786
N740G1X3.6214
N745G3X3.6464Y1.3786I3.6214J1.3786
N750G1Y1.3833
N755Y3.6214
N760G3X3.6391Y3.6391I3.6214J3.6214
N765G1X3.5891Y3.5891Z-0.8
N770G3X3.5714Y3.5964I3.5714J3.5714
N775G1X1.4286
N780G3X1.4036Y3.5714I1.4286J3.5714

N785G1Y1.4286
N790G3X1.4286Y1.4036I1.4286J1.4286
N795G1X3.5714
N800G3X3.5964Y1.4286I3.5714J1.4286
N805G1Y3.5714
N810G3X3.5891Y3.5891I3.5714J3.5714
N815G1X3.5391Y3.5391Z-0.85
N820G3X3.5214Y3.5464I3.5214J3.5214
N825G1X1.4786
N830G3X1.4536Y3.5214I1.4786J3.5214
N835G1Y1.4786
N840G3X1.4786Y1.4536I1.4786J1.4786
N845G1X3.5214
N850G3X3.5464Y1.4786I3.5214J1.4786
N855G1Y3.5214
N860G3X3.5391Y3.5391I3.5214J3.5214
N865G1X3.4891Y3.4891Z-0.9
N870G3X3.4714Y3.4964I3.4714J3.4714
N875G1X1.5286
N880G3X1.5036Y3.4714I1.5286J3.4714
N885G1Y1.5286
N890G3X1.5286Y1.5036I1.5286J1.5286
N895G1X3.4714
N900G3X3.4964Y1.5286I3.4714J1.5286
N905G1Y3.4714
N910G3X3.4891Y3.4891I3.4714J3.4714
N915G1X3.4391Y3.4391Z-0.95
N920G3X3.4214Y3.4464I3.4214J3.4214
N925G1X1.5786
N930G3X1.5536Y3.4214I1.5786J3.4214
N935G1Y1.5786
N940G3X1.5786Y1.5536I1.5786J1.5786
N945G1X3.4214
N950G3X3.4464Y1.5786I3.4214J1.5786
N955G1Y3.4214
N960G3X3.4391Y3.4391I3.4214J3.4214
N965G1X3.3892Y3.3892Z-0.9999
N970G3X3.3715Y3.3965I3.3715J3.3715
N975G1X1.6285
N980G3X1.6035Y3.3715I1.6285J3.3715
N985G1Y1.6285
N990G3X1.6285Y1.6035I1.6285J1.6285
N995G1X3.3715
N1000G3X3.3965Y1.6285I3.3715J1.6285
N1005G1Y3.3715
N1010G3X3.3892Y3.3892I3.3715J3.3715
N1015G0Z1.0
N1020X0.Y0.M2

APPENDIX D

FIXTURE DESIGNS

The following section presents the final designs of the various components built during manufacture of the fixture.

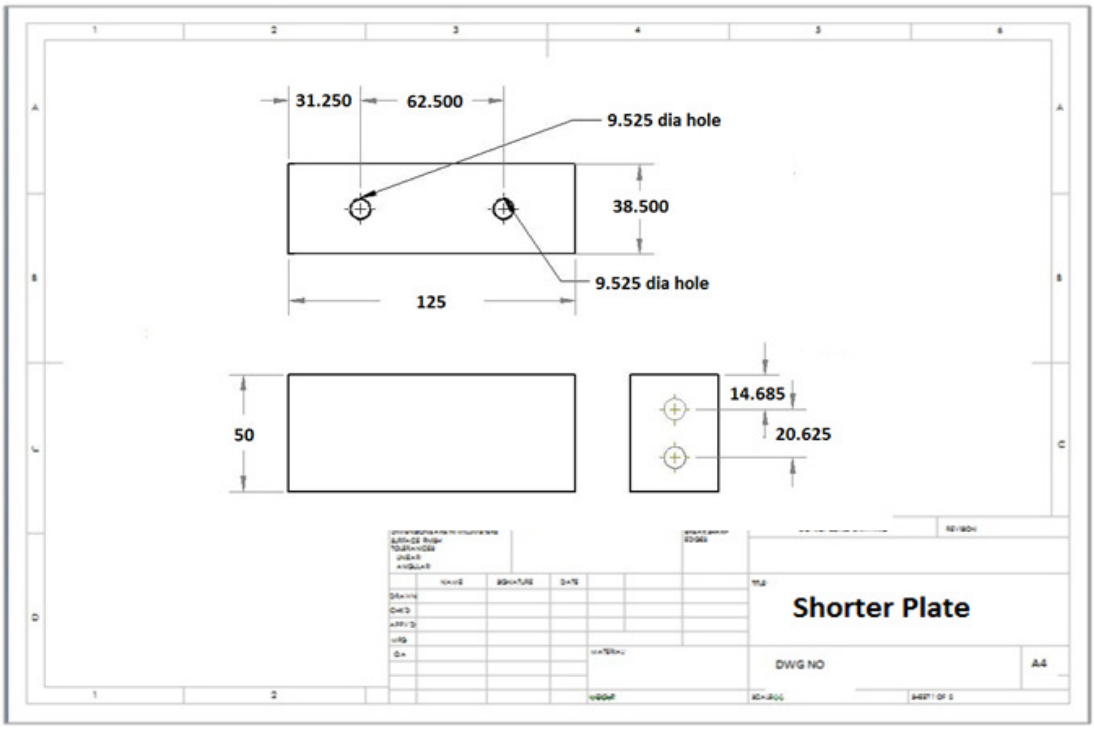

Fig. D1. Design of the shorter plate

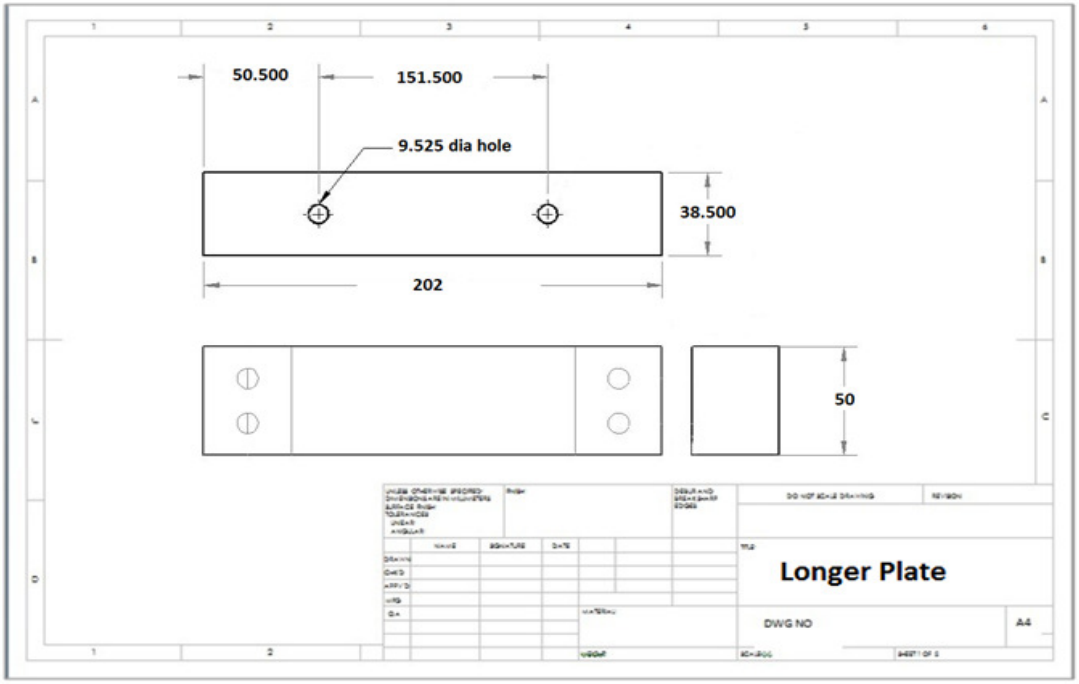

Fig. D2. Design of the longer plate

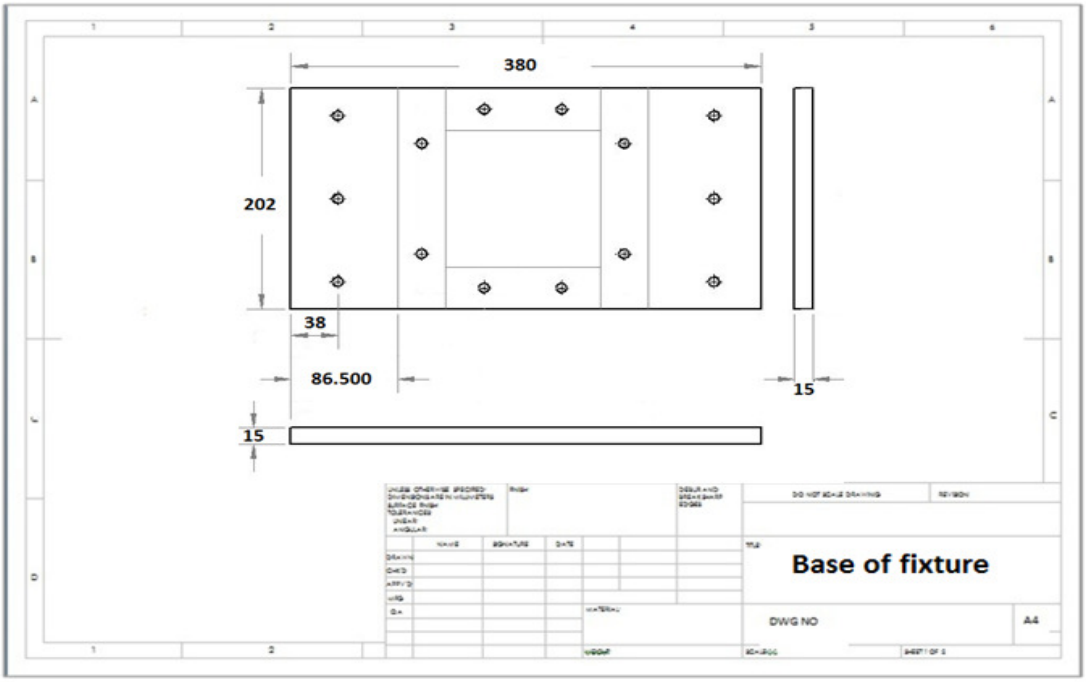

Fig. D3. Design of the fixture base

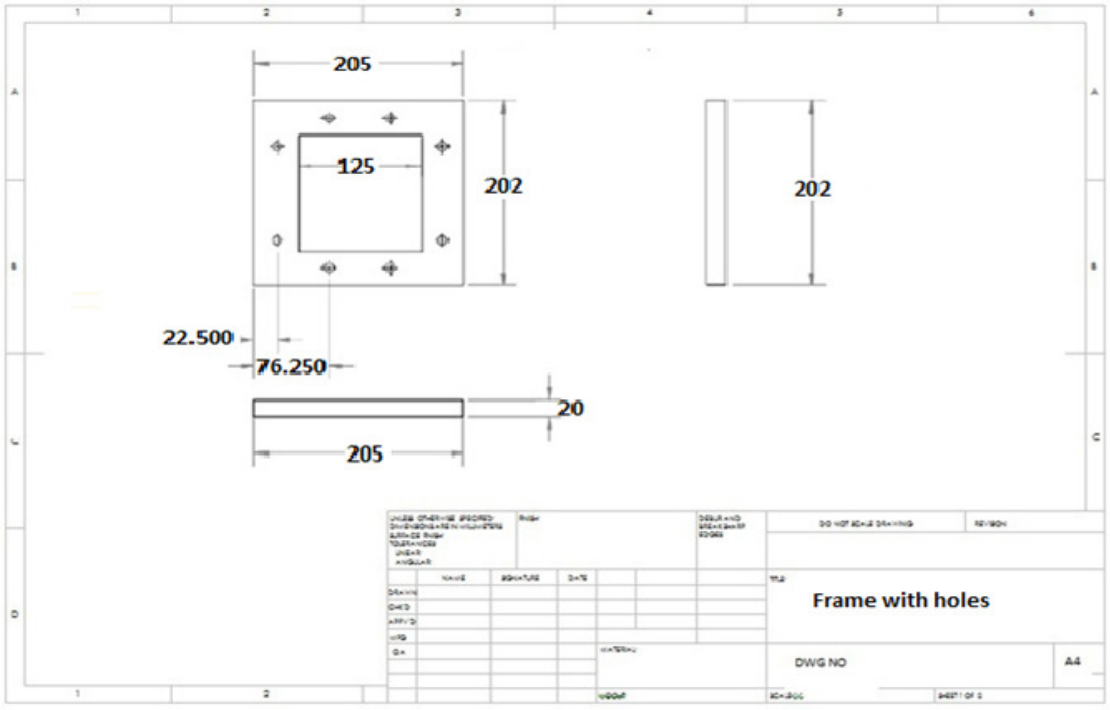

Fig. D4. Design of the frame

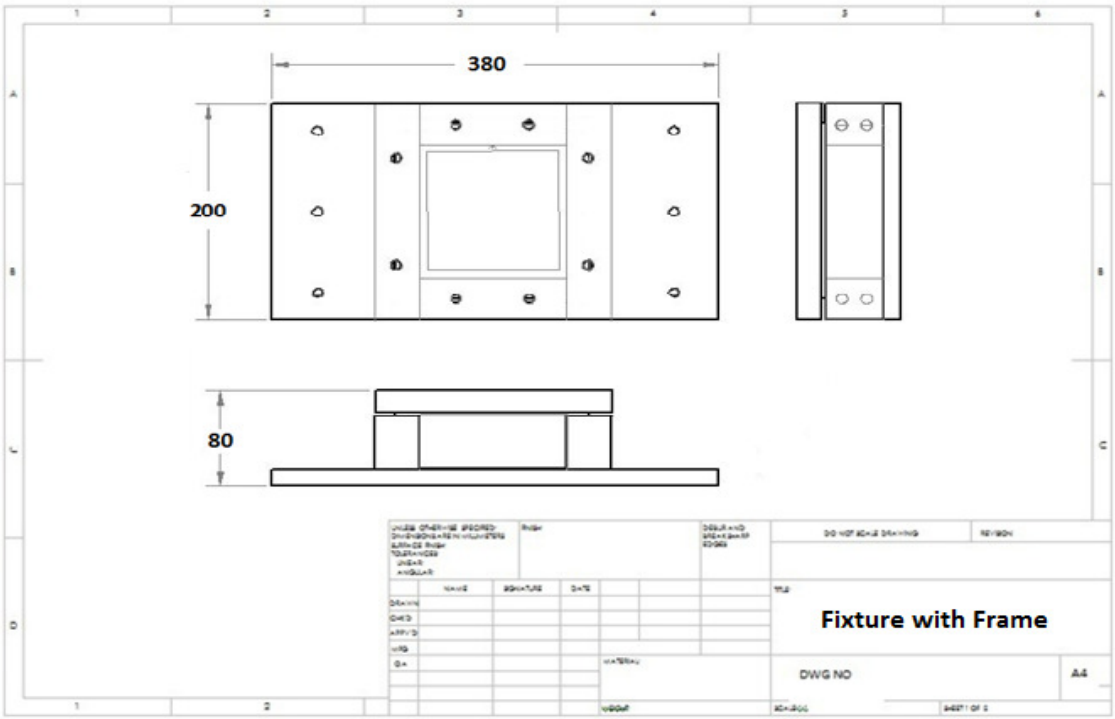

. Fig. D5. Design of the fixture with the frame

VITA

Mahesh Nair obtained his Bachelor of Engineering (Hons.) degree in mechanical engineering from Birla Institute of Technology and Science, Pilani – Goa Campus, Goa, India in June 2009. He enrolled in the mechanical engineering graduate program at Texas A&M University in August 2009 and received his Master of Science degree in August 2011. His research interests include stress analysis and manufacturing.

Permanent Address: Department of Mechanical Engineering, ENPH, 3123 TAMU, College Station, Texas 77843.

Email: maheshkeliye@gmail.com